

2021-09

NUMERICAL EVALUTION OF EPS GEOFOAM AND GEOTEXTILE FOR THE PROTECTION OF BURIED PIPES IN DIFFERENT BACKFILLS

BINYAM, GEZAHEGN

<http://ir.bdu.edu.et/handle/123456789/14617>

Downloaded from DSpace Repository, DSpace Institution's institutional repository



BAHIR DAR UNIVERSITY
BAHIR DAR INSTITUTE OF TECHNOLOGY
SCHOOL OF RESEARCH AND POSTGRADUATE STUDIES
FACULTY OF CIVIL AND WATER RESOURCE ENGINEERING
GEOTECHNICAL ENGINEERING

MSc. Thesis on:

NUMERICAL EVALUATION OF EPS GEOFOAM AND
GEOTEXTILE FOR THE PROTECTION OF BURIED PIPES IN
DIFFERENT BACKFILLS

By

BINYAM GEZAHEGN

December, 2021
Bahir Dar, Ethiopia



BAHIR DAR UNIVERSITY
BAHIR DAR INSTITUTE OF TECHNOLOGY
SCHOOL OF RESEARCH AND POSTGRADUATE STUDIES
FACULTY OF CIVIL AND WATER RESOURCES
ENGINEERING

**Numerical Evaluation of EPS Geofoam and Geotextile For The
Protection of Buried Pipes in Different Backfills**

By

Binyam Gezahegn

A thesis submitted

in Partial Fulfillment of the Requirements for the Degree of
Master of Science in Geotechnical Engineering

Yebeltal Zerie (Ph.D.)

December, 2021

Bahir Dar, Ethiopia

© 2021 Binyam Gezahegn

© Copyright by Binyam Gezahegn
December 13, 2021. All Rights Reserved

DECLARATION

This is to certify that the thesis entitled “**Numerical Evalution of EPS Geofoam and Geotextile for the Protection of Buried Pipes in Different Backfills**”, submitted in partial fulfillment of the requirements for the degree of Master of Science in **Geotechnical Engineering** under the **Faculty of Civil and Water Resource Engineering**, Bahir Dar Institute of Technology, is a record of original work carried out by me and has never been submitted to this or any other institution to get any other degree or certificates. The assistance and help I received during this investigation have been duly acknowledged.



Binyam Gezahegn

Name of the Candidate

Signature


December 2021

Date

BAHIR DAR UNIVERSITY
BAHIR DAR INSTITUTE OF TECHNOLOGY
SCHOOL OF RESEARCH AND GRADUATE STUDIES
FACULTY OF CIVIL AND WATER RESOURCE ENGINEERING

APPROVAL OF THESIS FOR DEFENSE

I hereby certify that I have supervised, read, and evaluated this thesis titled “**Numerical Evaluation of EPS Geofoam and Geotextile for the Protection of Buried Pipes in Different Backfills**” prepared by **Binyam Gezahegn** under my guidance. I recommend the thesis to be submitted for oral defense.

<u>Yebeltal Zerie (Ph.D.)</u>		<u>September, 2021</u>
Advisor's name	Signature	Date

BAHIR DAR UNIVERSITY
BAHIR DAR INSTITUTE OF TECHNOLOGY
SCHOOL OF RESEARCH AND GRADUATE STUDIES
FACULTY OF CIVIL AND WATER RESOURCE ENGINEERING







APPROVAL OF THESIS FOR DEFENSE RESULT

I hereby confirm that the changes required by the examiners have been carried out and incorporated in the final thesis.

<u>Binyam Gezahegn</u>		<u>12/14/ 2021</u>
Name of the Candidate	Signature	Date

As members of the board of examiners, we examined this thesis entitled “Numerical Evaluation of EPS Geofoam and Geotextile for the Protection of Buried Pipes in Different Backfills” by Binyam Gezahegn. We hereby certify that the thesis is accepted for fulfilling the requirements for the award of the degree of Masters of Science in “Geotechnical Engineering”.

Board of Examiners

<u>Yebeltal Zerie (Ph.D.)</u>		<u>26/01/2022</u>
Advisor's name	Signature	Date
<u>Binyam Bekele (Ph.D.)</u>		<u>26/01/2022</u>
External Examiner	Signature	Date
<u>Henok Fkrie (Ph.D.)</u>		<u>26/02/2022</u>
Internal Examiner	Signature	Date
<u>Fekadu Wubetu</u>		<u>05/04/2022</u>
Defense Chairman	Signature	Date
<u>Melkam U Abebe</u>		<u>05/04/2022</u>
Chair	Signature	Date
<u>Melkamu Demewez Gebeye</u>		<u>Apr. 6 / 2022</u>
Faculty Academic Program Officer (V/Dean)	Signature	Date

Melkamu Demewez Gebeye
Faculty Academic Program
Officer (V/Dean)



Acknowledgment

First of all, thank you God for the chance, the strength and wisdom you gave me to complete this study successfully. Next, University of Gondar and Bahir Dar University will take my appreciation for sponsoring and arranging this MSc program. Finally, I would like to express my gratitude to Dr. Yebeltal Zerie for his willingness to counsel me, for giving me the initial idea of this thesis, and for helping me in the process.

Nomenclatures

<u>Symbol</u>	<u>Description</u>	<u>Units</u>
B	– Width of the loading plate	[m]
b	– Width of geofoam block	[m]
c'	– Cohesion	[kPa]
D	– Diameter of the pipe	[m]
E	– Modulus of elasticity	[MPa]
G	– Shear modulus	[MPa]
H	– Depth of placement of the pipe	[m]
h	– Thickness of EPS geofoam block	[m]
L	– Length of the pipe	[m]
K _g	– Stiffness of the geofoam	[MPa]
PS	– Stiffness of the pipe	[MPa]
n	– Number of reinforcement	number
p	– Applied pressure	[kPa]
q	– Vertical stress on the crown	[kPa]
Q	– Ultimate bearing capacity reinforced backfill	[kPa]
T	– Tensile strength of geotextile	[kN/m]
w	– Settlement of loading plate	[m]
u	– Depth of the first layer of the reinforcement	[m]
z	– Depth of placement of geofoam	[m]
σ	– Normal stress	[kPa]
τ	– Shear stress	[kPa]
ε	– Strain	-
ϕ'	– Internal friction angle	[°]
ν	– Poisson's ratio	-
ρ	– Density	[kg/m ³]

Abbreviations

Abbreviations

Description

ALE	Arbitrary Lagrangian-Eulerian
ANSI	American National Standards Institute
ASME	American Society of Mechanical Engineers
ASTM	American Society for Testing and Materials
CAE	Complete Abaqus Environment
CU	Consolidated Undrained
EN-ISO	European International Organization for Standardization
FEA	Finite Element Analysis
FEM	Finite Element Method
FRP	Fiber Reinforced Plastic
HDPE	High Density Polyethylene
ITI	Imperfect Trench Installation
LDPE	Low Density Polyethylene
NPRA	Norwegian Public Road Administration

Table of Contents

Declaration	I
Approval of Thesis for Defense	III
Approval of Thesis for Defense Result	IIII
Nomenclatures	V
Abbreviations	VI
List of Tables	IX
List of Figures	XI
Abstract	XIII
Chapter 1 Introduction	1
1.1 Background	1
1.2 Problem Statement	1
1.3 Objective of the Research	3
1.4 Scope of the Study.....	4
1.5 Significance of the Study	4
Chapter 2 Literature Review	6
2.1 Introduction	6
2.2 Buried Pipes	6
2.3 Types of Pipes	7
2.3 Soil-Pipe Interaction.....	7
2.3.1 Contact Pressure Distribution on the Wall of Buried Pipes	8
2.3.2 Deflection of Buried Pipes	9
2.4 EPS Geofom	9
2.5 Geotextile	12
2.5.1 Reinforcement Mechanism.....	13
2.6 Backfill	14
2.6.1 Quarry Dust	14
2.6.2 Fly Ash	15
2.7 Finite Element Method (FEM)	16
Chapter 3 Research Methodology	24
3.1 Introduction	24
3.2 Geometry of the Model	25
3.2.1 Geometry of Trench Models without any Additional Protecting Material	25

3.2.2 Geometry of EPS Included Trench Models.....	26
3.2.3 Geometry of Geotextile Reinforced Trench Models	26
3.2.4 Boundary of the Model.....	27
3.3 Material Modeling.....	29
3.3.1 Constitutive Models.....	29
3.3.2 Materials	33
a. Quarry Dust.....	33
b. Fly ash.....	36
c. Soil for Trench Fill.....	37
D. The Surrounding Soil	39
e. Pipe.....	40
f. EPS Geofoam	41
g. Geotextile.....	46
3.4 Meshing.....	50
3.4.1 Element Type.....	51
3.4.2 Mesh Size	53
3.5 Loading and Boundary Conditions	55
3.5.1 Loading.....	55
3.5.2 Boundary Conditions.....	59
3.6 Validation of the Methodology	60
3.6.1 Basic Research Idea.....	61
3.6.2 Structural Model.....	62
3.6.3 Finite Element Modeling of the Model Trench Test	62
3.6.4 Comparison of the Model Trench Test and the Numerical Model.....	62
Chapter 4 Result and Discussions	65
4.1 Introduction	65
4.2 Study on Base Models.....	66
4.2.2 Vertical Stress on the top of the Pipe	66
4.2.3 Circumferential Strain	70
4.2.4 Performance of EPS Geofoam.....	72
4.2.5 Performance of Geotextile.....	73
4.3 Parametric Study	74

4.3.1 Effect of Pipe Diameter	74
a. Results in Unreinforced Trench Models	76
b. Results in Geotextile Reinforced and EPS Geofoam Included Models	77
4.3.2 Effect of Pipe Stiffness	77
4.3.3 Effect of EPS Geofoam Thickness	79
4.3.4 Effect of EPS Geofoam Location	80
4.3.5 Effect of Double Layer of EPS Geofoam Blocks.....	82
4.3.6 Effect of Tensile Stiffness of Geotextile Reinforcement.....	83
4.2.7 Effect of Number of Geotextile Reinforcement Layers	84
4.4 Combined Use of EPS Geofoam and Geotextile	85
Chapter 5 Conclusions and Recommendations.....	89
5.1 Conclusions	89
5.2 Recommendations	90
References.....	92
Appendix.....	100

List of Tables

Table 2.1 Summary of literature reviews.....	18
Table 3.1 Summary of the result of sensitivity analysis for deciding the side boundaries of the model	27
Table 3.2 Chemical composition of fly ash	37
Table 3.3 Properties of stone dust fly ash and soil	38
Table 3.4 Summary of input parameters for the three fill materials in FEA	39
Table 3.5 Parameter used in FEA for the surrounding soil.....	39
Table 3.6 Steel pipe dimensions	40
Table 3.7 Summary of material and geometrical model of the pipe.....	41
Table 3.8 Summary of EPS geofoam material and geometrical model.....	43
Table 3.9 Different geotextiles with their tensile strength values	47
Table 3.10 Calculated modulus of elasticity.....	49
Table 3.11 Effect of geotextile Poisson's ratio on the crown vertical stress	50
Table 3.12 Element types, used for each materials.....	51
Table 3.13 Result of mesh sensitivity analysis on the model with fly ash fill.....	54
Table 3.14 Materials, used by Beju and Mandal (2017a).....	61
Table 4.1 Summary of stress ratio results on the crown for minimum and maximum diameter pipe in different trench conditions	75
Table 4.2 Summary of stiffness of different pipes.....	79

List of Figures

Figure 3.1 Geometry of the unreinforced trench model..	28
Figure 3.2 Geometry of EPS geofoam included trench model	28
Figure 3.3 Geometry of Geotextile reinforced trench model.....	29
Figure 3.4 Mohr's circle of effective stress	32
Figure 3.5 Mohr-coulomb yield surface in principal stress space	33
Figure 3.6 Particle size distribution curves for soil, stone dust and fly ash.....	35
Figure 3.7 (a) Mohr-Coulomb failure envelop, (b) Deviatoric stress-axial strain curve ..	36
Figure 3.8 (a) Mohr-Coulomb failure envelop, (b) Deviatoric stress-axial strain curve ..	37
Figure 3.9 (a) Mohr-Coulomb failure envelope, (b) Deviatoric stress-axial strain curve.	38
Figure 3.10 General configuration of the pipe and the EPS geofoam	44
Figure 3.11 Default pressure-overclosure relationship in abaqus.....	46
Figure 3.12 General configuration of the pipe and a single geotextile reinforcement.....	48
Figure 3.13 Schematic representation of geotextile tensile strength test.....	48
Figure 3.14 Eight noded hexahedron element	52
Figure 3.15 Vertical stress on the crown of the pipe at different element size.....	53
Figure 3.16 Sample meshed trench model parts	54
Figure 3.17 Empty trench	55
Figure 3.18 Trench with bedding.....	56
Figure 3.19 Installation of the pipe	56
Figure 3.20 Filled unreinforced trench model	57
Figure 3.21 Partially backfilled trenches	57
Figure 3.22 Installation of (a) EPS geofoam, (b) geotextile	58
Figure 3.23 Final fill for (a) EPS included, (b) geotextile reinforced trenches	58
Figure 3.24 ASHTO SH-25 loading	59
Figure 3.25 Loading step in the finite element model	59
Figure 3.26 Schematic representation of trench model boundary conditions.....	60
Figure 3.27 Boundary condition in the 3D model	60
Figure 3.28 Schematic representation of model trench test set up	62
Figure 3.29 Finite element model of the model trench test	62

Figure 3.30 Comparison of the experiment and FEM results based on Variation of settlement ratio with the applied pressure.....	63
Figure 3.31 Comparison of the experiment and FEM results based on Variation of pipe deflection with applied pressure	63
Figure 4.1 Vertical stress variation at the crown of the pipe with time (for fly ash fill) ..	66
Figure 4.2 Variation of radial stress around the pipe in fly ash fill	67
Figure 4.3 Variation of vertical stress at the crown of the pipe along the length of the pipe in fly ash fill.....	67
Figure 4.4 Variation of vertical pressure at the crown of the pipe in different backfills..	69
Figure 4.5 Comparisons of stress ratio on the crown for different fill materials.....	70
Figure 4.6 Circumferential strain.....	71
Figure 4.7 Performance of EPS geofoam	72
Figure 4.8 Performance of geotextile.....	74
Figure 4.9 Variation of vertical stress ratio with pipe diameter to thickness ratio.....	75
Figure 4.10 Variation of vertical pressure ratio for different pipe stiffness values	79
Figure 4.11 Effect of EPS geofoam thickness on the performance of the trench.....	80
Figure 4.12 Effect of EPS geofoam location on the performance of the trench.....	81
Figure 4.13 Comparison of maximum vertical stress at the crown for different spacings of double EPS geofoam,.....	82
Figure 4.14 Variation of vertical pressure at the crown with time for different tensile strength geotextiles	84
Figure 4.15 Variation of vertical stress at the crown with time for different no of geotextile reinforcement layers.....	85
Figure 4.16 Schematic representation of combined use of EPS geofoam and geotextile.	86
Figure 4.17 Comparison of combined used of EPS geofoam and geotextile with other case of trench system	87

Abstract

The use of underground buried pipes is growing fast in transporting clean water, sewage, telecom lines, gases and other chemicals. These buried pipe lines can affect the lives of people directly. Therefore, studies all over the world have been conducted on methods of protecting the pipelines; and those studies have suggested different scientific protection methods. On the contrary, the habit of protecting buried pipes in Ethiopia is very low. This is costing the country millions of dollars already. It is believed that this research will encourage the use of different new and economical protection methods. In this paper, the behavior of Steel buried pipes with the inclusion of expanded polystyrene (EPS) geofoam and geotextile reinforcement in different backfills (local soil, fly ash and quarry dust) was analyzed numerically. The contact pressure and the circumferential strain were the main parameters to discuss the performance of the pipes in those different cases. The research also studied the effect of pipe stiffness, pipe diameter, EPS geofoam thickness & location, tensile stiffness and the number of reinforcements on the performance of the pipe along with the protective materials. A finite element analysis software, i.e., Abaqus/CAE was utilized to fulfill the objectives of the study. The results indicated that the vertical pressure on the top of the steel pipe, which was installed at 3D from the surface, could be reduced up to 40.1% and 29.3% under EPS geofoam included and geotextile reinforced trenches respectively. Since the three backfills that were used in this study had comparable shear strength parameters, it did not alter the vertical stress on the pipes significantly and this result strengthens the idea of using fly ash and quarry dust as an alternative backfill material. However, the above results were affected by the thickness and location of EPS geofoam, the tensile strength of the reinforcement and the number of geotextile reinforcements provided. Moreover, it is found that the performance of the steel pipe was found to be affected by its diameter and stiffness. Finally, the combined use of EPS geofoam and geotextile gave a positive result in reducing both the vertical pressure on the pipe and the surface settlement.

Keywords: Abaqus, EPS geofoam, Geotextile, Stone dust, Fly ash, Buried pipe

Chapter 1

Introduction

1.1 Background

Pipelines are a reliable and cost-effective way to carry gas, water, sewage, and other fluids. They are usually buried in the ground to provide protection and support. However, pipelines without proper installation could result in loss of life and a huge amount of money. This has been observed in different countries of the world. For example, records show that about one-third of the gas explosions in the United Kingdom are caused by gas escaping from broken pipes. Therefore, huge care should be given for the protection of buried pipelines.

Different methods of protecting buried pipes have been suggested by researchers. Nevertheless, the most effective and recent technology of protecting buried pipes is the inclusion of lightweight geosynthetic materials. Thanks to the development of polymer science, different types of geosynthetic materials have been produced, for example geocells, geogrid, geofoam, geotextile, etc. In addition, using selected lightweight backfill has been suggested to reduce the earth pressure on the pipes. Those different suggestions have been experimented with and tried by researchers around the world.

With the growing demand of the Ethiopians' government to invest in pipelines, the safety of buried pipes should also be guaranteed. The main aim of this research is to reinvestigate the use of some of the geosynthetic materials and selected backfill in protecting the buried pipes and to introduce them at least numerically. It is believed that this research will be a springboard to initiate further researches on the protection of buried pipes in Ethiopia.

1.2 Problem Statement

In Ethiopia, the use of buried pipes for different infrastructures is growing fast. Telecom lines, urban sewage lines and gas lines (the ones the government planned to install) are examples of this demand. However, the interest of companies and the government to protect the buried pipes with scientific methods is very low. Currently, the failure of buried pipes may not cause direct problems to the people and the environment but as the country

tries to use buried pipe lines for the transportation of gas and chemicals, every single pipe failure starts to affect the health and the environmental condition of the country.

Before the beginning of this research, it was tried to undertake a preliminary survey on the condition of buried pipe lines. This survey was conducted on some water supply agencies, the telecom company and city municipalities as a sample. Even though the willingness of those companies and agencies to give the necessary information on their pipes is very low, the researcher gathered enough information to conclude that the companies are far behind buried pipe protection science. From this survey, it is found that water supply agencies are the big spender for the maintenance of their pipes. For example in the city of Gondar, the Ethiopian water supply agency has five stations. Each station spends over 1.4 million birrs a year for the maintenance of the pipes. That money does not include the salary of the maintenance personnel. Such an amount of money could be reduced by installing pipes with some type of protection.

Based on the preliminary study, it is not said that the agencies are not using any protection. They use different protection techniques at different sections of the pipelines, especially for road crossing pipes and other sensitive pipeline sections. For example, using more flexible PVC pipes instead of steel pipes; installing pipes in greater depth; sending the pipe through a larger steel pipe and sometimes covering the pipe with cement concrete at the joints. Nevertheless, each technique has its own limitation. For instance, installing pipes in a greater depth may protect them from the loads that could be applied at the surface of the ground but the vertical earth pressure on the pipe will get bigger and this will make the maintenance work a bit difficult. Protecting pipe lines with another large-diameter steel pipe is not economical. Therefore a new, economical and effective method of protecting buried pipes should be introduced.

In addition to the water supply agency, it was tried to gather information on other service providers that use buried pipes, like city municipality and telecom offices. However, no one was willing to give any necessary information. Even though it is not supported by actual quantitative data, the sewerage and drainage pipelines in Gondar are exposed to damage. These conditions are observed in many parts of the city. There might be many

reasons for those damages but it is believed that installing pipelines with some protective techniques could reduce the level of damage.

In this research, it was planned to introduce and encourage the use of a new scientific protection technique in the country. The first technique is applying imperfect trench installation (ITI) with expandable polystyrene geofom (Spangler and Handy, 2007). Almost all types of pipes in Ethiopia are buried in trench/ditch installation method. Pipelines around sensitive areas could be buried with the inclusion of some type of lightweight and compressible materials like expandable polystyrene geofom. The second technique that will be studied and encouraged in this research is reinforcing the backfill soil with a geotextile.

The waste disposal problem was the second issue that this study aimed to address. Currently, the world is facing a problem with disposing of wastes from different factories. Among these wastes, stone dust and fly ash are some of them. In Ethiopia, stone dust and fly ash are currently produced as waste from stone crushing plants and from different factories which use coal as an energy source. Before Ethiopia face a series of problems with those wastes like western and far-east countries, the wastes should be either reused or disposed of in an environmentally friendly way. In this research, the use of those waste materials as a non-conventional backfill material in combination with the above protective materials was also assessed.

1.3 Objective of the Research

The general objective of this research is to analyze the behavior of buried pipes with the inclusion of EPS geofom along with geotextile reinforcement in quarry dust, fly ash and soil as a backfill numerically.

The specific objectives of the research are:

- a. Determining the contact pressure and circumferential strain of the pipe in unreinforced, EPS included and geotextile reinforced trench models numerically.
- b. Comparing the results of unreinforced trench models with geotextile reinforced and EPS included trench models.

- c. Study the effect of different parameters on the performance of the pipe, i.e., pipe stiffness and diameter, thickness and location of the EPS geofoam, and tensile stiffness and number of layer of the geotextile reinforcement.
- d. Comparison of this study with previously published works.

In addition to the objectives stated above, there are also some practical objectives regarding to the materials that were used in this research. These are:

- a. Suggesting some buried pipe protection techniques to the local users.
- b. Introducing some geosynthetic materials for the use of pipe protection to the local users.
- c. Protecting the environment by utilizing waste products of different industries.

1.4 Scope of the Study

With strong intension of protecting buried pipes, this research analysed buried pipe models with various properties of pipes, different backfills and different protection materials. From geosynthetic materials, EPS geofoam and woven geotextile was used as a compressible inclusion and reinforcement respectively. Three materials (soil, fly ash and quarry dust) were also utilized as a backfill. The numerical analysis in this study involved shallow buried pipes with diameter from 141 mm to 273 mm and only one type of EPS geofoam (EPS 15) was used as compressible material. Moreover, four types of geotextiles were applied in the models.

Due to time, cost and resource constraints, this research has its own limitations. The research was conducted only numerically. However, the index properties and the shear parameters of the backfill materials were obtained using standard laboratory tests. Furthermore, some parameters of the materials that were necessary for the analysis were taken reasonably from Standard books, literatures and manufacturers descriptions. Since it is hard to find the test machine nearby, other researchers with much resources could validate this research experimentally.

1.5 Significance of the Study

The contribution of this research could be explained in two ways. The first one is its impact on the future pipeline construction of the country. As it was attempted to reveal in section 1.2 of this document, the application of modern pipeline protection techniques in Ethiopia

is low. This research is expected to create awareness for companies about the use of EPS geofoam and geotextile in trenches. The second contribution of this research is for the academic world. The use of EPS geofoam for the protection of buried pipes has been studied widely but the study of geotextile with a buried pipe is very limited. In addition, the performance of both EPS geofoam and geotextile within different backfills has not been studied widely. The parametric studies, which were conducted in this research, are also expected to fill some of the gaps and strengthen some of the theoretical aspects regarding the above materials.

Moreover, this research will introduce some non-conventional fill material for the local users. The use of these non-conventional fill materials will solve the disposal problem of those materials and keep the environment clean.

Chapter 2

Literature Review

2.1 Introduction

Due to the wide range of applications of pipelines, studies on the pipelines and pipeline-related issues have been conducted broadly. In this section of the document, some literatures that are related to the objective of this research are reviewed. It was tried to classify the studies in different categories and it is presented in sub-topics. These categories involve the reviews of studies, which were conducted on the buried pipes, soil-pipe interaction, protection techniques of buried pipes and buried pipe analysis techniques. Mostly, recent studies were selected for this report but some old and basic researches were also involved. Based on the reviews made, some gaps were identified and those gaps were used as a motivation for this research work. Finally, all the reviewed studies were summarized and presented in Table form.

2.2 Buried Pipes

Underground conduits and pipes have been in use since ancient human civilization. Remnants of such structures from ancient civilizations have been found in Europe and Asia. In addition, some of the ancient inhabitants of South and Central America had water and sewer systems. However, most of the underground conduits from those ancient civilizations were constructed by trial and error and experience.

Unlike ancient underground pipes, modern age conduits are constructed based on scientific principles and experiments. So, extensive researches and studies have been made on the mechanics of buried pipes. Among these studies, Marston and Anderson (1913) was the fundamental one. Today, the design and analysis of buried pipes is being done by using finite element and finite difference based software.

Generally piping materials are categorized in one of two classifications: rigid or flexible but it is hard to find pure flexible and pure rigid material. Based on the method of installation, buried pipes are divided into two main categories: ditch conduits (trench conduits) and projecting conduits (embankment conduits) (Spangler and Handy, 2007).

During the design of buried pipes internal pressure, external pressure and other types of loads are considered. (Moser and Folkman, 2008). The effect of those loads on the pipes is expressed in different parameters. However, in this paper, only three parameters (contact pressure on the wall of the pipe, deflection and circumferential strain of the pipe) were considered.

2.3 Types of Pipes

The main classification of pipes came from the stiffness the pipe material. Generally piping materials are categorized in one of the two classifications: rigid or flexible but it is hard to find pure flexible and pure rigid material. According to Moser and Folkman (2008), rigid pipes are sufficiently strong (within both the pipe wall and joints) to withstand most anticipated live and dead loads. Rigid pipes include reinforced non-cylinder concrete, reinforced concrete cylinder, pre-stressed concrete cylinder, vitrified clay, polymer concrete, cast iron, asbestos cement and cast-in-place pipes. On the other hand, flexible pipes are less strong and the load carrying capacity of such pipes came from their ability to deflect without structural damage (Moser and Folkman, 2008). Flexible pipes include steel, ductile iron, thermoplastics such as Polyvinyl Chloride (PVC) and High Density Polyethylene (HDPE), thermosetting plastics such as fiberglass-reinforced polymer (FRP), bar-wrapped concrete cylinder pipe, and corrugated steel pipes. Some standards' define a flexible pipe as one that can deflect more than 2% without cracking.

There are other criteria to classify pipes. For example, based on the method of installation, buried pipes are divided into two main categories: ditch conduits (trench conduits) and projecting conduits (embankment conduits) (Spangler and Handy, 2007). A ditch conduit is one that is built in a relatively small ditch and then covered with earth fill. Sewers, drains, and water and gas mains are all examples. Whereas, a projecting conduit is installed in shallow bedding with its top projecting above the surface of the natural ground and then is covered with an embankment. This is how most railway and highway culverts are installed.

2.3 Soil-Pipe Interaction

As literatures from old to the recent ones indicate, the performance of buried pipes is greatly affected by the interaction of the pipe with the surrounding soil. According to the

famous Marston theory (Moser and Folkman, 2008), the soil-pipe interaction depends on the method of installation of the pipe (trench conduit and embankment conduit). In addition to method of installation, stiffness of a pipe is the major factor on the soil-pipe interaction. Rigid pipes support a given earth load through the strength inherent in the pipe material. Although no additional support is gained from the side soil, the bedding material type and trench geometry are important in distributing the load over the entire pipe and preventing concentrated loads (Boldon and Jeyapalan, 1986). On the other hand, flexible pipes transfer loads to the side fills through its flexible ability. Flexible pipes deflect due to loads and mobilize the support of embedment materials on both sides of the pipe. Terzaghi (1943) called this condition ‘arching’. Therefore, flexible pipes distribute the imposed vertical load to the surrounding soil.

2.3.1 Contact Pressure Distribution on the Wall of Buried Pipes

Contact pressure is one of the main concept in mechanics of buried pipes. Based on Marston theory, the contact pressure on the buried pipes can be calculated depending on their method of installation (Marston and Anderson, 1913). Even though it is an old theory, it is still widely accepted and widely used concept. According to Marston, there are two major methods of installations. These are trench condition and embankment condition. In the same study, the formula to calculate the vertical pressure on the walls of the pipe was derived for each type of installation methods and for different type of pipes. The net vertical force acting on a buried conduit was evaluated as the weight of the soil column plus or minus the shear forces acting on the sides of the column. The direction of the shear forces is controlled by the arching phenomena (Spangler and Handy, 1973). With some modification of other researchers, this theory is still a good analytical method. The main limitation of those analytical approaches is they cannot be applied for trench conditions with some reinforcement of the backfill and other pipe protective materials.

In addition to the above analytical approaches, FEM is widely used recently to evaluate the contact pressure distribution on the walls of the pipes but the small scale laboratory test remains the best choice for an accurate results.

2.3.2 Deflection of Buried Pipes

Deflection is another important parameter in buried pipe design, especially for flexible pipes. Elastic deflection is calculated in the same way for both rigid and flexible pipes. However, elastic deflection for rigid pipe is small enough to be neglected. During the design of pipes, two types of analysis are always conducted independently: longitudinal and ring analysis. As Watkins and Anderson (2000) explained, ring instability is the worst case of collapse analysis. Because instability is reduced by the interaction of ring stiffness and longitudinal stiffness. So here after, when it is said deflection in this paper, it is to refer the ring deflection.

After Marston's load theory, Spangler (1941) showed that Marston's theory was not enough for the design of flexible buried pipes and the author derived the famous formula to calculate the deflection of flexible pipes, i.e., 'Iowa formula'.

Later Watkins (1958) examined the Iowa formula dimensionally. From the analysis, the author determined that modulus of passive resistance of side fill which is used in Iowa formula could not possibly be a true property of the soil. Because the dimensions of modulus of passive resistance of side fill are not those of a true modulus (Moser and Folkman, 2008).

In addition to the above methods of determining the deflection of buried pipes, 'beam on elastic foundation approach' (Hetényi, 1946) and finite element method (FEM) are developed. However, the most comprehensive analysis method is FEM. This method gives the best tool for predicting the detailed performance of buried structures. Many researchers studied pipe deflection by using finite element method (e.g. Anil et al., 2015; Meguid et al., 2017; Abdollahi and Tafreshi, 2017) and most of the analysis from those researches gave a result, which is very close to the experimental values.

2.4 EPS Geofom

Expanded polystyrene (EPS) geofom, here after called EPS geofom, is a polymeric material, which has cellular (generally closed cell) structure. EPS geofom has a widespread use in geotechnical problems among other types of geofoms. This is because of some basic reasons according to Horvath (1994). The first one is; it is least expensive and widely available. The second one is that it is the only polymeric foam that does not use

a blowing agent (Chlorofluro carbon, Hydro Chlorofluro carbon etc.) and it does not release formaldehyde, i.e., a toxic gas produced for extended periods (years) by some polymeric foams after their production.

After EPS geofoam was first introduced and used in 1970 in Norway by the Norwegian Public Road Administration (NPRA), extensive studies have been done on the engineering properties of the material. The first engineering property of the EPS geofoam that allows it to be used in different geotechnical problems is its ultra-lightweight. It has a density of only about 1% of the density of soil (Horvath, 1994). During the application of EPS geofoam to geotechnical problems, great attention should be given to its density. According to Beju and Mandal (2017b), the water absorption, compressive strength and cohesion of the EPS geofoam blocks are directly affected by their density, especially low-density EPS geofoam blocks. Most of the time EPS blocks are produced within a range of densities between approximately 10 kg/m^3 and 40 kg/m^3 . The second property of EPS geofoam that allows it to be used widely is its thermal conductivity. Horvath (1994) showed that the thermal conductivity of the EPS geofoam is very low with a coefficient of conductivity approximately 20-40 times less than that of soil.

The mechanical behavior of EPS geofoam can be determined by using unconfined compression tests, constrained (uniaxial) tests or triaxial compression tests at least below their elastic strain limit (Atmatzidis et al., 2001). However, the mechanical behavior of the EPS geofoam could be best investigated using true triaxial test apparatus (Leo et al., 2008). Based on these tests, EPS geofoam is an elastoplastic hardening material with plastic contractive volume change under compressive loading and yielding can be represented reasonably well by a Drucker–Prager yield surface. In addition to those earlier explained type of tests, repeated load test method could be used as a method for the evaluation of the ability of EPS geofoam to obtain their elastic response (Mohamed et al., 2017). Due to these mechanical properties, EPS geofoam is the most compressible material among all geosynthetic materials (Horvath, 2005). Generally EPS geofoam is a lightweight and compressible material with very low thermal conductivity.

With the knowledge of those special engineering properties of EPS geofoam, it is not hard to select it as a protective material for different underground structures. EPS geofoam

blocks could protect soil retaining structures by reducing the heavy lateral load from the retained soil. The protection is done by using EPS geofoam as a compressible inclusion to induce or allow ‘controlled yielding’ within a normal soil (Horvath, 2005).

EPS geofoam could also be used to protect underground buried pipe lines and culvert systems. The protection can be implemented in four ways, especially under transportation systems. These are: (1) light-weight embankments, (2) imperfect trenches, (3) slot-trench cover systems and (4) post and beam cover systems (Bartlett et al., 2015). Most of the time, the first three types of installation systems that mostly focused on protecting the pipe from vertical loads have been analysed, evaluated and implemented. However, some very important and sensitive pipes could be protected by two EPS geofoam blocks, “posts” placed on each side of the structure, an EPS block capping, “beam” on the top of two posts, and soil cover on the beam (Abdollahi and Tafreshi, 2017).

The vertical contact pressure of soil on buried pipes and culverts is significantly reduced by the compressible inclusion of EPS geofoam due to the mobilization of positive soil arching depending on the stiffness of the EPS geofoam (Al-Naddaf et al., 2019). The contribution of this EPS geofoam do not only expressed by the reduction of the vertical contact pressure. The physical model tests and the finite element analysis of the models showed that EPS geofoam could also reduce the concentration of the contact pressure along the walls of buried pipes (Meguid et al., 2017). This property of EPS geofoam is very advantageous when the pipe is buried in expansive soil. (Rajeev and Kodikara, 2011). In addition to reducing and distributing the contact pressure, EPS geofoam is a good geosynthetic material in developing less uplift force to the corresponding environment. The geofoam cover system could develop about four times less uplift force than that of the corresponding soil backfill (Bartlett et al., 2014).

Besides the vertical and horizontal static load conditions, the performance of EPS geofoam has been investigated and analysed under different conditions. It is clearly shown that EPS geofoam block has a positive contribution on impact behavior of pipe systems by reducing acceleration, displacement and it increases energy absorption values significantly (Anil et al., 2015). This property of the EPS geofoam protects the buried pipes and culverts from sudden impact loads such as rock falls. Buried pipes could also be subjected to cyclic load

during their design life. EPS geofoam is the best choice to reduce the stress on the pipe due to such type of loadings. Inclusion of EPS geofoam can significantly enhance the response of buried pipes particularly for shallow-buried structures under repeatable loading especially at the crown of the pipes (Meguid and Ahmed, 2020).

So far, many researches have been conducted on the EPS geofoam and its application on the protection of buried pipes. Most of them focused on the mechanical behavior EPS geofoam and response of EPS geofoam to different type loadings depending on the type of installation. However, the response of this geosynthetic material at different backfills was not studied and compared. In fact, it was tried to analyze the response of EPS geofoam in mixed back fill (fly ash bed and quarry dust fill) in Beju and Mandal (2017a). In this paper, the numerical analysis of the EPS geofoam protected buried pipe system in different backfills was conducted and discussed.

2.5 Geotextile

Geotextile is one of the geosynthetic types, which are now becoming common in geotechnical sites. According to EN-ISO 10318-1, as cited by Shirazi et al. (2020), a geotextile is defined as: planar, permeable, polymeric (synthetic or natural) textile material, which may be nonwoven, knitted or woven, used in contact with soil and other materials in geotechnical and civil engineering applications.

Basically geotextile is a product of either natural or synthetic fiber. Most of the time, natural fiber geotextiles are used in geotechnical problems because natural fibres have light weight, cost effective and they are fully biodegradable/Non-toxic for the soil and for the people who work with it (Shirazi et al., 2020). However, fire hazard problems and durability of natural fiber geotextile should also be considered. These natural fibers are directly obtained from basic sources, such as vegetables, animals and minerals, and are converted into non-woven fabrics. Natural plant fibres can generally be classified into three types (Satyanarayana et al., 1990): (a) bast fibres, (b) leaf fibres, and (c) fruit fibres. Among these natural fiber geotextiles, jute geotextile is mostly selected and used. Because the availability of jute fiber is high in the world due to its systematic cultivation and processing in Asian countries.

In geotechnical problems, geotextiles have been used for many purposes. Depending on the type of the geotextile and type of the problem, there are different functions of geotextile, for example separation, reinforcement, filtration, drainage, containment, and combination of these (Koarner, 1993). In this paper, the reinforcement function of geotextiles was utilized. Since the main purpose of this research is to protect buried pipes by reducing the total stress, which reaches on it, the backfill soil around the pipe could be reinforced.

The general stress-strain behavior of geotextile reinforced soil has been studied using triaxial, direct shear and other test methods (Parihar et al., 2015; Athanasopoulos, 1996; Tuna and Altun, 2012; You-chang et al., 2009; Mahmood et al., 2000). These researches showed that adding geotextile reinforcement to soil improves the soil's performance by boosting the peak strength. Especially in granular soils, geotextile reinforcements reduce dilation and help the soil to stay at its peak strength. In addition, the general performance of woven geotextile reinforced soil was found to be higher than that of unwoven geotextile reinforced soils. However, the amount of the geotextile, which would be used to reinforce the soil layer, should be limited up to 10% by weight of soil (Parihar and Shukla, 2015).

Now a day, the application of geotextile reinforcement is covering different geotechnical sites. In the construction of highway, reinforcing the sub grade soil will increase the CBR value. In addition, strain relieving and reinforcing property of geotextiles allows it to be used in asphaltic concrete overlays (Negi and Singh, 2019; Lytton, 1989). Geotextiles could also be used to reinforce the backfill soil around the pipes. An experimental study on the protection of buried pipes with the reinforcement of the fill in combination with EPS geofoam showed positive result (Beju and Mandal, 2017a).

Most of researches, conducted on geotextile so far, concentrated on the general engineering property of the geotextile and the study on the application of geotextile reinforcement for buried pipe protection was limited. In this paper, the performance of woven geotextile in protecting buried pipes was studied in different fill materials. Moreover, different tensile stiffness geotextiles and different number of layers of reinforcement was analysed.

2.5.1 Reinforcement Mechanism

According to Chen (2007), geosynthetics reinforce foundations in three mechanisms. When geosynthetic materials are used in multiple layers and if the top layer spacing is

greater than a certain value, the reinforcement would act as a rigid boundary and the failure would occur above the reinforcement. This condition is called boundary effect and it has been proved by different researchers (e.g., Ghosh et al., 2005).

The second mechanism is membrane effect. It is obvious that the loading on the reinforced foundation will create a downward movement of the soil beneath the foundation. This will leave the geosynthetic reinforcement under deformation and tension. As a result the deformed and tensioned reinforcement will develop an upward force to support the applied load. To mobilize this effect, a certain amount of settlement is needed and the settlement should not be created by pull out or rupture. This effect has been investigated by different literatures (e.g., Shukla and Chandra, 1990; Bourdeau, 1989).

In addition to those two effects, a frictional force is induced at the interface as the result of relative displacement between the soil and the reinforcement. Consequently, lateral deformation or potential tensile strain of the soil is restrained and the vertical settlement of the soil will be reduced. This is called the confining effect (lateral restraint effect) and it has been studied in various literatures (e.g., Madhav and Poorooshab, 1989).

2.6 Backfill

It is known that bedding and backfill materials play a critical role in the long-term structural integrity of buried pipelines. Different older and recent studies have shown that the engineering property of backfills and the way of applying them affect the general performance of pipes (Marston and Anderson, 1913; Spangler and Handy, 1982; Handy, 2004). Therefore, attention should be given in selecting the type of backfill and bedding material around the pipes.

Common types of backfill materials range from native soils (which usually have fines, silt and clay) to imported crushed rock, to soil-cement slurry (flowable fill) (Watkins et al., 2010). In this paper the local soil, quarry dust and fly ash were studied as a bedding and back fill material in combination with some geosynthetic protection of pipes.

2.6.1 Quarry Dust

During the production of aggregate through the crushing processes of rocks in rubble crusher units, quarry dust or stone dust is obtained as a by-product. Most of the time, this

waste material is composed of fine particles less than 4.75 mm. With the increase in demand of coarse aggregate in the construction industry, the production of the by-product is also increasing. Therefore, the world is facing a problem with the way of disposing this waste material without jeopardizing environmental protection requirements.

Even though quarry dust is a waste product, it has some special properties, which makes it suitable to be used in different areas especially in the construction industry. For example, it has good shear strength (Prakash and Rao, 2017). In addition, it is available at a low cost. So far, the concrete production industry is the famous area for utilizing quarry dust. Many studies showed that quarry dust could be used as a partial replacement of fine aggregate in concrete production. Based on these studies, up to 50 % replacement of fine aggregate could increase the strength of the concrete (Sinha et al., 2017; Prakash and Rao, 2016; Agrawal et al., 2017; Subramanian and Kannan, 2013). Quarry dust can also be used as a good construction material in highway or expressway embankments (Prakash and Rao, 2017).

Studies on the utilization of quarry dust were mostly focused on concrete production and highway construction related areas. Some previously conducted studies showed that stone dust could be used as a bedding material for the pipe with some geosynthetic reinforcement and an encouraging result was found (Beju and Mandal, 2017a). A further way of utilizing quarry dust should be studied and applied. Therefore, in this research, the performance of quarry dust as a fill material around pipes was studied.

2.6.2 Fly Ash

Fly ash is a finely divided residue that results from the combustion of pulverized coal. It is mostly produced by coal-fired and steam-generating plants. In the case of Ethiopia, more than 50% of the energy consumption of cement factories is fulfilled by coal (Kifle, 2019). There are also some factories, which use the combustion of coal. According to the data presented at the Ethiopian investment forum in 2011, Ethiopia has an exploitable potential of 400 million tons of coal. Currently, there are different coal-based power plants in Ethiopia. For example, a coal-based urea fertilizer factory was integrated with the 90 MW coal-fired power plant for an electrical energy source in the Oromia regional state, the

Ilubabor Zone, Yayu Wereda. It is expected that this power plant will produce 75,000 tons of coal ash annually (Kifle, 2019).

Proper disposal of waste products of industries is one of the main concerns of the world and re-use these waste products is the best way of handling it. Different researches have been conducted on the utilization of fly ash to support the proper handling of wastes and to find good construction material. Based on this studies fly ash has low unit weight and high shear strength. (Rai et al., 2010). This makes it a very suitable material for the construction of highway embankments and it is also recommendable material in stabilizing weak soils (Karthik et al., 2014; Deb Nath et al., 2017). In addition to this, it was tried to replace cement in concrete production with fly ash and the result was very encouraging, especially in the late stages of curing of concrete (Banerjee and Chakraborty, 2016; Soni and Saini, 2014).

The study of utilization of fly ash as a backfill material around the pipe is very, especially in Ethiopia. Therefore, in this research, performance of fly ash will be studied with the intention of protecting buried pipes.

2.7 Finite Element Method (FEM)

The finite element method is one of the most powerful, versatile, and mathematically sound discretization techniques for models written in terms of partial differential equations. (Luca et al., 2002). It is a numerical method seeking an approximated solution of the distribution of field variables in the problem domain that is difficult to obtain analytically. Even though there is some debate on who could be called the "creator" of the finite element method, it still is mostly accepted that the method was originally introduced from aerospace engineering research in the 1950s. The two key initial contributors of the method are Professors Jon Turner (in the United States) and John Argyris (in Europe) (Ioannis, 2018 and Robbert, 1995).

According to Robbert (1995), FEM can be defined in sophisticated and unsophisticated ways. Unsophisticated description of FEM is that it involves cutting a structure into several elements (a piece of structure), describing the behavior of each element in a simple way, then reconnecting elements at 'nodes' as if nodes were pins or drops of glues that hold together. On the other hand, sophisticated description of FEM regards it as piecewise

polynomial interpolation. That is a field quantity at the element such as displacement is interpolated from the values of field quantity at the nodes. By connecting elements, the field quantity becomes interpolated over the entire structure in a piecewise fashion, by as many polynomial expressions as there are elements.

The theory of FE includes matrix manipulations, numerical integration, equation solving, and other procedures carried out automatically by commercial software. The user may see only hits of these procedures as the software process data. The user deals mainly with preprocessing (describing loads, supports, materials and generating the FE mesh) and post-processing (sorting outputs, listing, and plotting of results).

FEM has been applied in many fields of engineering. However, it was very late (over thirty years from the creation) to be widely used for analyzing geotechnical problems. (David and Lidija, 1999). This is because there are many complex issues that are specific to geotechnical engineering and have only been resolved relatively in recent years.

Generally, the summary of all works of literature is summarized in tables as shown in Table 2.1. However, this summary does not include books and standards.

Table 2.1 Summary of literature reviews

Researcher	Materials used	Test/analysis used	Findings
Abdollahi et al., 2017	<ul style="list-style-type: none"> • EPS geofoam 	<ul style="list-style-type: none"> • 3D numerical analysis using ABAQUS (6.14.1) 	<ul style="list-style-type: none"> • EPS show favorable performance for protecting sensitive infrastructures.
Agrawal et al., 2017	<ul style="list-style-type: none"> • Quarry dust • Cement • Sand • Aggregate 	<ul style="list-style-type: none"> • Compressive strength test 	<ul style="list-style-type: none"> • The maximum compressive strength of concrete was obtained by replacing 50 % (Mix 3) of sand with quarry dust.
Al-Nadda et al., 2019	<ul style="list-style-type: none"> • Concrete culvert • EPS geofoam 	<ul style="list-style-type: none"> • Three reduced-scale model tests of induced trench installation system in a test box 	<ul style="list-style-type: none"> • The EPS geofoam reduced the vertical stresses on the buried structure. • The lower stiffness geofoam had more effect on the vertical stress reduction.
Anil et al., 2015	<ul style="list-style-type: none"> • Steel and composite pipe • EPS Geofoam • Sand 	<ul style="list-style-type: none"> • Physical model test which simulates the falling rocks on buried pipes • Finite element analysis of the physical model using ABAQUS 6.13 	<ul style="list-style-type: none"> • Protective layers have a positive contribution on impact behavior of pipe systems by reducing acceleration, displacement and increase energy absorption values significantly.
Athanasopoulos, 1996	<ul style="list-style-type: none"> • near-saturated silty clay soil • Woven and non-woven geotextile 	<ul style="list-style-type: none"> • Direct shear test 	<ul style="list-style-type: none"> • Based on total stress analysis, the strength of non-woven geotextile reinforced wet soil was increased. • The inclusion of woven geotextiles did not offer any strength increase.
Atmatzidis et al., 2001	<ul style="list-style-type: none"> • EPS geofoam(density of 10 kg/m³-35kg/m³) 	<ul style="list-style-type: none"> • Unconfined compression test • Constrained (uniaxial) test • Triaxial compression test 	<ul style="list-style-type: none"> • Unconfined compression test could represent the mechanical behavior of EPS geofoams with normal stress below their elastic strain limit. • Size and aspect ratio have a significant effect on the initial modulus of elasticity • EPS geofoams do not exhibit lateral expansion during compression.

Banerjee and Chakraborty, 2016	<ul style="list-style-type: none"> • Fly ash • Cement • Aggregate 	<ul style="list-style-type: none"> • Compressive strength test 	<ul style="list-style-type: none"> • Compressive strength of concrete mixes decrease with increased presence of Fly Ash. • Fly Ash has an adverse effect on early strength of concrete. • The optimum limit of mixing of Fly Ash is 45 %
Bartlett et al., 2014	<ul style="list-style-type: none"> • Light weight EPS geofom cover/backfill system and • Conventionally constructed backfill/cover with soil 	<ul style="list-style-type: none"> • Two full-scale uplift tests using <ol style="list-style-type: none"> 1 EPS geofom 2 Conventional backfill soil 	<ul style="list-style-type: none"> • The geofom cover system developed about four times less uplift force than that of the corresponding soil backfill. • The force displacement behavior of the geofom system was more desirable than the conventional backfill system
Bartlett et al., 2015	<ul style="list-style-type: none"> • No test or model 	<ul style="list-style-type: none"> • Discussion of the previous papers regarding the topic 	<ul style="list-style-type: none"> • EPS geofom could be used for the protection of underground pipes and culverts in four ways.
Beju and Mandal, 2017a	<ul style="list-style-type: none"> • polyethylene(HDPE) pipes • fly ash as a fill material • stone dust(quarry dust) as a bedding material • EPS geofom as a compressible inclusion • Jute geotextile as reinforcement 	<ul style="list-style-type: none"> • Experimental model test • Numerical model of the experiment using PLAXIS 3D 	<ul style="list-style-type: none"> • The performance of the pipes was affected by number of layer, width, density, shape, thickness, location of EPS. And reinforcement of the fill with Jute geotextile. • Using fly ash and quarry dust could solve the pollution of the environment and disposal problem
Beju and Mandal, 2017b	<ul style="list-style-type: none"> • Low density expanded polystyrene (EPS) geofom 	<ul style="list-style-type: none"> • water absorption test • compressive strength test • flexural strength test • Triaxial test(UU) 	<ul style="list-style-type: none"> • water absorption property of EPS geofom is very less and decrease as its density increase • The quality, the compressive strength and the modulus values of the EPS geofom are affected by the density and specimen size of the material. • cohesion is a major parameter which contributes the shear strength of EPS geofom and it is a function of density
Horvath, 1994	<ul style="list-style-type: none"> • Previously Published papers about EPS geofom 	<ul style="list-style-type: none"> • Discussion 	<ul style="list-style-type: none"> • The density, the load deformation and the thermal conductivity of the EPS geofom should be determined before it is applied for geotechnical problems.

Karthik et al., 2014	<ul style="list-style-type: none"> • Soil • Fly ash 	<ul style="list-style-type: none"> • Proctor compaction test • California Bearing Ratio value (CBR) test • Un Confined Compressive strength • Direct shear test... 	<ul style="list-style-type: none"> • The bearing capacity and CBR value of stabilized soil were increase up to 350% and 150% respectively of the original soil.
Leo et al., 2008	<ul style="list-style-type: none"> • EPS geofoam 	<ul style="list-style-type: none"> • Triaxial compression test in true triaxial apparatus 	<ul style="list-style-type: none"> • EPS geofoam is an elastoplastic hardening material, which also softens stiffness-wise under increasing confining pressure. • The EPS geofoam can be modeled as a Drucker–Prager material.
Lytton, 1989	<ul style="list-style-type: none"> • Geotextile and asphalt concrete 	<ul style="list-style-type: none"> • Discussion 	<ul style="list-style-type: none"> • Equations, which lead to the selection of the overlay thickness in conjunction with the properties of the geotextiles both in the strain-relieving and reinforcing modes, are presented.
Mahmood et al., 2000	<ul style="list-style-type: none"> • organic silty clay • Sandy soil as a fill material • Geotextile 	<ul style="list-style-type: none"> • Shear box test 	<ul style="list-style-type: none"> • The shear strength of the interface (geotextile/ organic clay) increasing with the increases tensile strength of the geotextile. • The shear strength of geotextile/fill interfaces did not show a consistent relationship with the geotextile tensile strength.
Meguid and Ahmed, 2020	<ul style="list-style-type: none"> • EPS geofoam block • Granular back fill 	<ul style="list-style-type: none"> • Physical model test which simulates the buried pipe system in granular back fill under cyclic load 	<ul style="list-style-type: none"> • EPS geofoam inclusion can significantly enhance the response of buried pipes particularly for shallow buried structures under repeatable loading especially at the crown section of the pipe.
Meguid et al., 2017	<ul style="list-style-type: none"> • Hollow structural steel section (HSS) • EPS geofoam bolck 	<ul style="list-style-type: none"> • Physical modeling to investigate the earth pressure distribution on a rigid box-shaped structure buried in granular material and overlain by EPS. • A finite element analysis using ABAQUS 6.13 	<ul style="list-style-type: none"> • Contact pressure distribution on the walls of the buried box was found to be non-uniform with significant increase at the corners for positive projecting installation. • Addition of the EPS block above the structure significantly decreases the stress concentrations. • EPS density contributed significantly to the positive arching developed above the structure.
Mohamed et al., 2017	<ul style="list-style-type: none"> • EPS geofoam 	<ul style="list-style-type: none"> • Compression test using compression test apparatus 	<ul style="list-style-type: none"> • EPS material is loading rate dependent. • The repeated load test method could be used as method for the evaluation of the ability of expanded polystyrene foam to maintain their elastic response.

Nath, et al., 2017	<ul style="list-style-type: none"> • Organic soil • Types of fly ashes 	<ul style="list-style-type: none"> • Standard Proctor compaction • Unconfined compressive strength test 	<ul style="list-style-type: none"> • Properties of organic soil can be improved by using fly ash but the amount of this improvement depends on the characteristics of organic soil
Negi and Singh, 2019	<ul style="list-style-type: none"> • Woven an unwoven geotextile • Sand • Clay 	<ul style="list-style-type: none"> • CBR test • Finite element analysis of the test using ABAQUS 	<ul style="list-style-type: none"> • Inclusion of woven geotextile reinforcement in the subgrade increases the CBR value. • woven geotextile performs better than non-woven geotextile
Parihar et al., 2015	<ul style="list-style-type: none"> • Woven and non-woven geotextile • c-φ soil 	<ul style="list-style-type: none"> • Triaxial test 	<ul style="list-style-type: none"> • The stress-strain behavior of soil has improved with the addition of geotextiles • Optimum amount of geotextiles threads are found to be varying from 5% to 10% by weight of soil. • woven geotextile performs better than non-woven geotextile
Prakash and Rao, 2017	<ul style="list-style-type: none"> • Quarry dust from 40 different sites 	<ul style="list-style-type: none"> • Specific gravity • Particle size distribution • direct shear tests • compaction test 	<ul style="list-style-type: none"> • Quarry dust can be used as a good construction material in the highway or expressway embankments. • Quarry dust is easily exposed to wind and water;
Prakash and Rao, 2016	<ul style="list-style-type: none"> • Quarry dust • Cement • Sand • Aggregate 	<ul style="list-style-type: none"> • Compressive strength test 	<ul style="list-style-type: none"> • 40% replacement of fine aggregate by quarry dust gives maximum result in strength than normal concrete and then decreases from 50%.
Rai et al., 2010	<ul style="list-style-type: none"> • fly ash 	<ul style="list-style-type: none"> • sieve analysis • specific gravity test • compaction test • direct shear test • permeability test 	<ul style="list-style-type: none"> • Fly ash has low unit weight and high shear strength. • Fly ash could be subject to erosion by wind or water • Fly ash can be a good construction material for highway or expressway embankments.
Rajeev et al., 2011	<ul style="list-style-type: none"> • Expansive soil (Merri Creek clay) • A polyethylene pipe 	<ul style="list-style-type: none"> • Large scale physical model test • Three dimensional finite deference continuum model analysis of the laboratory experiment using FLAC^{3D} 	<ul style="list-style-type: none"> • The pipe- soil interaction in expansive soil could be modeled with pipe as linear elastic, soil as nonlinear elastic and Swelling induced stresses are computed in terms of the change in the soil moisture content.

			<ul style="list-style-type: none"> • Along the pipe, the higher stresses are occurred at the ends of the pipe and lower stress is at the middle of the pipe.
Satyanarayan et al., 1990	<ul style="list-style-type: none"> • Natural fibers-polymer composite 	<ul style="list-style-type: none"> • Describes systematic work carried out until then on the structure property relationship of fibers including fracture modes. 	<ul style="list-style-type: none"> • Durability of the natural fibers is lowered by their degradable property. • Fire hazard is another problem. Processes should be developed to minimize these limitations.
Singh et al., 2015	<ul style="list-style-type: none"> • sandy clay • Woven and non-woven geotextile 	<ul style="list-style-type: none"> • Unconfined compressive strength test 	<ul style="list-style-type: none"> • The failure plane of reinforced soil was observed above the level of geotextile. • Peak strength of reinforced soil with woven geotextile is increased compared with unwoven geotextile reinforced soil
Sinha et al., 2017	<ul style="list-style-type: none"> • Quarry dust • Cement • Sand • Aggregate 	<ul style="list-style-type: none"> • compressive strength test • workability test (compaction factor) 	<ul style="list-style-type: none"> • 50% replacement of sand by quarry dust gives higher compressive strength than natural sand concrete
Soni and Saini, 2014	<ul style="list-style-type: none"> • Fly ash • Cement • Aggregate 	<ul style="list-style-type: none"> • Compressive strength test 	<ul style="list-style-type: none"> • Compressive strength of concrete decreased with the increase in cement replacement with Class-F fly ash. However, at each replacement level of cement with fly ash, an increase in strength was observed with the increase in age.
Subramanian and Kannan, 2013	<ul style="list-style-type: none"> • Quarry dust • Cement • Sand • Aggregate 	<ul style="list-style-type: none"> • Compressive strength test 	<ul style="list-style-type: none"> • Concrete made of 20% replacement of fine aggregates with quarry dust equals the compressive strength of concrete made of pure sand. • it is advisable to carry out trial casting with quarry sand proposed to be used, in order to arrive at the water content and mix proportion to suit the required workability levels and strength requirement
Tuna and Altun, 2012	<ul style="list-style-type: none"> • Granular soil (sand) • Geotextile 	<ul style="list-style-type: none"> • direct shear tests 	<ul style="list-style-type: none"> • In reinforced soils, the loss of shear strength seen after peak strength was considerably reduced. This effect was further modified by increasing the layer of reinforcement.
Watkins et al., 2010	-----	<ul style="list-style-type: none"> • Qualitative and analytical discussions on back fill materials regarding flexible pipes. 	<ul style="list-style-type: none"> • Common types of backfill material can range from native soils (which usually have fines, silt and clay) to imported crushed rock, to soil-cement slurry (or flowable fill/CLSM).

You-chang et al., 2009	<ul style="list-style-type: none">• Mixture of crushed stone and clay• Non-woven geotextile	<ul style="list-style-type: none">• Resilient Modulus Test• CBR test• Unconfined Compression Test	<ul style="list-style-type: none">• Compressive strength of geotextile-reinforced soil increases significantly with the decrease in reinforcement spacing or with the increase in the degree of the relative compaction of fill.• Standard laboratory soil resilient modulus and CBR test methods are unsuitable for geotextile-reinforced soil.
------------------------	--	---	---

Chapter 3

Research Methodology

3.1 Introduction

This section of the research presents three-dimensional numerical modeling of buried pipes using finite element analysis software (Abaqus 6.0). Each model was constructed in such a way that it can achieve the objective of the research. Following the general procedures of modeling and analysis in Abaqus, each step was conducted carefully. These general steps are:

1. Geometrical modeling: The first task in FEA is developing a geometrical model of the problem. This task is conducted by considering the boundary effects. Different parts of the model were prepared independently which are called instances/parts in Abaqus.
2. Material definition and assignment: In this step, the material properties are defined based on the appropriate constitutive model and it was assigned for the corresponding instances.
3. Assembling the independent instances: The instances, which were developed independently, were assembled in this step to make the problem complete.
4. Discretize the domain: After the assembly, the whole domain of the problem was discretized into smaller parts called elements. This process is called meshing.
5. Apply loading and boundary conditions,
6. Run the analysis,
7. Post-processing: After the analysis was finished, the output was collected in such a way that it can fulfill the objective of the research.

To achieve the specific objectives of this research, the whole ‘pipe- protective material-backfill’ system with the surrounding native soil was generally configured carefully. Three types of materials, i.e., quarry dust, fly ash and conventional soil was used as backfill. Moreover, EPS geofoam and geotextile materials were used as compressible inclusion and reinforcement materials respectively.

All the models simulate two types of pipe installation techniques depending on the method of protection. If the installation system is assumed to include EPS geofoam, the whole

system was modeled to simulate the imperfect trench installation (ITI). Otherwise, it was modeled, as it is trench/ditch installation. Before all the parametric studies were conducted, nine base models were simulated and comparisons were made. These models were simulated for the three types of fill materials with the same geometry, pipe dimension and protecting materials.

In this section of the research, all the methodologies, which were used to model the whole research problem, are described in detail. This includes the geometry of the model, the material properties, the meshing, the loading and boundary condition and finally the validation for the methodology.

3.2 Geometry of the Model

As it was explained earlier, the model in this research represents a trench and its surrounding soil. The trench part involves the bedding, the pipe and the fill materials. Basically, all the developed models could be divided into three categories. The first one is a trench model without any additional pipe protective material. The second one is a trench with EPS geof foam included in it and finally a trench with geotextile reinforcement.

3.2.1 Geometry of Trench Models without any Additional Protecting Material

According to ASTM D2321, the minimum width of a trench is provided to give a sufficient space to insure working room for proper and safe placement and compacting the hunching and other embedment materials. In addition to this, if the trench is constructed in unstable soil, the minimum width of the trench depends on the size and stiffness of the pipe, stiffness of the embedment and in-situ soil, and depth of cover. With these considerations ASTM D2321 suggests a minimum width to be the greater of the pipe outside diameter plus 400 mm or the pipe outside diameter times 1.25 plus 300 mm. Therefore in this research a 680 mm width of the trench was used by considering the highest diameter pipe i.e. 273 mm. ASTM D2321 also suggests that a minimum of bedding between 100 and 150 mm should be provided before the installation of the pipe. So 110 mm depth bedding was used for the current research.

The location of the pipe affects the contact pressure, which will be created around the pipe and the settlement of the top surface during loading. Different literatures showed that as the pipe is embedded close to the surface, the settlement of the loading plate will decrease.

However, the stress on the crown of the pipe will increase. So for this study, all the analyses were made by putting the pipe 3D from the top surface of the trench, Where D is the diameter of the pipe. This depth is higher than 1.5B, which is the depth; most of the load from the isolated footing spreads out. The whole geometry of the unreinforced model is shown in Figure 3.1 (a), (b) and (c).

3.2.2 Geometry of EPS Included Trench Models

Researches showed that under constant density and thickness of EPS geofoam and under the same embedment depth of the pipe, the vertical stress on the pipe will decrease as EPS geofoam block is installed near to the top of the pipe (e.g. Beju and Mandal, 2017a; Kang et al., 2008; Soylemez and Huvaj, 2018). In this research, all base models were created by putting a single layer of EPS geofoam at 0.25D above the top of the pipe as shown in Figure 3.2.

EPS geofoam is fabricated in different shapes and sizes. In this research, 40 mm thick rectangular shape of EPS geofoam was used because the rectangular section EPS geofoam allows more amount of deformation than the circular section EPS geofoam (Beju and Mandal, 2017a). The width of the EPS geofoam was modeled as 1.5D. As Kim et al., 2010 showed, with 1.5D width of geofoam, up to 73% of vertical stress at the top of the pipe could be reduced. Moreover, during the installation, it was assumed to be installed at the center of the trench following the length of the pipe.

3.2.3 Geometry of Geotextile Reinforced Trench Models

The location of the reinforcement material greatly affects the performance of the reinforcement material. According to Shukla (2016), the reinforcement material should be located within the depth of influence of the foundation and the optimum embedment depth of single reinforcement is 0.3B from the top surface, where B is the width of the foundation. Therefore in the current research, the geotextile reinforcements in the base models were located 0.3B from the surface of the trench, where B is the width of the longer side of the loading area, i.e., 0.508 m. The whole configuration of the trench with geotextile reinforcement is shown in Figure 3.3.

3.2.4 Boundary of the Model

In finite element analysis of geotechnical problems, the boundary of the model affects the final output. When it said boundary, it is to refer the extent or the size of the model. In the current research, the size of the trench was decided based on international standards as it was explained earlier. However, the part of the model beyond the trench was decided in different ways.

One of the boundaries of the model is the depth below the bedding of the trench. The location of the research problem was assumed to be in Gondar town. According to the ongoing geotechnical investigation by the University of Gondar technical groups, in most of the areas, the depth below 3 m is dominated by hard rock (mostly igneous rock). So in this research, the depth of the model was assumed to be 3 m.

The horizontal extent of the model was decided by using the preliminary sensitivity analysis. This analysis was conducted on one of the base models in fly ash fills with the same loading and boundary condition of the main analysis. The final size of the model was determined based on the vertical pressure on the crown of the pipe. The result of the sensitivity analysis was summarized in Table 3.1. Based on this sensitivity analysis, a 10 m width and length was selected for the model. Generally, the size of the model was 10 by 10 by 3 meters as shown in Figure 3.1 (a). At this point, it should be noted that the limit of the boundary and the size (the width and depth) of the trench for all types of models is similar and the part of the model beyond the trench was assumed to be filled with the insitu soil.

Table 3.1 Summary of the result of sensitivity analysis for deciding the side boundaries of the model

Size of the model (m)	Vertical stress on the crown (kPa)	Remark
3 x 3 x 3	13.975	
3 x 5 x 5	14.671	
3 x 8 x 8	15.912	
3 x 10 x 10	16.669	selected
3 x 15 x 15	16.691	

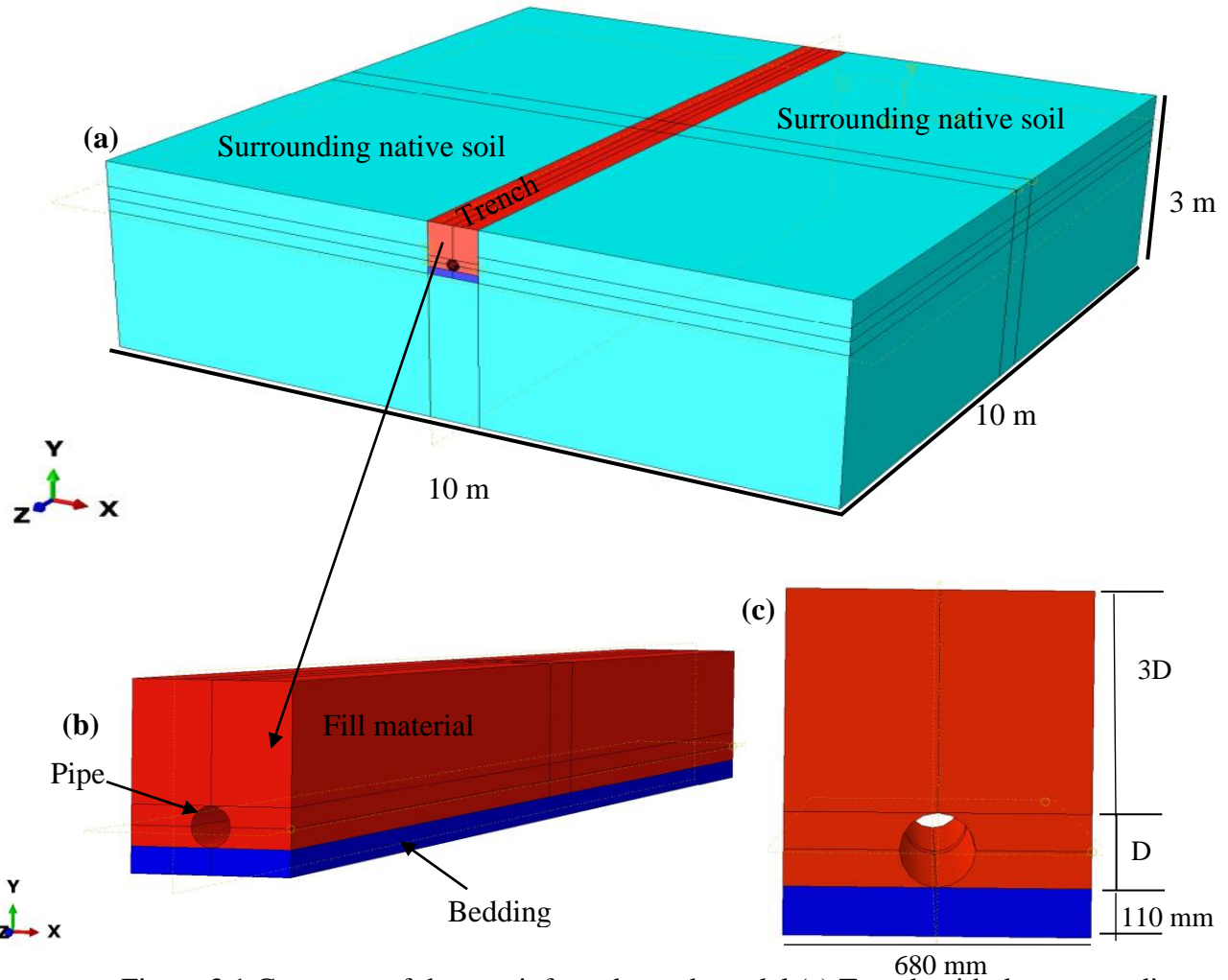


Figure 3.1 Geometry of the unreinforced trench model (a) Trench with the surrounding soil, (b) Magnified unreinforced trench model, (c) sectional view of unreinforced trench model (without the surrounding soil)

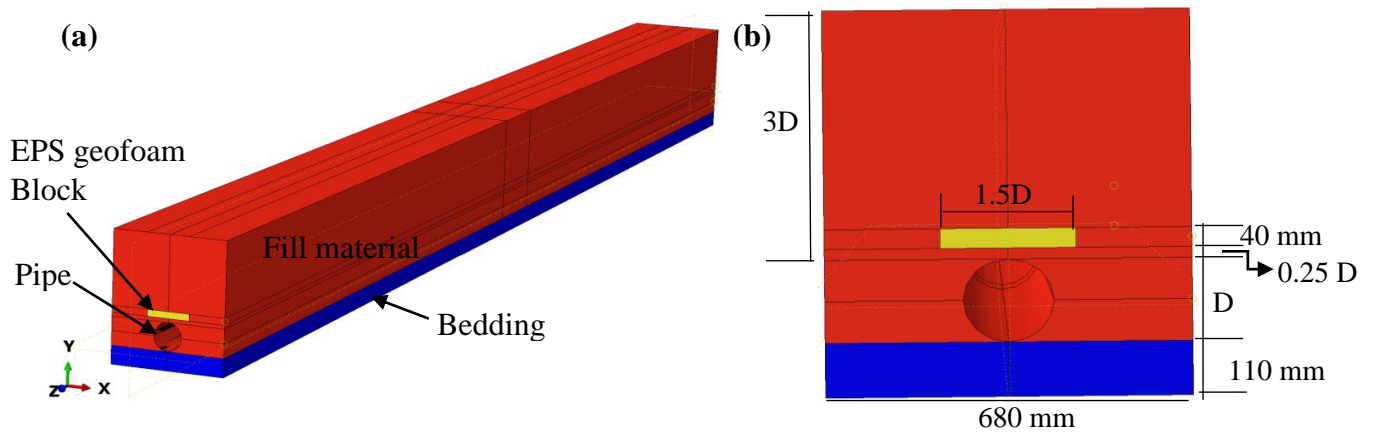


Figure 3.2 Geometry of EPS geofoam included trench model (a) 3D view of EPS geofoam included trench model, (b) sectional view of EPS geofoam included trench model

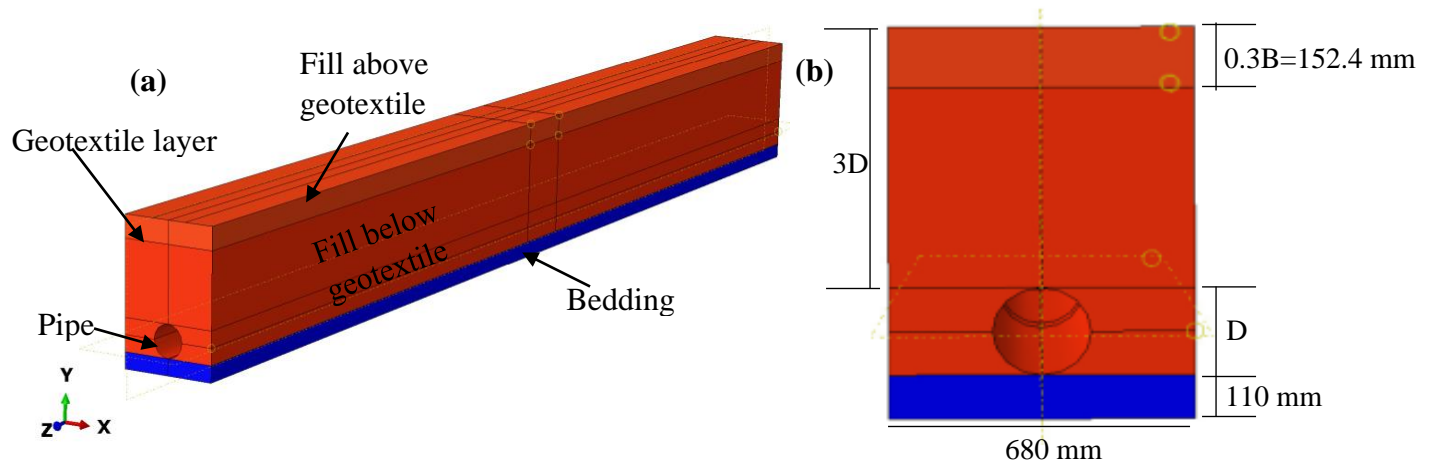


Figure 3.3 Geometry of Geotextile reinforced trench model (a) 3D view of geotextile reinforced trench model, (b) sectional view of geotextile reinforced trench model

3.3 Material Modeling

After the geometry of the model was finished, the next task was to model the materials' behavior. This includes selecting an appropriate constitutive model for each type of materials. Constitutive models are mathematical expression of the materials' behavior and response to loads. These models are not the exact representation of the materials' behavior but it gives an approximate resemblance by taking different reasonable assumptions on complicated real situations. The models in this research include four types of fill materials (fly ash, stone dust, and two types of soils, i.e., the selected fill soil and the surrounding soil), EPS geof foam and geotextile. Based on the behavior of these materials from literatures, two type of constitutive models were used, i.e., linear elastic and Mohr-Coulomb elasto-plastic constitutive models.

3.3.1 Constitutive Models

a. Linear Elastic Material Model

Many materials exhibit an initial region of a stress strain diagram in which the material behaves both elastically and linearly. For that straight-line portion of the diagram stress is directly proportional to strain. This property is expressed mathematically by Hooke's law. Based on this law, stress (σ) in a particular direction is the vector product of strain (ϵ) in that direction and the modulus of elasticity (E).

Starting from the basic theories and assumptions of Hooke's law, a generalized three dimensional constitutive law for linear elastic material was developed mathematically as shown in Equation 3.1 and 3.2. In these expressions, for a three-dimensional state of stress, each of the six stress (three normal and three shear stresses) components are expressed as a linear function of six components (three normal and three shear strains) of strain within the linear elastic range, and vice versa.

$$\begin{aligned}
 \sigma_x &= C_{11}\varepsilon_x + C_{12}\varepsilon_y + C_{13}\varepsilon_z + C_{14}\gamma_{xy} + C_{15}\gamma_{yz} + C_{16}\gamma_{xz} \\
 \sigma_y &= C_{21}\varepsilon_x + C_{22}\varepsilon_y + C_{23}\varepsilon_z + C_{24}\gamma_{xy} + C_{25}\gamma_{yz} + C_{26}\gamma_{xz} \\
 \sigma_z &= C_{31}\varepsilon_x + C_{32}\varepsilon_y + C_{33}\varepsilon_z + C_{34}\gamma_{xy} + C_{35}\gamma_{yz} + C_{36}\gamma_{xz} \\
 \tau_{xy} &= C_{41}\varepsilon_x + C_{42}\varepsilon_y + C_{43}\varepsilon_z + C_{44}\gamma_{xy} + C_{45}\gamma_{yz} + C_{46}\gamma_{xz} \\
 \tau_{yz} &= C_{51}\varepsilon_x + C_{52}\varepsilon_y + C_{53}\varepsilon_z + C_{54}\gamma_{xy} + C_{55}\gamma_{yz} + C_{56}\gamma_{xz} \\
 \tau_{xz} &= C_{61}\varepsilon_x + C_{62}\varepsilon_y + C_{63}\varepsilon_z + C_{64}\gamma_{xy} + C_{65}\gamma_{yz} + C_{66}\gamma_{xz}
 \end{aligned}
 \tag{Equation 3.1}$$

In matrix form

$$\begin{bmatrix} \sigma_x \\ \sigma_y \\ \sigma_z \\ \tau_{xy} \\ \tau_{yz} \\ \tau_{xz} \end{bmatrix} = \begin{bmatrix} C_{11} & C_{12} & C_{13} & C_{14} & C_{15} & C_{16} \\ C_{21} & C_{22} & C_{23} & C_{24} & C_{25} & C_{26} \\ C_{31} & C_{32} & C_{33} & C_{34} & C_{35} & C_{36} \\ C_{41} & C_{42} & C_{43} & C_{44} & C_{45} & C_{46} \\ C_{51} & C_{52} & C_{53} & C_{54} & C_{55} & C_{56} \\ C_{61} & C_{62} & C_{63} & C_{64} & C_{65} & C_{66} \end{bmatrix} \begin{bmatrix} \varepsilon_x \\ \varepsilon_y \\ \varepsilon_z \\ \gamma_{xy} \\ \gamma_{yz} \\ \gamma_{xz} \end{bmatrix}
 \tag{Equation 3.2}$$

Where: the 36 coefficients, C_{11}, \dots, C_{66} , are called elastic coefficients (stiffnesses) and they are material dependent constants.

There are different types of linear elastic models. Among these, isotropic linear elastic model is the simplest one. Abaqus presents an option with name 'elastic' to represent this model. In the current research, all the materials are considered as isotropic materials. In this type of constitutive model, the elastic properties (coefficients) from Equation 3.2 are completely defined by giving young's modulus (E) and Poisson's ratio (ν) as shown in Equation 3.3.

So linear isotropic elastic constitutive model was considered for elastic materials (Pipe, geotextile) and for an elastic portion of other materials (soil, stone dust, fly ash, EPS geof foam).

$$\begin{bmatrix} \sigma_x \\ \sigma_y \\ \sigma_z \\ \tau_{xy} \\ \tau_{yz} \\ \tau_{xz} \end{bmatrix} = \begin{bmatrix} \frac{1}{E} & \frac{-\nu}{E} & \frac{-\nu}{E} & 0 & 0 & 0 \\ \frac{-\nu}{E} & \frac{1}{E} & \frac{-\nu}{E} & 0 & 0 & 0 \\ \frac{-\nu}{E} & \frac{-\nu}{E} & \frac{1}{E} & 0 & 0 & 0 \\ 0 & 0 & 0 & \frac{1}{G} & 0 & 0 \\ 0 & 0 & 0 & 0 & \frac{1}{G} & 0 \\ 0 & 0 & 0 & 0 & 0 & \frac{1}{G} \end{bmatrix} \begin{bmatrix} \varepsilon_x \\ \varepsilon_y \\ \varepsilon_z \\ \gamma_{xy} \\ \gamma_{yz} \\ \gamma_{xz} \end{bmatrix} \quad \text{Equation 3.3}$$

Where G is shear modulus of the material and can be expressed in terms of E and ν as $G=E/2(1+\nu)$.

As it was explained earlier, in this research, elastic constitutive model was applied for the pipe and the geotextile material. In addition, it was used to cover the elastic sections of the rest of the elasto-plastic materials (all fill materials and the EPS geof foam). Therefore, the parameters which are necessary to apply the liner elastic constitutive model (elastic parameters, i.e. modulus of elasticity and Poisson's ratio) for each type materials are explained in section 3.3.2 of this paper.

b. Mohor-Coulomb Material Model

Mohor-Coulomb model is one of the elasto-plastic constitutive models provided by Abaqus. It is used in combination with the linear elastic models. This model is developed from the combination of both Mohr and Coulomb theories of material response for loading. In this model, there are two parameters which defines the failure criteria (the friction angle, ϕ and cohesion, c) and also a parameter to describe the flow rule (dilatancy angle, which comes from the use of non-associated flow rule which is used to model a realistic irreversible change in volume due to shearing). This model has been used in many geotechnical problems, like stability of dams, slopes, embankments and shallow

foundations. Recently, this model has also been applied in pipe line analysis in shallow and deep trenches.

The formulation of Mohr-Coulomb model is started with a coulomb failure line equation (Equation 3.4) based on Figure 3.4.

$$\tau_f = c' + \sigma'_{nf} \tan \phi' \quad \text{Equation 3.4}$$

Where τ_f and σ'_{nf} are the shear and normal effective stresses on the failure plane, and the cohesion c' , and angle of shearing resistance, ϕ' , are material parameters.

Using the Mohr's circle of stress, shown in Figure 3.4, and by considering that $\sigma_1' = \sigma_v'$ and $\sigma_3' = \sigma_h'$, Equation 3.4 can be rewritten as:

$$\sigma_1' - \sigma_3' = 2c' \cos \phi' + (\sigma_1' - \sigma_3') \sin \phi' \quad \text{Equation 3.5}$$

Equation 3.5 is often called Mohr-Coulomb failure criterion and it is adopted as the yield function:

$$F(\{\sigma'\}, \{k\}) = \sigma_1' - \sigma_3' - 2c' \cos \phi' - (\sigma_1' - \sigma_3') \sin \phi' \quad \text{Equation 3.6}$$

In principal effective stress space, the yield function is an irregular hexagonal cone as shown in Figure 3.5.

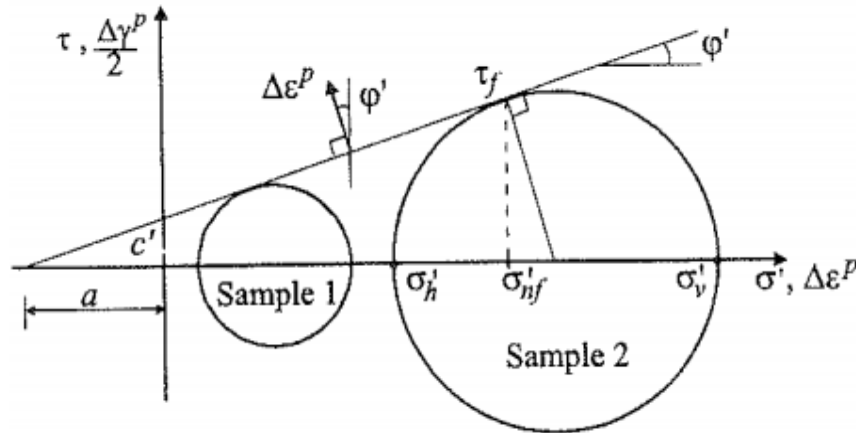


Figure 3.4 Mohr's circle of effective stress (Potts and Zdravkovic, 1999)

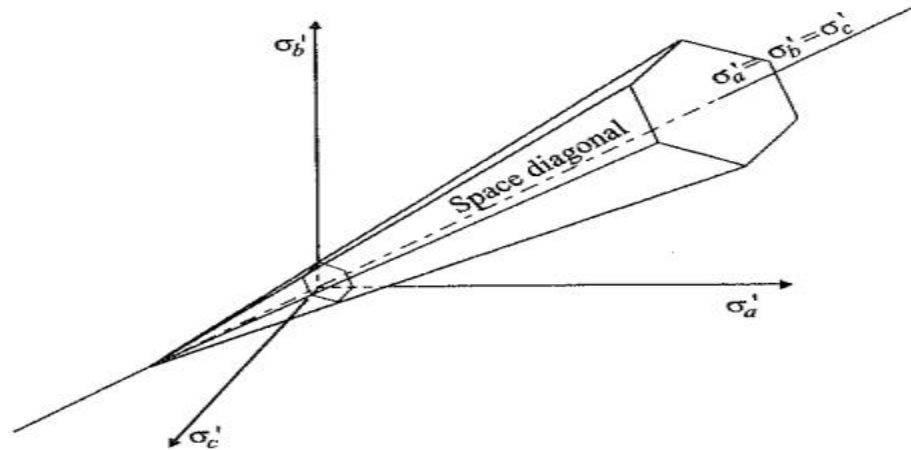


Figure 3.5 Mohr-coulomb yield surface in principal stress space

The main disadvantage in Mohr-coulomb model is that the material is assumed to be perfectly plastic. Therefore, no hardening and softening law is required. This idea is adopted by setting the space parameter, $\{k\}$ constant independent of plastic strain or plastic work, where $\{k\} = \{c', \phi'\}^T$. To complete the plastic part of the model a plastic potential function, $P(\{\sigma'\}, \{m\})$ is required. For this purpose an associated flow rule could be adopted, i.e., $P(\{\sigma'\}, \{m\}) = F(\{\sigma'\}, \{k\})$. Using this, a dilatant plastic volume strain resulted. But here the dilation angle is almost equal to angle of internal friction, ϕ' . This will over estimate the plastic strain compared with real material behavior. This problem is partly solved by adopting a non associated flow rule, i.e., the ϕ' in associated flow rule is replaced by dilation angle, ψ .

In this research, the plastic section of the elasto-plastic materials (all the fill materials and the EPS geofoam) was modeled using the the Mohr-Coulomb constitutive model. Abaqus gives an option to use this model in combination with the elastic models independently. Therefore both the elastic and plastic parameters are necessary at this point. These parameters for each type of material is explained in the next section of the paper.

3.3.2 Materials

a. Quarry Dust

One of the backfill materials, which are the concern of this study, is quarry dust or stone dust. The property of the quarry dust that was used in the finite element analysis was

brought from a large stone crushing site. This site is located in a small town called 'Meshenti' around Bahir Dar city.

All the index tests were conducted on quarry dust based on ASTM standards and all the characteristics of quarry dust are shown in Table 3.3. However, all the necessary calculations and graphs are incorporated in the appendix section of this document. During sieve analysis, more than 50% of the sample was retained on no 200 sieve. For the sample that passed sieve no 200, a hydrometer analysis was conducted; and the particle size distribution curve was constructed as shown in Figure 3.6. Generally, according to ASTM D2487-98 (unified soil classification system), the sample stone dust could be taken as an equivalent silty sand (SM).

In finite element analysis, the commonly used elastoplastic model with Mohr-Coulomb failure criteria was selected to represent the plastic section and linear elastic model for elastic section of the stone dust. This type of material behavior representation for backfill materials has been seen in many literatures. (Madhu and Singh, 2019; Beju and Mandal, 2017a; Abdollahi and Tafreshi, 2017). The model parameters are Young's modulus (E), Poisson's ratio (ν) (this behavior is valid until the stress-path reaches the stress yield envelope at which point plastic deformation begins to develop), friction angle of the soil (ϕ) and cohesion (c). The Mohr-Coulomb criterion assumes that failure is controlled by the maximum shear stress and this failure shear stress depends on the normal stress. For this purpose, the shear strength input parameters were obtained from CU triaxial compressive tests according to ASTM D4767-02. Two CU tests were conducted at confining pressures of 40 kPa and 50 kPa on compacted and prepared samples at stone dust's OMC. In normal soil triaxial tests, the first two tests are conducted at confining pressures, which represent the past effect vertical pressure at the site and future expected effective pressure. However, finding past effective stress for stone dust is not feasible whereas the future expected confining pressure for buried pipes is the sum two types of loads. The first one is the weight of the fill material. This can be calculated easily using the unit weight and the height of the fill. The second one is the confining load form nearby surcharge loads, which is hard to estimate unless the specific area of the site is known. Therefore, the above two medium confining pressures were selected to represent the stone dust in a trench. Then, the friction

angle (ϕ') and the cohesion (c') of the quarry dust sample were obtained from the mohr-Columb failure envelop as shown in Figure 3.7 (a). In a dry state, quarry dust is a cohesionless material. However, with the addition of moisture, the cohesion property could be mobilized. This has been proven in Kandolkar and Mandal (2015), Beju and Mandal (2017a), and other literatures.

To find the modulus of elasticity (E), the deviatoric stress against strain curve, which is given in Figure 3.7 (b), was used. This method of determining E was described in Yang et al., (2011). The axial strain at 50% of the deviatoric stress was found and this point is highlighted on the curve. A line was drawn through the origin and the highlighted point. The slope of this line is found by regression and was used to determine E . The Poisson's ratio of stone dust was taken as 0.35, which is similar to the values taken in Beju and Mandal (2017). The dilation angle for all fill materials could be calculated from the internal friction angel, i.e. below 6° . However, the effect of these values on the required result for this research is in significant. Generally, the input parameters of stone dust, which was used in the finite element analysis, are summarized in Table 3.2.

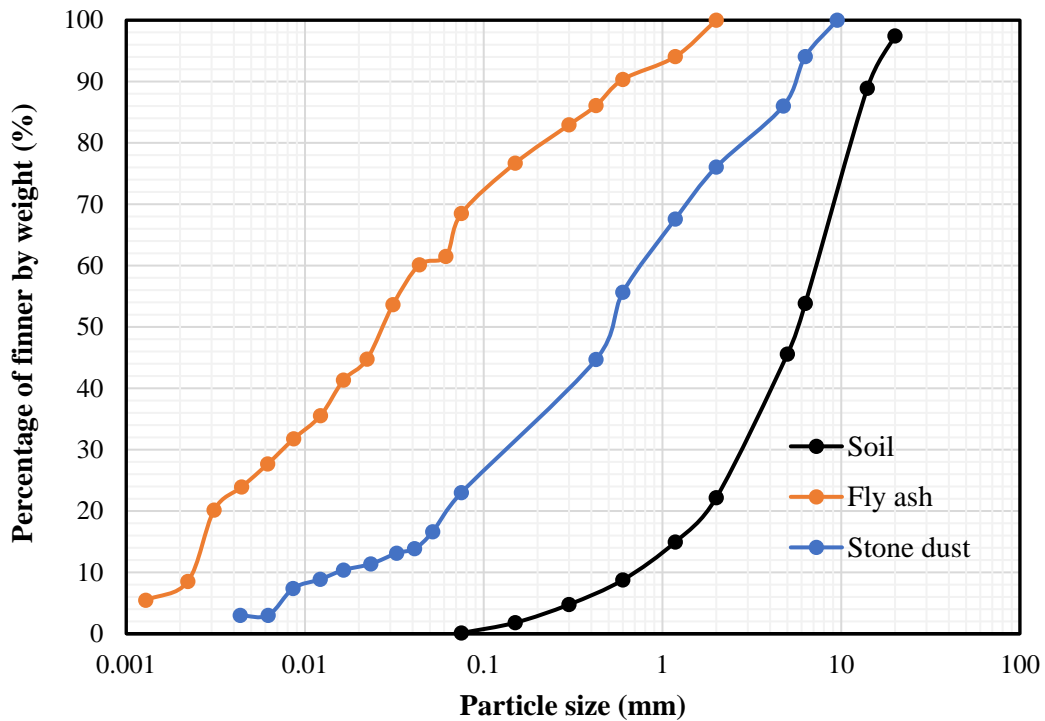


Figure 3.6 Particle size distribution curves for soil, stone dust and fly ash

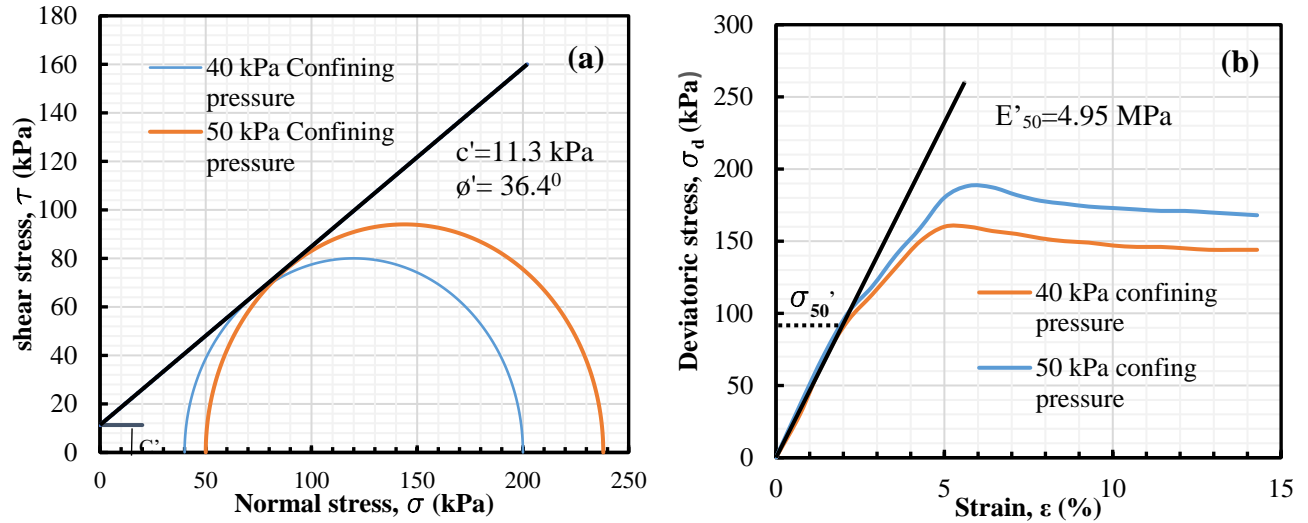


Figure 3.7 (a) Mohr-Coulomb failure envelop, (b) Deviatoric stress-axial strain curve

b. Fly ash

The purpose of fly ash in this thesis was to be used as an alternative backfill material. The fly ash sample was brought from Aika Addis textile factory, which is found in Akaki Kaliti, Addis Ababa. The chemical composition of the fly ash from the same source was determined previously by Kifle (2019) as shown in Table 3.2. According to Table 3.2, the sum of SiO_2 , Al_2O_3 and Fe_2O_3 is above 70. Based on this value and other compositions from Table 3.3, the fly ash was classified as an ASTM Class F fly ash. ASTM C618 explains class F fly ash as a material with pozzolanic property. Therefore it can be used as a non-conversional backfill material. A particle size analysis was conducted on fly ash (as shown in Figure 3.6) and almost similar particle size distribution curve with Kifle (2019) was found. From the particle size distribution test, it can be seen that 68.489% of the sample passed sieve no 200 (0.075 mm) and the sample generally was dominated by silt-sized particles. According to ASTM D2487-98, this sample fly ash can be classified as an equivalent silt with low compressibility (ML). Other index tests for fly ash were conducted and the results are summarized in Table 3.3.

In the finite element modeling, the fly ash was modeled as a homogenous solid element with a Mohr-Coulomb elastoplastic material model. The shear strength parameters for finite element modeling were determined from two consecutive triaxial CU tests under 40 kPa and 50 kPa confining stresses. The Mohr-Coulomb failure envelope and the stress-

strain curve are presented in Figure 3.8. The Poisson's ratio was taken as 0.36. This value was directly adopted from Beju and Mandal (2017a) who conducted appropriate tests to find the Poisson's ratio of fly ash sample. All the parameters of fly ash used in FEA are summarized in Table 3.4.

Table 3.2 Chemical composition of fly ash (Kifle, 2019)

Chemical compounds	SiO ₂	Al ₂ O ₃	Fe ₂ O ₃	CaO	MgO	Na ₂ O	K ₂ O	MnO	P ₂ O ₅	TiO	H ₂ O	LOI
Composition (%)	52.54	34.66	1.34	0.16	0.01	1.08	0.01	0.01	0.01	0.55	4.25	6.85

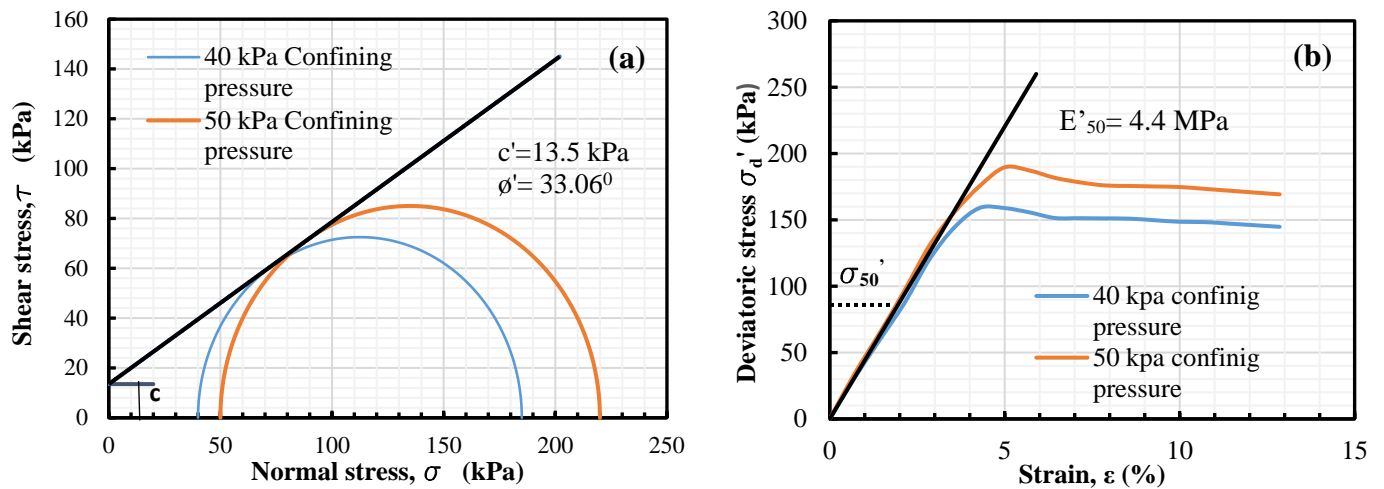


Figure 3.8 (a) Mohr-Coulomb failure envelop, (b) Deviatoric stress-axial strain curve

c. Soil for Trench Fill

The soil sample was brought from a dumped soil for the purpose of backfilling the trench, which was excavated along the newly ongoing road construction in Gondar town (airport-Arbegnoch square). This soil was originally obtained around Denbia. This makes it a good choice of sample to use as fill material in this thesis to compare with the above two backfills. A disturbed soil sample was taken and some of the necessary index tests were conducted as shown in Table 3.3. As the particle size distribution curve in Figure 3.6 shows, the sample was a mixture of gravel (31.5%), sand (43.15%) and some amount of fine particles (25.35%). Based on ASTM D2487-98 (unified soil classification system) the soil sample was classified as a clayey sand with gravel (SC).

In finite element analysis, the soil was modeled using the Mohr-Coulomb elastoplastic model as the other fill materials. A triaxial CU test (ASTM D4767 – 02) was conducted to find the elastic and plastic parameters of the soil. The stress-strain behavior and the Mohr-Coulomb failure envelope of the soil from two CU triaxial tests under 40 kPa and 50 kPa confining pressures are presented in Figure 3.9. The Poisson's ratio was taken as 0.35. This value was assumed based on the particle size distribution (Bowles, 1997). Generally, the parameters that were used in finite element analysis are summarized in Table 3.4.

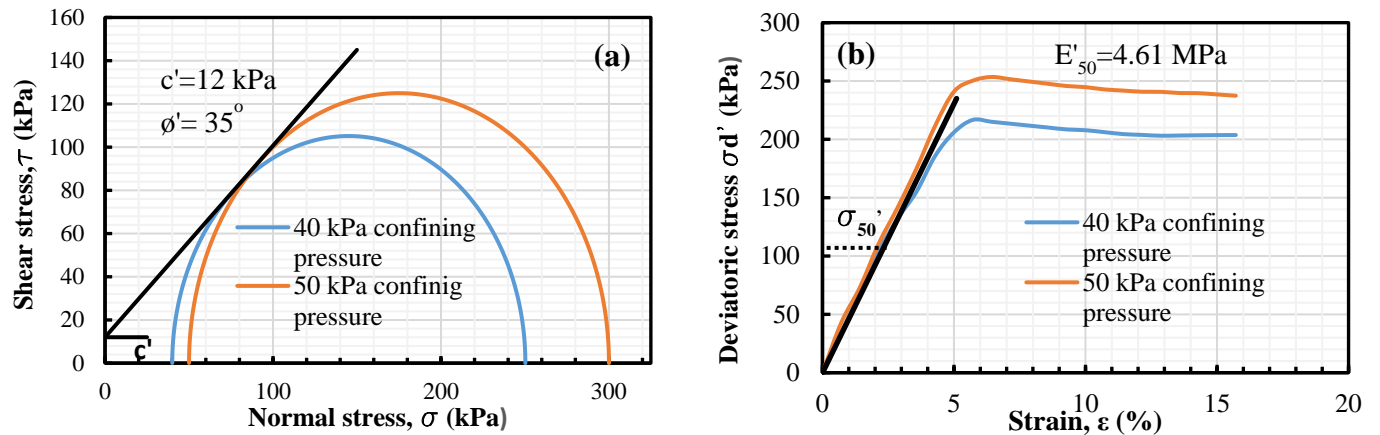


Figure 3.9 (a) Mohr-Coulomb failure envelope, (b) Deviatoric stress-axial strain curve

Table 3.3 Properties of stone dust fly ash and soil

Measurement	Test Method	Soil	Stone Dust	Fly ash
Natural moisture content (%)	ASTM D2216-98	15.5	Dry	dry
Specific gravity	ASTM D854-00	2.646	2.832	2.273
Liquid limit (%)	ASTM D4318-00	46.8	Non-plastic	Non-plastic
Plastic limit (%)	ASTM D4318-00	22.7	Non-plastic	Non-plastic
Maximum dry unit weight (kN/m ³)	ASTM D698-00	19.70	20.18	13.70
Optimum moisture content (%)	ASTM D698-00	12.3	9.8	24.1
Gravel sized particles (%)	ASTM D422/D2487-98	31.5	5.66	-
Sand sized particles (%)	ASTM D422/D2487-98	43.15	65.81	31.5
Silt sized particles (%)	ASTM D422/D2487-98	25.35 ¹	25.9	57.98
Clay sized particles (%)	ASTM D422/D2487-98		2.6	10.51
Classification based on USCS	ASTM D422/D2487-98	SC	SM	ML

¹ This number represents the sum of silt and clay sized particles (percentage of fine particles)

Table 3.4 Summary of input parameters for the three fill materials in FEA

Parameters	Stone dust	Fly ah	soil
Material model	Mohr-Coulomb	Mohr-Coulomb	Mohr-Coulomb
Bulk density (kg/m ³)	2393	1635	2136
Young's modulus (MPa)	4.95	4.407	4.63
Poisson's ratio	0.35	0.36	0.35
Cohesion (kPa)	11.3	13.5	12.0
Friction angle (°)	36.4	33.06	35

Table 3.5 Parameter used in FEA for the surrounding soil (Bowles, 1997)

Parameters	Surrounding soil
Material model	Mohr-Coulomb
Bulk density (kg/m ³)	1582
Young's modulus (MPa)	5
Poisson's ratio	0.4
Cohesion (kPa)	10
Friction angle (°)	15

D. The Surrounding Soil

As it was explained and showed in the geometry modeling, the trench model in this research involves the surrounding native soil. This soil type is different from the soil that was used to fill the trench. Since the ideal location of the trench was assumed to be Gondar town, the property Gondar soil should be used in the finite element analysis. According to the ongoing investigation conducted by university of Gondar geotechnical research group, different types of soil exist in Gondar. Among these, soft clay is one of them, which is assumed to surround the trench in this research.

Like the other fill materials, the surrounding soil was modeled using Mohr-Coulomb model in assentation with linear elastic model. For this purpose both the elastic and the plastic parameters are necessary. Since no mechanical tests were conducted on this soil, the property of soft clay soil from Bowls et al. (1997) was taken. Bowles et al. (1997) gives a

range of values of parameters for different types of soils based on the experimental data. Based on this, the assumed values to model the surrounding soil is summarized in Table 3.5.

The surrounding native soil interacts with the trench fills in three directions. These interactions are created at the bottom of the trench and at the two sides of the trench. According Dietz (2013), the frictional interaction between a trench fill and the walls of the excavation is known to be considerably low, approximately equal to $\mu = 0.13$. Therefore in the current study, the tangential frictional behavior was modeled using a surface to surface contact simulation with coefficient of interaction of 0.13 and the normal behavior of the interaction was simulated as a hard contact. The detail explanation of the surface to surface contact simulation in abaqus is explained in the coming sections of the paper.

e. Pipe

In this study, the property of commercially available AMSE/ANSI B36.10/19- carbon, alloy, and stainless steel pipes with a density of 7.85 g/cm^3 with different diameters, as shown in Table 3.6, was used. However, for the base models, only a diameter of 168 mm steel pipe was used in different backfills and protective materials. According to ASTM D2321-14, the bedding layer should be in a range of 100-150 mm. For this study, a minimum of 110 mm bedding was provided for all types of diameter of pipes and all the analyses were made by putting the pipe 3D from the top surface of the trench, Where D is the diameter of the pipe as it was explained in the geometrical model section.

Table 3.6 Steel pipe dimensions (Hebei Haihao PLC online specification)

Nominal Pipe size (in)	Diameter (mm)	
	External	Internal
5	141	128
6	168	154
8	219	203
10	273	255

During finite element modeling of the pipe in Abaqus, a homogenous shell element was used because shell elements represent objects with small thickness relative to their length

and width. To simulate the behavior of the steel pipe, a linear elastic model that is available in Abaqus 6.0 was used. The modulus of elasticity, Poisson’s ratio and density of the steel pipe were taken directly from the manufacturer specification. Generally, the material and geometrical models, which were used in this study, are summarized in Table 3.7.

Table 3.7 Summary of material and geometrical model of the pipe

Parameters	Values used in FEA
Density	7.85 g/cm ³
Modulus of elasticity	200 GPa
Poisson’s ratio	0.29
Diameter	From 141 mm to 273 mm
Location	3D from the top surface
Material model	Elastic material

Pipe-Fill Interaction

The performance of a buried pipe is heavily influenced by the interaction between the pipe and its surrounding soil (soil-pipe interaction). The soil-pipe interaction is a function of the combination of physical and geometric properties of the backfill soil and the pipe. The distribution of pressure at the pipe-soil interface and the total load transmitted to the pipe are useful parameters in evaluating the fill-pipe interaction (McGrath, 1993).

In this research, pipe–soil interaction was modeled using surface-based contact interaction, which is incorporated in Abaqus. This interaction behavior is explained in section 3.2.f of this document. Based on recommendations by USACE (1994), the interface shear strength was assumed to be one-half of the estimated soil shear strength (Kim and Watthofe, 2015). Therefore, a 0.5 coefficient of friction for tangential direction and a hard contact for normal behavior were adopted.

f. EPS Geof foam

There are many ways of reducing the earth pressure on buried pipes. The first one is to use a ‘lightweight’ material as backfill. The other one is to use a compressible inclusion to induce or allow 'controlled yielding' within a normal soil fill/backfill (Horvath, 2005). Since EPS geof foam is the most compressible material among geof foam types (Horvath, 1997), it was used as compressible inclusion in the present study.

During the installation, the location of the EPS geof foam affects the vertical earth pressure distribution on the pipe. When a buried pipe is installed in imperfect trench condition, the plane of equal settlement is developed within the embankment. The depth below this plane is the main factor to reduce the stress on the pipe by mobilizing shear stress between the inner prism and the outer prism of soil. Most of the time, under shallow burial depth (embankment), this plane is not real. Therefore, installing the EPS geof foam far from the pipe will decrease the depth of mobilized shear stress between the soil prisms.

Researches showed that under constant density and thickness of EPS geof foam and under the same embedment depth of the pipe, the vertical stress on the pipe will decrease as EPS geof foam block is installed near to the top of the pipe (e.g. Beju and Mandal, 2017a; Kang et al., 2008; Soylemez and Huvaj, 2018). Therefore, the lowest vertical stress on the pipe could be mobilized by installing the EPS geof foam close to the pipe. In this research, all base models were created by putting a single layer of EPS geof foam 0.25D from the top of the pipe.

EPS geof foam is fabricated in different shapes and sizes. In this research, 40 mm thick rectangular shape of EPS geof foam was used because the rectangular section EPS geof foam allows more amount of deformation than the circular section EPS could (Beju and Mandal, 2017a). The width of the EPS geof foam was modeled as 1.5D. As Kim et al., 2010 showed, with 1.5D width of geof foam, up to 73% of vertical stress at the top of the pipe could be reduced. Moreover, during the installation, it was assumed to be installed at the center of the trench following the length of the pipe.

It is obvious to select EPS geof foam based on its density because the density basically controls the compressibility, the water absorption behavior, the modulus values and the cohesion of EPS geof foam (Beju and Mandal, 2017b; Meguid et al., 2017). So in this paper, the property of medium density EPS geof foam (EPS15) based on ASTM D6817-13 was used. The general configuration of the pipe and the EPS geof foam is shown in Figure 3.9.

The other very important thing in modeling is to select a constitutive model, which simulates the actual material property of the EPS geof foam best. Many studies showed that the stress-strain behavior of EPS is close to linearly elastic perfectly plastic material. Therefore, EPS geof foam could be considered as an elastoplastic material (Aytekin, 1997;

Leo, et al., 2008). Having this thought, the linear elastic and Mohor-Columb plastic material behaviors were used in finite element modeling of EPS geofoam.

Since compressive strength tests on EPS geofoam was not conducted, the shear strength parameters and the unit weight of the EPS geofoam (EPS 15) were taken from literatures. Those values were taken from Beju and Mendal (2017a) who conducted the appropriate tests. Even though the poisson's ratio of geofoam becomes zero as the strain enlarges, it was calculated using Equation 3.7 which was suggested by Horvath (1995). This formula was used in different literature for finite element analysis (eg, Kim and Witthoeft, 2016; Beju and Mandel, 2017a; Mandal, 2012) and similar results with respective experimental works were found. Generally, all the EPS geofoam material properties and the geometries that were used in the present study are presented in Table 3.8.

$$v = 0.0056 \rho + 0.0024 \quad \text{Equation 3.7}$$

Where ρ = Density of EPS Geofoam (kg/m³)

Table 3.8 Summary of EPS geofoam material and geometrical model (Beju and Mandal, 2017a)

Parameters	Values
Density (kg/m ³)	15
Elastic modulus (MPa)	2.77
Poisson's ratio	0.1 ²
Undrained Cohesion (kPa)	32.25 at zero plastic strain
Friction angle (°)	1.38
Position	0.25D from the top of the pipe
Width (mm)	1.5D
Thickness (mm)	40
Material model	Mohr- Coulomb

² Using the empirical formula, the exact value was 0.0864. However, by the recommendation of the owner of the formula, it was approximated to 0.1.

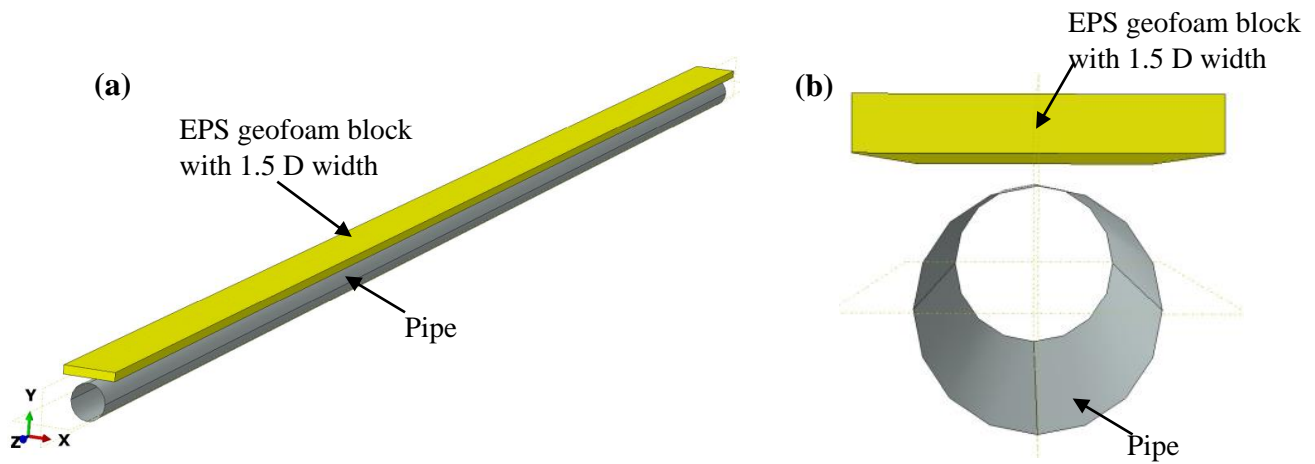


Figure 3.10 General configuration of the pipe and the EPS geofoam (a) 3D view, (b) sectional view

EPS –Fill Interaction

Abaqus presents a wide range of interaction simulation techniques. Among these options, the surface-based contact interaction was used in this study to model the EPS-fill interface. Similar contact interactions were used by different researchers (Abdollahi and Tafreshi, 2017; Kim and Witthoef, 2016; etc.). Surface-based contact simulations between two deformable bodies generally need to define mechanical contact property models in two directions: normal direction and tangential direction.

i. Tangential Behavior

It is known that there will be a small amount of relative motion between the EPS geofoam and the fill material. This behavior could be simulated in Abaqus by using a friction formulation option, i.e., 'penalty', which works based on the Coulomb friction model. This option uses the stiffness (penalty) method that permits some relative motion of the surfaces (an "elastic slip") when they should be sticking. While the surfaces are sticking (i.e., $\tau < \tau_{crit}$), the magnitude of sliding is limited to this elastic slip.

The stiffness method in Abaqus/Standard requires the selection of an allowable elastic slip, γ_{crit} . Using a large γ_{crit} in the simulation makes the convergence of the solution more rapid at the expense of solution accuracy (there is a greater relative motion of the surfaces when they should be sticking). Behavior in which no slip is permitted in the sticking state is approximated more accurately by allowing only a small γ_{crit} . If γ_{crit} is chosen very small,

convergence problems may occur. Abaqus/Standard by default provides an allowable elastic slip, which gives a conservative balance between efficiency and accuracy.

Abaqus/Standard calculates γ_{critc} as a small fraction of the “characteristic contact surface length,” l_{charc} , and scans all of the facets of all the slave surfaces when calculating l_{charc} .

Abaqus/Standard reports the value of l_{charc} used for each contact pair in the data (.dat) file if we request a detailed printout of contact constraint information. The allowable elastic slip is given as $\gamma_{\text{critc}}=F_f.l_{\text{chrac}}$, where F_f is the slip tolerance; the default value of F_f is 0.005.

Having the above concepts, the penalty friction formulation was adopted in the present study. The frictional coefficients were adopted by assuming the interface shear strength reduction coefficients. The interface strength factor is defined as the ratio of tangent values of interface friction angles and fill friction angles. Therefore, for the stone dust and fly ash, the interface shear strength reduction factor is taken from Beju and Mandal (2017) who assumes a reasonable reduction factor in the analysis and got similar results with the model tench tests. But for the soil, it was tried to take a coefficient of friction slightly below the stone dust because of the fact that stone dust particles are more angular and could create more interface strength than the soil particles. Generally, a frictional coefficient of 0.8, 0.75 and 0.67 for stone dust, soil and fly ash respectively was used.

ii. Normal Behavior

The other important interaction behavior that should be considered is the normal behavior of the interaction. The normal behavior of interactions depends on the clearance or over closure condition of the two interacting surfaces during loading. Abaqus gives different options for simulating the normal behavior of contact surfaces. In this study, it is assumed that there will not be any penetration between the EPS geof foam and the fill materials. Among all overclosure options Abaqus presents, a 'hard contact' option was used to simulate the normal behavior of interaction between EPS geof foam and all the three fill materials. The "hard" contact relationship minimizes the penetration of the slave surface into the master surface at the constraint locations and does not allow the transfer of tensile stress across the interface.

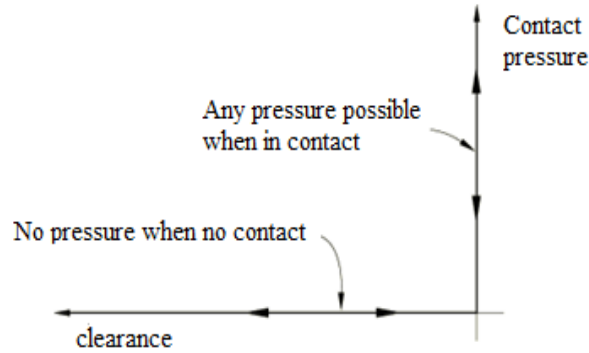


Figure 3.11 Default pressure-overclosure relationship in abaqus (Abaqus 6.14 user Manual)

In this overclosure option, the contact constraint is applied when the clearance between two surfaces becomes zero. There is no limit in the contact formulation on the magnitude of contact pressure that can be transmitted between the surfaces. The surfaces separate when the contact pressure between them becomes zero or negative, and the constraint is removed. This contact pressure-clearance relationship is summarized in Figure 3.11. From the enforcement techniques of the "hard" contact overclosure, the default enforcement method was used for the present research.

g. Geotextile

As it was explained in the literature review section, geotextiles have different purposes. However, for the present study, it was used as a reinforcement for the backfill and bedding materials. To mobilize this purpose of the geotextile, it was simulated as it was laid over the whole surface of the trench width at the required depth. In fact, Kou et al., (2018) showed that as the ratio of the reinforcement width to pipe diameter increases, the vertical pressure on the crown of the pipe will get decrease.

Geotextiles are fabricated in different specifications based on ASTM standard. For this particular study a property of 1.78 mm thick 'HP series' woven geotextiles, which are produced by MIRAFI Company, was used. These HP-series geotextiles are specially designed for the purpose of reinforcement, stabilization and other related purposes. Since one of the objectives of this research is to study the effect of tensile strength of the geotextile on the reinforcement of the fills, different geotextiles were selected based on

their tensile strength values, which were given directly by the producing company as shown in Table 3.9.

Table 3.9 Different geotextiles with their tensile strength values (MIRAFI Company online user manual)

Properties	Test method	Unit	HP370	HP570	HP665	HP770
Strength at 5% strain (MD)	ASTM D4595-98	kN/m	21.9	35	17.5	52.5
Strength at 5% strain (CD)	ASTM D4595-98	kN/m	22.8	39.4	61.3	52.5
Apparent opening size	ASTM D4751-98	mm	0.60	0.60	0.43	0.6
Mass per unit area	ASTM D5261-98	g/cm ²	0.71	0.91	1.81	2.62

MD: Machine Direction CD: Cross-Machine Direction

In Abaqus, the geotextile was modeled as a shell element. Then, this shell element was assigned as a membrane section. Membrane section in Abaqus represents thin surfaces, which give a strength along the plane of the surface. This makes it very suitable for the desired purpose of geotextile in the present study. The appropriateness of membrane elements for the simulation of the geosynthetic was supported by Perkin (2001) and was used by many researchers (e.g. Dondi, 1994; Leng, 2002). An advantage of using the membrane elements is that they do not have a tangible thickness within the modeling space. This means that the membrane can be placed in a plane where two soil sections meet without disrupting the contact adjacent to the area where there is no geotextile. The thickness of the membrane is specified as a property for calculating the membrane stiffness in the analysis procedure. If solid elements were to be used in place of membrane elements for the geotextile, voids would be created by the geotextile's thickness in the areas where the geotextile does not extend.

The location of the reinforcement material greatly affects the performance of the reinforcement material. According to Shukla (2016), the reinforcement material should be located within the depth of influence of the foundation and the optimum embedment depth of single reinforcement is 0.3B from the top surface. Therefore, the geotextile reinforcements in the base models were located 0.3B from the surface of the trench. The general configuration of single geotextile reinforcement is presented in Figure 3.12.

The mechanical property of the geotextile was modeled as a linear elastic material. Such assumption was used by different researchers previously (e.g. Madhu and Singh, 2019; Dondi, 1994; Leng, 2002 and Andrew and Dietz, 2013). To use linear elastic model, modulus of elasticity and Poisson's ratio of the geotextile should be determined.

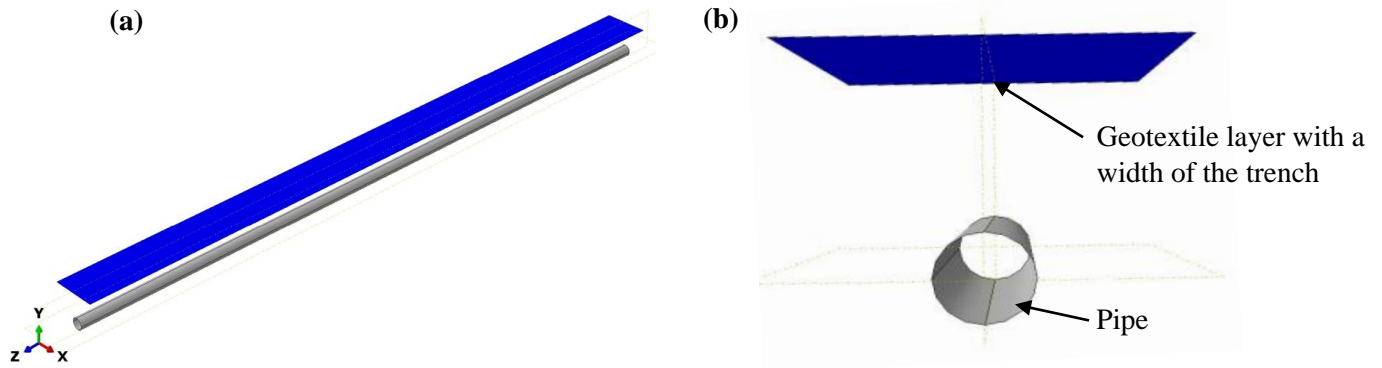
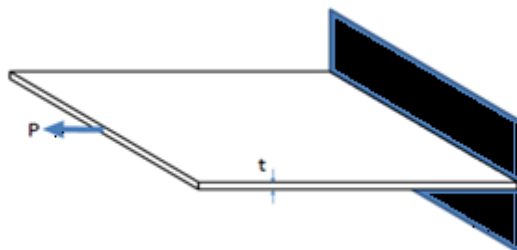


Figure 3.12 General configuration of the pipe and a single geotextile reinforcement (a) 3D view, (b) Sectional view

Geotextile Modulus of Elasticity

Usually, the modulus of elasticity of geotextiles is not provided by the companies. However, it can be calculated by using a combination of values supplied by the manufacturer (Robert, 2005). Among four types of geotextiles, which were used for the present study, a sample calculation to find the modulus of elasticity is shown below. The modulus of elasticity of the remaining geotextile types is presented in Table 3.10.

A Mirafi HP570 geotextile has a tensile strength of 35.0 kN/m and 39.4 kN/m at 5% strain in the machine and cross-machine directions respectively (TenCate Geosynthetics, 2012). Since the forces applied to the geotextile in the buried pipe problem are bi-directional, the smaller strength value was used to represent the worst case scenario and assure a conservative modeling approach. Using these values, combined with an average nominal thickness of 1.78 mm, the modulus of elasticity can be calculated as follows:



Where 'p' is the tensile strength and 't' is thickness

Figure 3.13 Schematic representation of geotextile tensile strength test

By dividing the tensile strength by the designated strain, an intermediate modulus of elasticity can be obtained. Through unit analysis, it is apparent that the modulus of elasticity can be generated by dividing the intermediate modulus of elasticity by material thickness.

$$M = \frac{P}{\varepsilon} = \frac{35 \text{ kN/m}}{0.05} = 700 \text{ kN/mm}$$

$$E = \frac{M}{t} = \frac{P}{t\varepsilon} = \frac{700 \text{ kN/mm}}{1.78 \text{ mm}} = 393.99 \text{ MPa}$$

Where M= intermediate modulus of elasticity

E=modulus of elasticity

ε = strain

Table 3.10 Calculated modulus of elasticity

Geotextile code	Strength at 5% strain (MD) (kN/m)	Thickness (mm)	Calculated modulus of elasticity (MPa)
HP370	21.9	1.5	292
HP570	35	1.78	393.26
HP665	17.5	1.35	259.26
HP770	52.5	2.06	509.71

Geotextile Poisson's Ratio

Like modulus of elasticity, Poisson's ratio of geotextile is not provided by the manufacturing companies. Therefore, finding a way of calculating the Poisson's ratio of geotextiles is up to the user. In the present study, no mechanical tests were conducted on geotextiles. However, it was tried to see the effect of Poisson's ratio on the vertical stress, which will reach the crown of the pipe using the finite element analysis. This preliminary study was conducted on the three fill materials with a single geotextile reinforcement layer above the pipe. By setting all other parameters constant, only the Poisson's ratio of the geotextile was varied from 0.1 up to 0.45. As the result of these models in Table 3.11 indicates, the effect of Poisson's ratio of geotextiles in protecting buried pipes is very small. The biggest difference between the vertical stress on the crown of the pipe from the smallest and largest Poisson's ratio values is below 1%. So for this research, a 0.4 Poisson's

ratio value was used in all models. This value was taken directly from Andrew (2013). For the base model, the property of MIRAFI HP570 properties was used.

Table 3.11 Effect of geotextile Poisson's ratio on the crown vertical stress

Fill material	Poisson's ratio of geotextile used	Stress on the crown of the pipe (kPa)	Stress Differenc b/n hieighest and lowest poisson's ratio
soil	0.1	14.25	0.89%
	0.45	14.38	
Fly ash	0.1	12.19	0.36%
	0.45	12.23	
Stone dust	0.1	15.19	0.64%
	0.45	15.28	

Geotextile – Fill Interaction

The contact between the geotextile and the fill material is the main factor in resisting the vertical loading at the surface. Through this frictional contact, some of the magnitudes of the vertical load is transferred to the geotextile and diverted into the tangential direction of the textile plane.

Two types of interactions were defined between the fill materials and geotextile layers, i.e., normal behavior and tangential behavior. For the normal behavior, it was assumed that there is no relative motion between two surfaces for all three fill materials (referred to as 'hard contact' in Abaqus). For the tangential behavior, it was assumed that some amount of slip will occur at the interface. To simulate this condition 0.54, 0.703 and 0.79 frictional coefficients for fly ash, stone dust and soil fill respectively were adopted. These values were assumed based on the particle size and internal friction angle of the fill materials by taking Beju and Mandal (2017a) as a reference. Because many researches showed that, soil with higher particle size will have higher interface shear strength with the geotextiles. (E.g. Lopes, 1999; Lopes and Lopes, 2001; Jewell, 1990).

3.4 Meshing

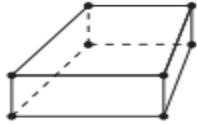

In finite element analysis (FEA), it is very important to determine the type of element, the shape of the element and the number of elements of the mesh in order to obtain more

accurate results based on the available computational capacity of the computer. The topology of the mesh is not changed by adaptive meshing technology in Abaqus and it is involved in the characteristics of pure Lagrangian and pure Eulerian analysis simultaneously. This adaptive meshing type is called Arbitrary Lagrangian-Eulerian (ALE) analysis (Huang et al., 2008).

3.4.1 Element Type

In the present study, eight noded (linear) hexahedron and four noded quadrilateral elements were used for solid and shell elements respectively to mesh the whole model independently as it is explained in Table 3.12.

Table 3.12 Element types, used for each materials

Material	Element type	First-order (or linear) interpolation	
Soil, fly ash, stone dust, EPS geofom, and loading plate	Reduced integration continuum element	C3D8R	
Pipe and geotextile	Reduced shell element	S4R	

In finite element analysis, based on the selected type of element, the elemental stiffness matrix are constructed in the following general steps. (**N:B** only eight noded hexahedron element as shown in Figure 3.14 is selected to show the general steps)

- I. A displacement vector (U) will be expressed in terms of the nodal displacements and shape functions which are a function of the natural coordinate system as:

$$U = Nd \tag{Equation 3.8}$$

where, d is the nodal displacement vector in three global directions (x, y, z) which can be expressed as:

$$u = \sum_{i=1}^8 N_i u_i, \quad v = \sum_{i=1}^8 N_i v_i, \quad w = \sum_{i=1}^8 N_i w_i \tag{Equation 3.9}$$

3.4.2 Mesh Size

The size of the elements relative to the size of the model affects the accuracy of the final result and the running time of the analysis. Therefore, in the present research, an optimized size of elements with accuracy and the running time was selected through a preliminary mesh sensitivity analysis. This section of the thesis presents the result of the sensitivity analysis of sample base model with fly ash fill. Abaqus gives an option to mesh parts manually using global seeds and local seeds. Global seeds allows the user to mesh the whole part once with the desire size of elements, where as the local seeds are used to refine different sections of the part by allowing the user to select single edges and mesh it.

In this research, all the parts were meshed independently. Primarily, global seeds were used to generate mesh in Abaqus. But, some refinement or manual adjustments were made at sensitive areas and at the contact surfaces of instances using local edge seeds. Finally from the sensitivity analysis, an appropriate mesh size was selected based on the accuracy, running time and computational capacity of the computer. The element size used for each part, the no of elements and the vertical stress at the crown of the pipe in the sensitivity analysis is summerized in Table 3.13. In this table, the size of the elements is expressed in ranges, i.e, maximum and minimum. The maximum value indicates the size of the global seeds and the minimum values represents the local seeds which were used to refine sensitive areas. The results are more illustreted in Figure 3.15. This grapgh was drawn as the minimum elemnt size vs the verticsl stress at the crown. Based on this grapgh, the third option was used for the rest of the models and a sample meshed model is presented in Figure 3.16.

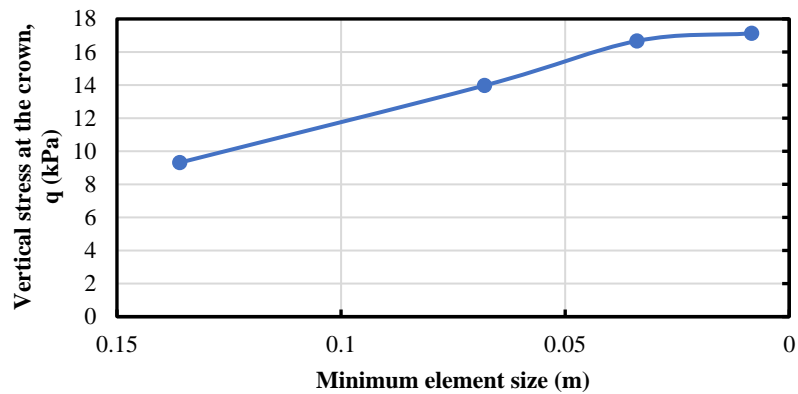


Figure 3.15 Vertical stress on the crown of the pipe at different element size (in fly ash fill)

Table 3.13 Result of mesh sensitivity analysis on the model with fly ash fill

Trials	Parts/ Instances	size of elements	No of elements	Vertical stress on the crown (kPa)
Trial 1	native soil	1-0.296	5984	9.314
	bedding	0.5-136	100	
	embedmnet and fill	0.5-0.056	4360	
	pipe	0.36	336	
Trial 2	native soil	0.75-0.146	8096	13.378
	bedding	0.5-0.068	200	
	embedmnet and fill	0.5-0.028	6720	
	pipe	0.18	504	
Trial 3	native soil	0.5-0.073	12848	16.669
	bedding	0.5-0.034	400	
	embedmnet and fill	0.5-0.014	9600	
	pipe	0.09	840	
Trial 4	native soil	0.5-0.073	12848	17.032
	bedding	0.5-0.034	400	
	embedmnet and fill	0.5-0.0084	13440	
	pipe	0.09	840	

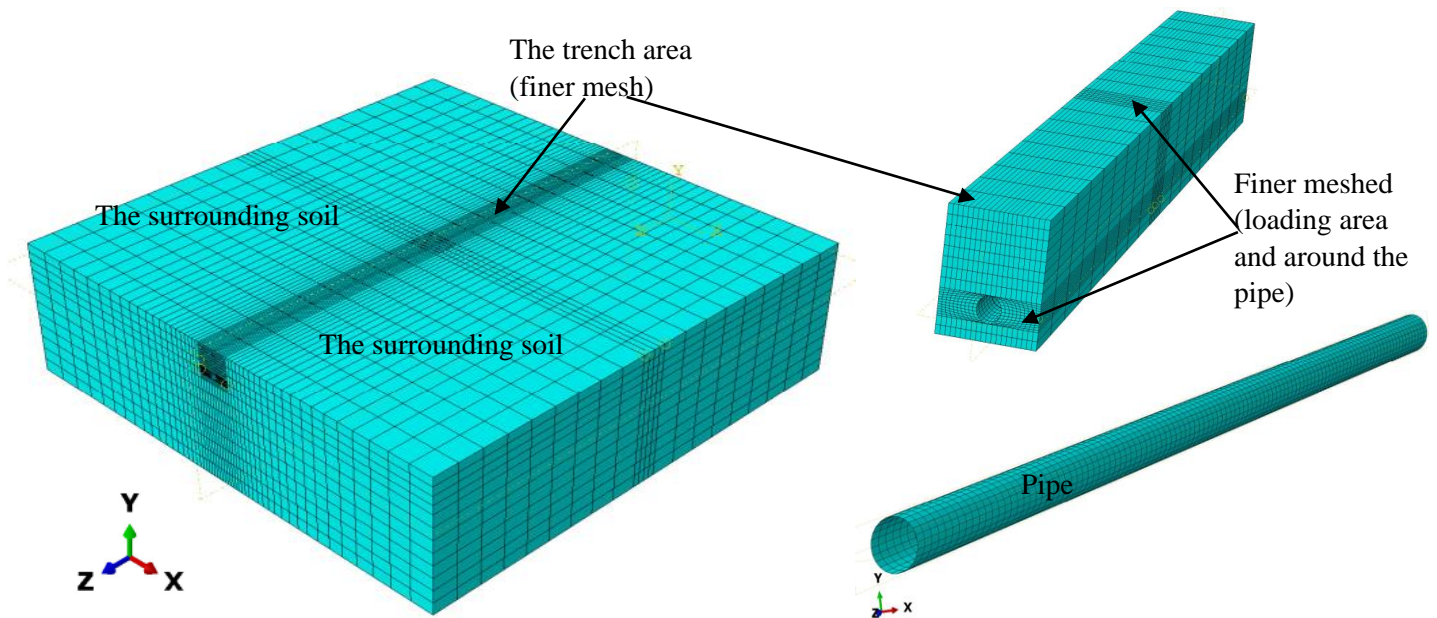


Figure 3.16 Sample meshed trench model parts

3.5 Loading and Boundary Conditions

3.5.1 Loading

In addition to the applied load, the loading in this research simulated the actual construction stages of a trench after the excavation is finished. Therefore the total loading condition can be seen in two categories:

- i. Geostatic loading
- ii. Applied loading

i. Geostatic loading

The total geostatic load of the whole model was applied in four or six steps depending on specific trench condition. Each geostatic step was simulated by activating the gravitational force for that particular instance/part and by allowing this force to propagate for the rest of the steps including the applied loading step.

Step 1- Geostatic load of the empty trench: This includes the self weight of the surrounding native soil within the boundary of the model as shown in Figure 3.17

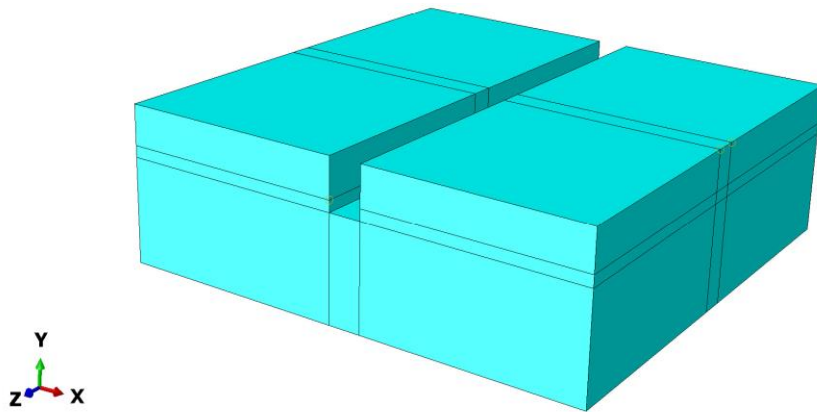


Figure 3.17 Empty trench

Step 2- Geostatic load of the bedding: In this step, 110 mm bedding material, which was prepared to install the pipe on it, was simulated to be placed within the empty trench as shown in Figure 3.18. During compacting and preparing the bedding, different additional loads are used in the construction sites. However, for this study, the effect of such forces was neglected in all steps.

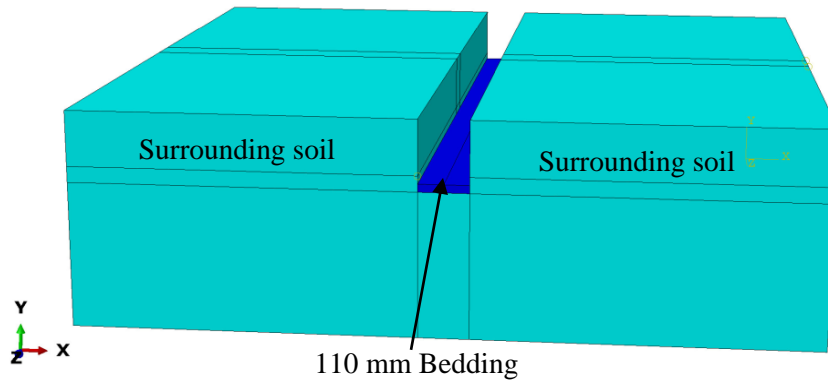


Figure 3.18 Trench with bedding

Step 3- Installation of the pipe: In this step, placement of the pipe on the prepared bedding was simulated by allowing the self weight of the pipe to be active. This condition is presented in Figure 3.19

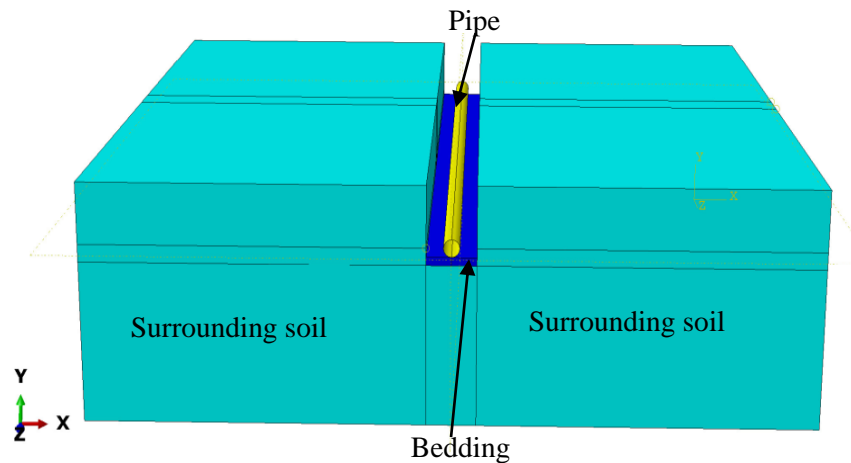


Figure 3.19 Installation of the pipe

Step 4- Embedment and Backfilling: This stage of construction is conducted in different ways depending on the type of the trench that is intended to use. If the trench is constructed without an additional protecting material, the embedment and backfilling will be conducted up to the ground level and this will be the end of the construction as shown in Figure 3.20. In this research, since the effect of compacting force was neglected, the two basic construction stages (embedding the pipe and backfilling the trench) were simulated in a single step. The other reason for such type of simulation is that a single type of embedment and backfilling material and degree of compaction was used. However, if either the trench

is constructed in of EPS included or geotextile reinforced type, step-4 will be embedding the pipe and backfilling the trench up to the level where those additional materials are installed as shown in Figure 3.21.

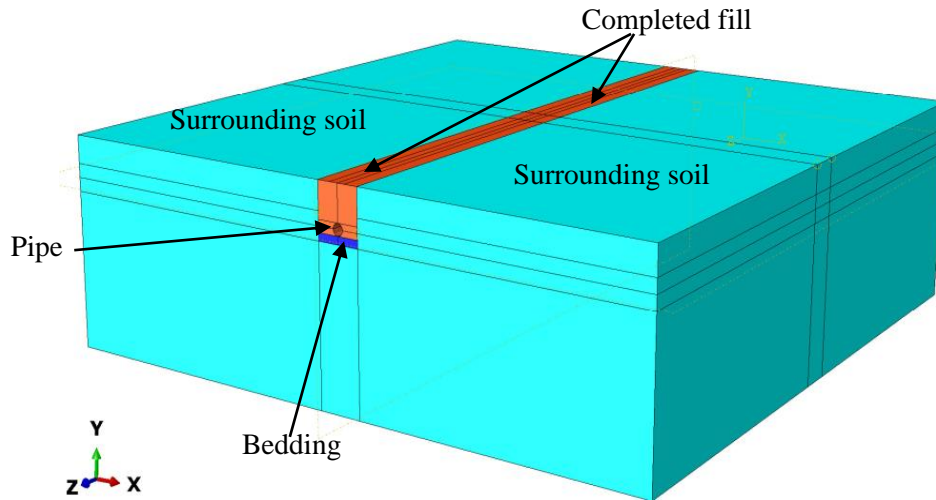


Figure 3.20 Filled unreinforced trench model

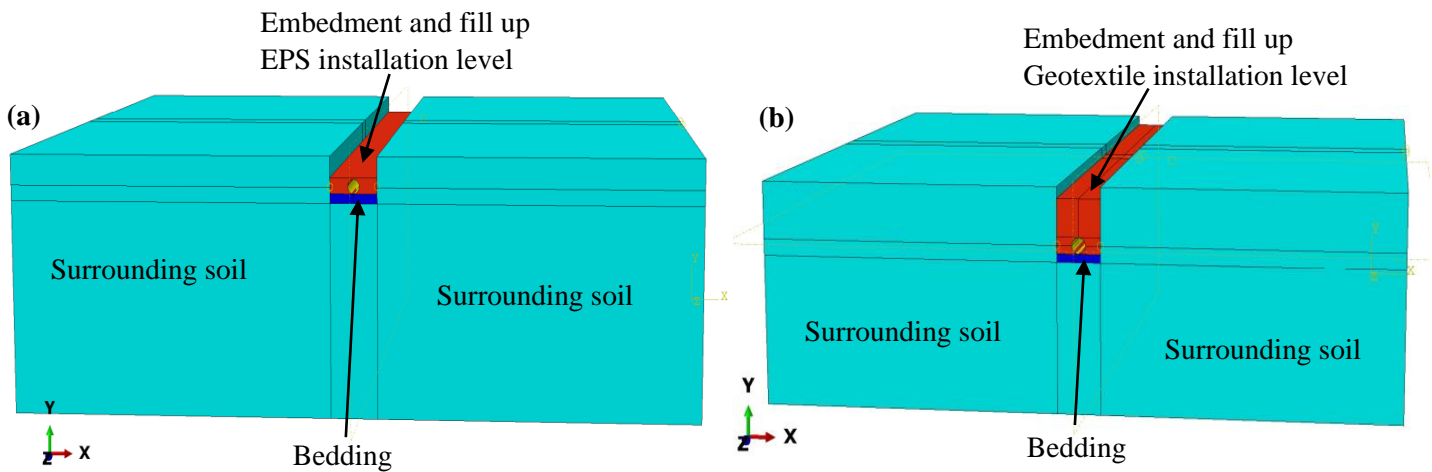


Figure 3.21 Partially backfilled trenches (a) for EPS included trench, (b) for geotextile reinforced trench

Step 5- Installation of protective materials: This step was applied for EPS included or geotextile reinforced trench models. In actual construction sites, after the placement of the pipe, the embedment and backfilling will be continued. However, during backfilling, the placement of EPS geofoam and geotextile will be conducted at the required depths and backfilling will be continued and finished at the surface of the ground. In this research, step

5 loading was created to express the installation of either of the two protective materials at the required depth.

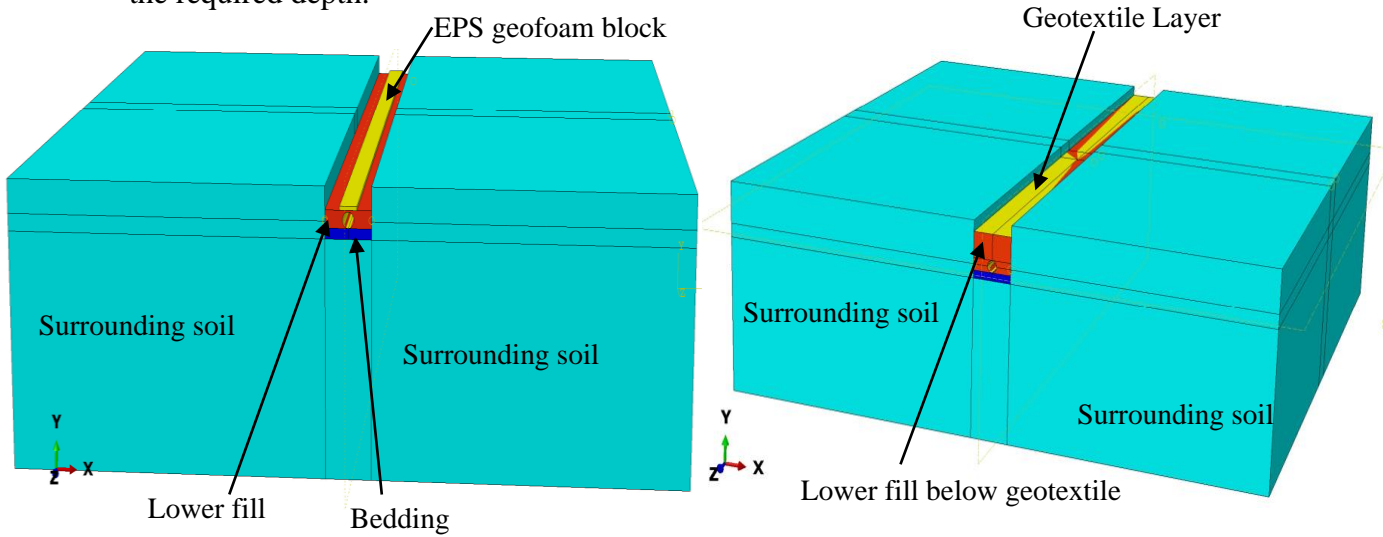


Figure 3.22 Installation of (a) EPS geofoam, (b) geotextile

Step-6- Backfilling up to the surface of the ground: With this step, the construction of EPS included and geotextile reinforced trenches will be finished. So the geostatic loading in this research was also finished in this step as shown in Figure 3.23.

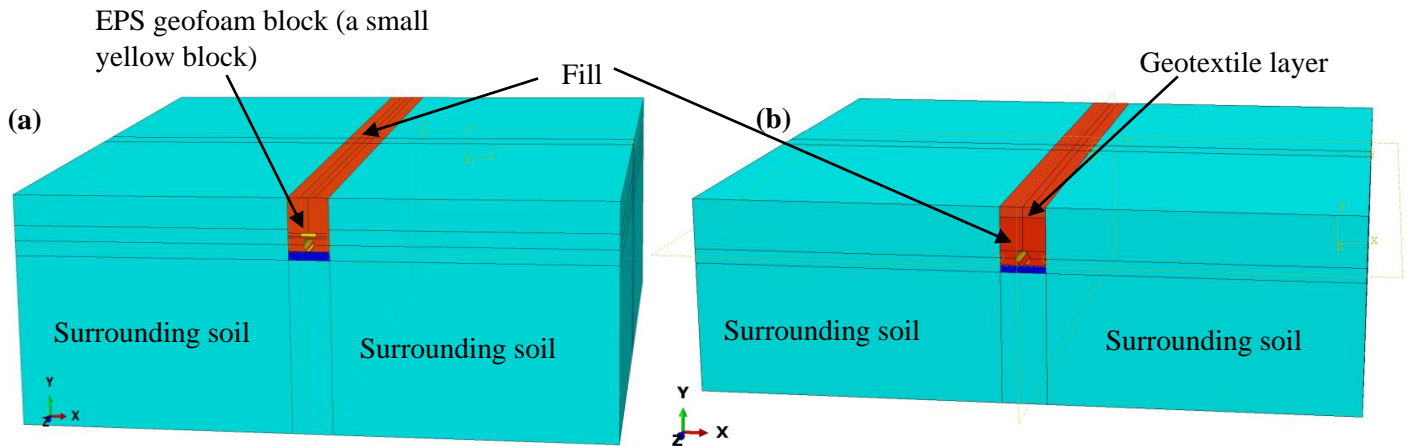


Figure 3.23 Final fill for (a) EPS included, (b) geotextile reinforced trenches

ii. Applied load

In this research, a static load, which simulates a single ASHTO standard SH-25 wheel load, was applied at the center of the model. An ASHTO standard SH-25 truck wheel load represents 13.79 kPa load over an area of 0.508 m X 0.254 m as shown in Figure 3.24. In

the present trench model, this amount of pressure was applied at center of the top surface of the trench in the seventh step as shown in Figure 25.

Another load associated with pipe lines is the internal pressure from the transported fluid. In the current research, this load was not taken into account because most deformation of buried pipelines occurs in the absence of pipe flow except for highly pressurized pipes.

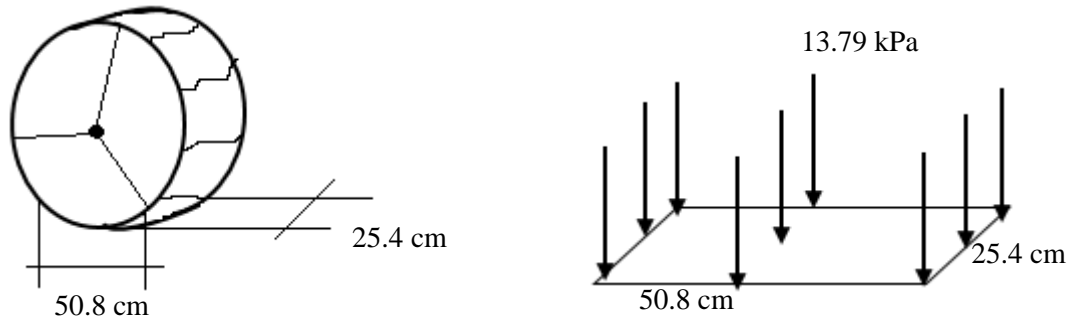


Figure 3.24 ASHTO SH-25 loading

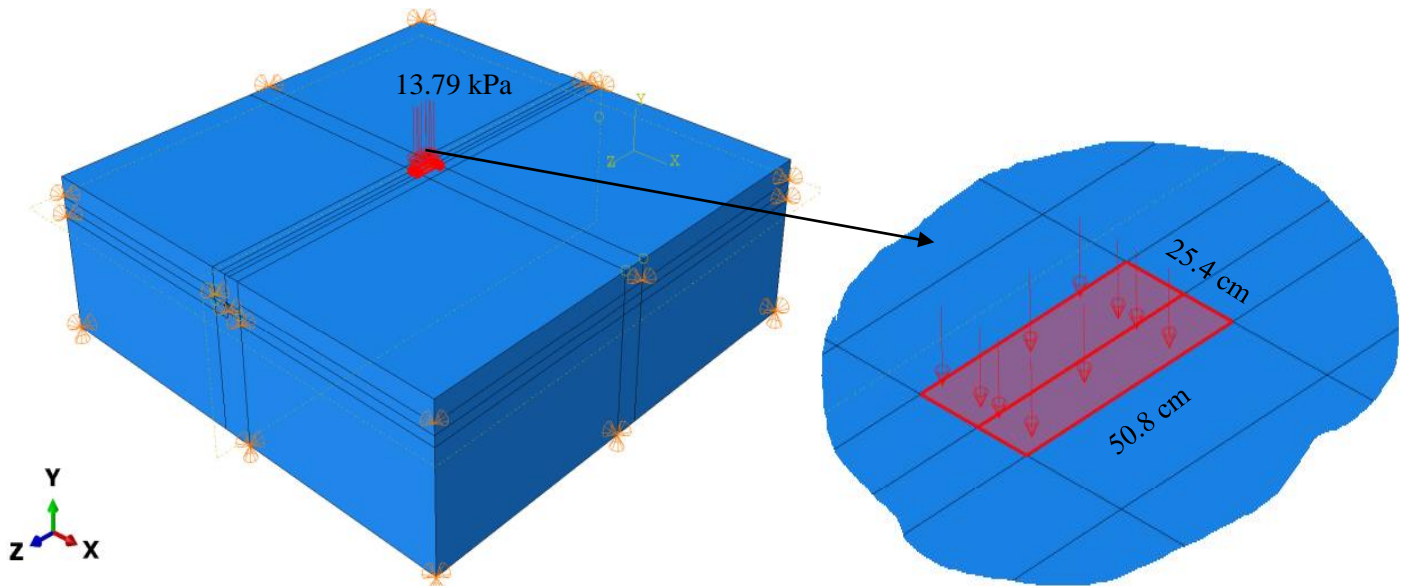


Figure 3.25 Loading step in the finite element model

3.5.2 Boundary Conditions

Different types of initial boundary conditions were applied for the trench model in the finite element analysis. The bottom boundary of the model was restricted from vertical and horizontal translations because it was assumed that the portion below 3m was assumed to be hard rock. Whereas, all the side boundaries were restricted only from horizontal translations. In addition to this, the two ends of the pipe were restricted from horizontal

translation in the longitudinal direction by considering the fittings at the end of the length of the pipe. All the boundary conditions are summarized in schematic view as shown in Figure 3.26 and the 3D view of the model with boundary condition applied on it is presented in Figure 3.27.

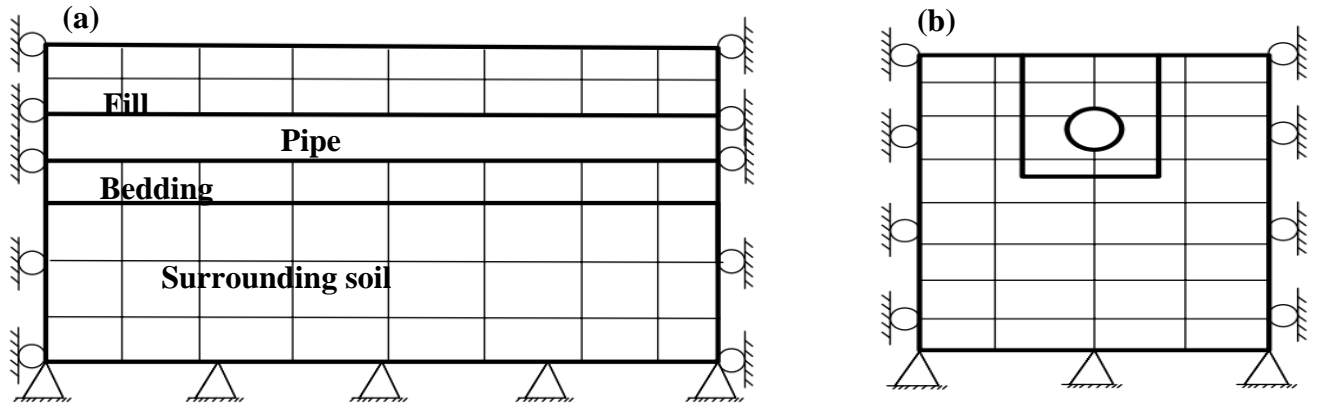


Figure 3.26 Schematic representation of trench model boundary conditions, (a) longitudinal section, (b) Crosssection

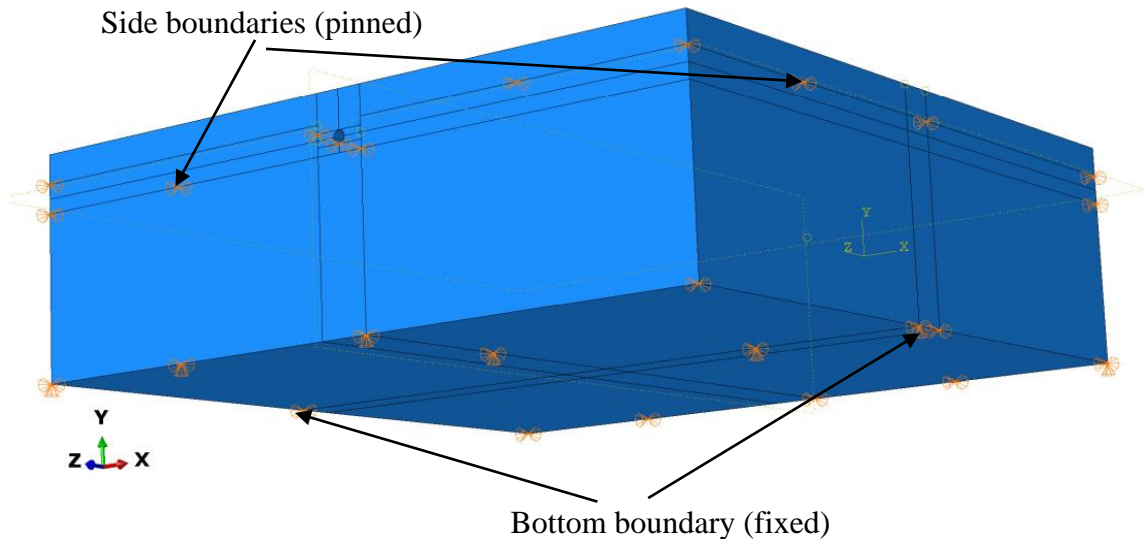


Figure 3.27 Boundary condition in the 3D model

3.6 Validation of the Methodology

As the finite element approach was selected to achieve the objective of this research, its accuracy and consistency should be checked. Therefore, in this section, the suitability of the Abaqus software for the analysis of buried pipe and its protection is assessed and verified. With all the features Abaqus has, it has been used by many geotechnical

researchers and it gave very similar result with the laboratory tests (e.g. Meguid et al., 2017; Anil et al., 2015; Abdollahi and Tafreshi, 2017; Negi and Singh, 2019).

There are several research works, which were conducted on buried pipes and their protection. Most of them used small-scale model tests. Among these researches, Beju and Mandel (2017a) was selected to verify the consistency of the methodology of this thesis. This is because of many reasons. The first one is its similarity in terms of the materials used. Most materials used in Bajju and Mandal (2017a) are similar to that of the material that was used in this thesis, but not identical. The second reason is that Bajju and Mandal (2017a) used a physical model test and the result of this test was validated in finite element software (Plaxis 3D). Therefore, it can be said that the result of this literature is accurate.

3.61 Basic Research Idea

The literature investigated and presented the results on the combined use of jute geotextile and EPS geofoam for the protection of buried HDPE pipes. It showed how these protections reduce the vertical stress on the pipe. Furthermore, different parametric studies were performed. The materials used in the study are shown clearly in Table 3.12. In addition to these materials, 1.33 mm thick jute geotextile with 502 g/m² mass per unit area and 146.8 kN/m tensile stiffness was used.

Table 3.14 Materials, used by Beju and Mandal (2017a)

Parameters	Fly ash	Stone dust	EPS geofoam(EPS 15)	Pipe
Material model	M-C	M-C	M-C	Elastic
Drainage type	Drained	Drained	Non-porous	-
Unit weight (kN/m ³)	14.2	22.6	0.15	9.57
Young's modulus (MPa)	4.6	4.8	2.77	816
Poisson's ratio	0.36	0.35	0.1	0.46
Cohesion (kPa)	15	13	32.25	-
Friction angle (°)	34	38	1.38	-
Thickness (mm)	-	-	40	4.2

3.6.2 Structural Model

In the selected literature, a small-scale trench model test was conducted. The whole physical model comprises the pipe, the bed and backfills, the protective materials and other sensors and measuring equipment as shown in [Figure 3.28](#).

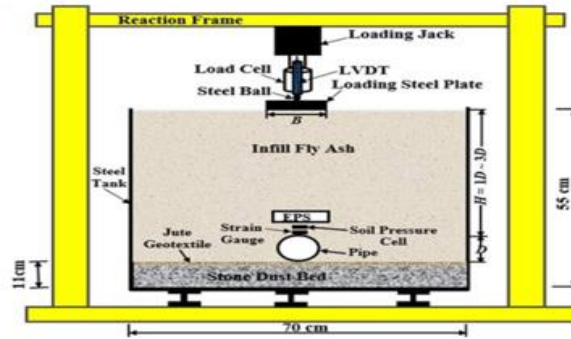


Figure 3.28 Schematic representation of model trench test set up (Beju and Mandel, 2017a)

3.6.3 Finite Element Modeling of the Model Trench Test

Using exactly the same material property and geometries of [Table 3.12](#), the model trench tests were simulated using a finite element software, Abaqus 6.0. The basic procedures of numerical analysis were used in the process. A sample finite element model of the trench with a pipe installed 3D from the top surface is shown in [Figure 3.29](#).

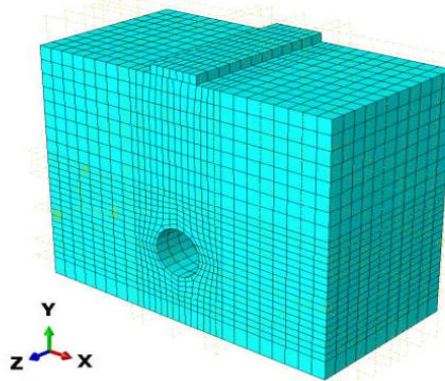


Figure 3.29 Finite element model of the model trench test

3.6.4 Comparison of the Model Trench Test and the Numerical Model

After the numerical analysis is completed, the results are compared with model trench test results. For comparison, settlement of the loading plate at the surface and the deflection of

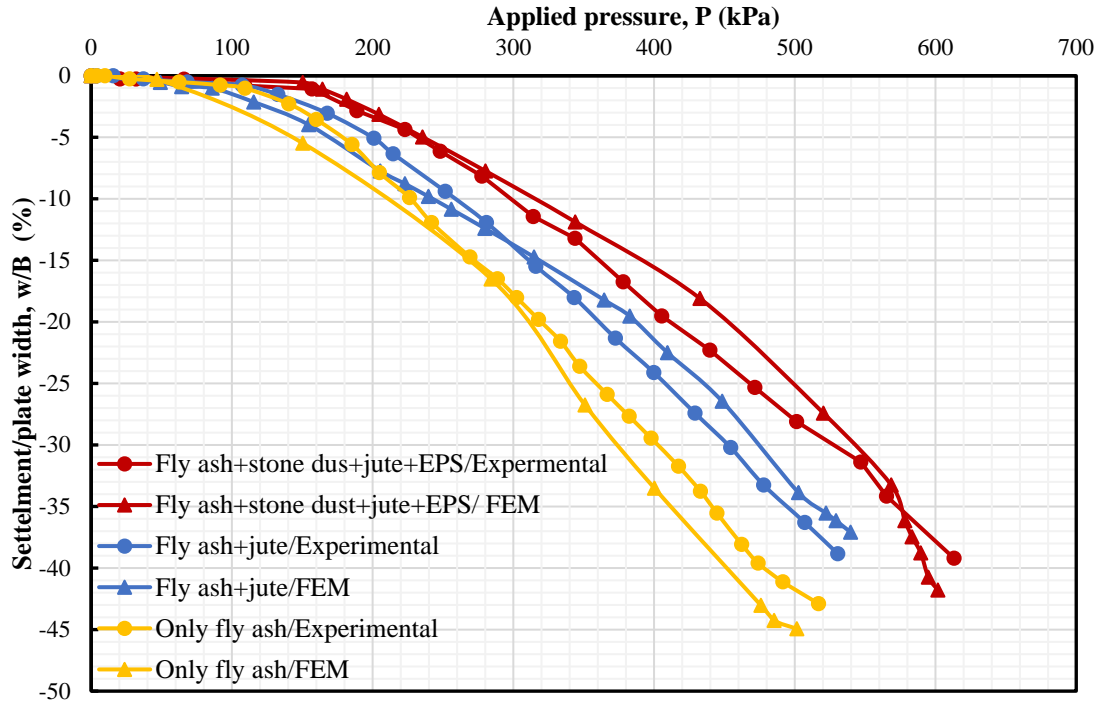


Figure 3.30 Comparison of the experiment and FEM results based on Variation of settlement ratio with the applied pressure

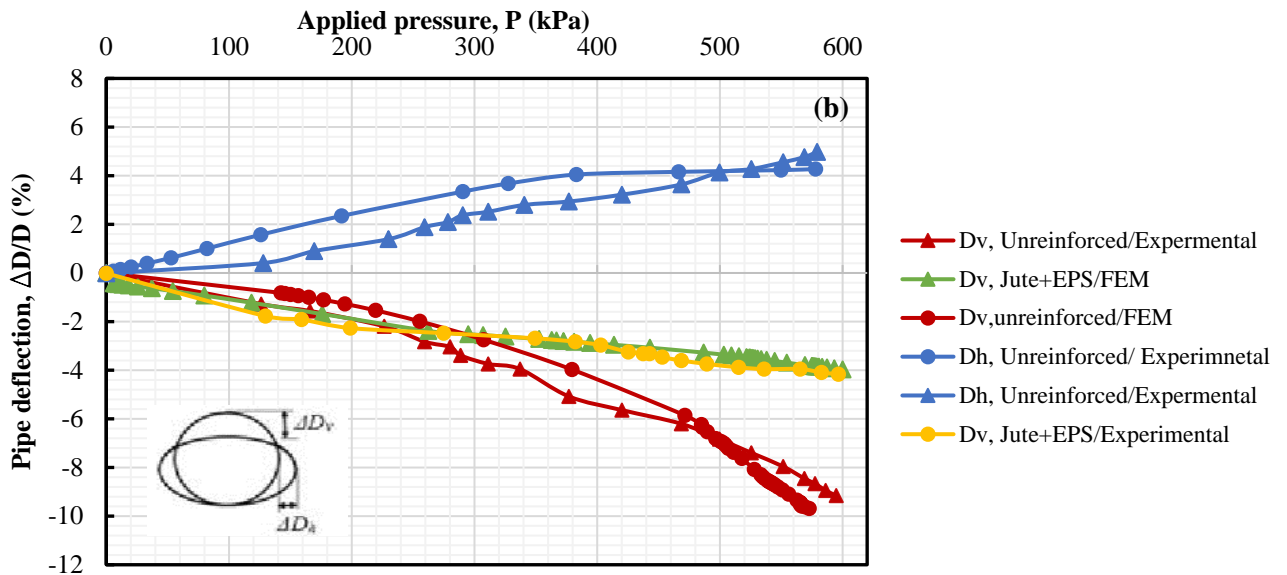


Figure 3.31 Comparison of the experiment and FEM results based on Variation of pipe deflection with applied pressure

the pipe were selected. As it can be seen from Figure 3.30 and 3.31, the results from Abaqus have good agreement with the physical test regarding the two parameters. The slight

difference possibly came from the accuracy level of the modeling software, from the mesh condition of the model, and other uncontrolled laboratory conditions. Generally, it can be said that Abaqus could be applied for similar studies.

Chapter 4

Result and Discussions

4.1 Introduction

This chapter covers all the results and the discussions of the research. The results and discussions are presented in different sub-titles. The first portion of this chapter discusses only the first nine base models, i.e., the results of unreinforced, reinforced, and EPS geofilm included trench models within three backfill materials were compared. Then, the results of different parametric studies were discussed accordingly. The parametric studies include the effect of pipe diameter, pipe stiffness, EPS geofilm location, EPS geofilm thickness, tensile stiffness of geotextile, and the number of geotextile layers. This chapter also includes the result and discussion on the combined effect of EPS geofilm and geotextile. In this research, each model was analyzed under the same bedding, embedment and backfill material. Therefore, in the discussions, the word 'fill' is used to express the whole bedding, embedment and backfill materials.

The default output of Abaqus is a function of time. This time express the percentage of loads which are applied at each increment up to hundred percent of the load is applied. Each step has its distinct time of load application. This will help to collect the results in separate steps. Since the main concern of this research is the condition of the pipe, the output should be started at a step where the direct force is started to be applied at the pipe. This is the embedment and backfilling step. However, it was the researcher's intension to discuss the response of the pipe with the wheel pressure at the surface. So all the graphs were drawn for the last step (for applied loading step). In these graphs, the vertical stress at the crown of the pipe did not start at origin of the coordinate. Because, the embedment and the backfilling steps already put the pipe in stress before the wheel load was applied. This can be seen clearly in sample time vs. vertical stress at the crown for the fly ash fill trench model in Figure 4.1.

Figure 4.1 shows a sample of time vs. vertical stress at the crown graph in different trench conditions for fly ash fill. All the plots in this figure have two segments. As it was explained earlier, the trench models simulate the actual loading condition by applying the geostatic

pressure and the wheel pressure in separate steps. The first segment, which is plotted up to the end of the first second, represents the vertical stress on the crown of the pipe due to the geostatic load from the fill materials and the second segment of the plots represent the vertical pressure variation on the crown of the pipe due to the wheel pressure. Therefore, for most of the discussions, only the second segment of the analysis was used.

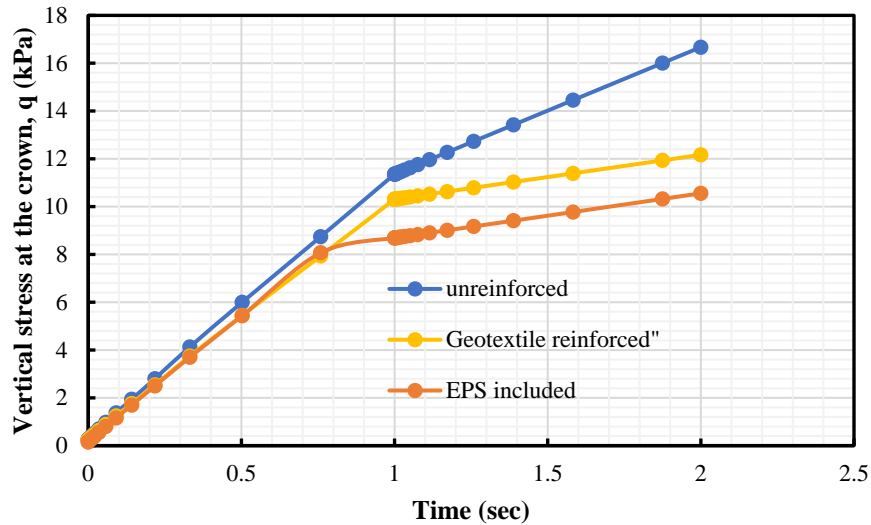


Figure 4.1 Vertical stress variation at the crown of the pipe with time (for fly ash fill)

4.2 Study on Base Models

In this section, the result of the first nine models (base models) is presented. Basically, these models could be divided into three categories based on the type of backfill used, i.e., stone dust, fly ash and soil. In each type of fill, three different models were analyzed. First, only pipes with fill materials without any protecting method were modeled. Second, EPS geof foam was included right above the pipe. Finally, the fill was reinforced with a single layer of geotextile at 0.3B below the surface. All the properties of pipe, EPS geof foam and geotextile used for this section were constant.

4.2.2 Vertical Stress on the top of the Pipe

In this thesis, the researcher intended to study the performance of the pipe regarding maximum stress around the pipe. Therefore, a critical area throughout the pipe should be found. This area should be a part of the pipe, which receives higher pressure than the rest part of the pipe. For this purpose, a sample radial stress around the pipe section, which was installed under fly ash fill, was drawn in a radar graph at the end of the analysis as shown

in Figure 4.2. Similarly, the vertical pressure at the crown along the length of the pipe was also compared for the same fill material as shown in Figure 4.3. From the combination of these plots, it is understood that the crown of the pipe received a higher amount of radial stress than the invert, spring lines and haunches of the pipe and maximum vertical stress at the crown was registered at the mid-section of the pipe. These results were not changed by the application of EPS geof foam or geotextile. Similar results were found in stone dust and soil fills. Therefore, from this moment onwards, most of the discussions were made based on the vertical stress on the crown of the mid-section of the pipe.

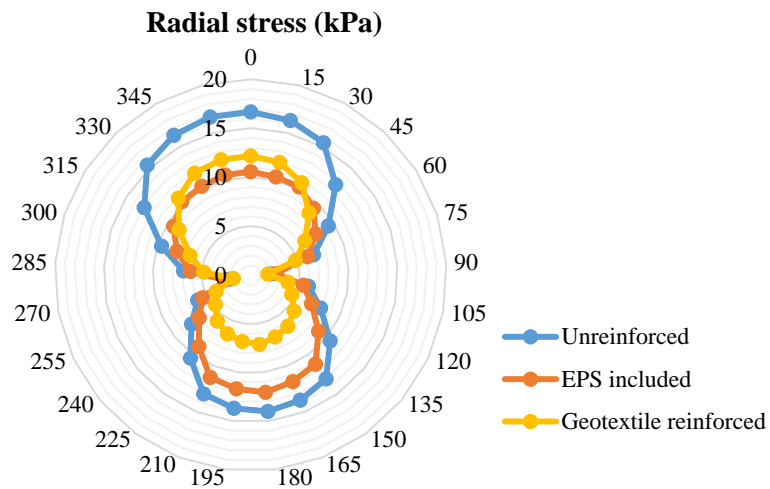


Figure 4.2 Variation of radial stress around the pipe in fly ash fill

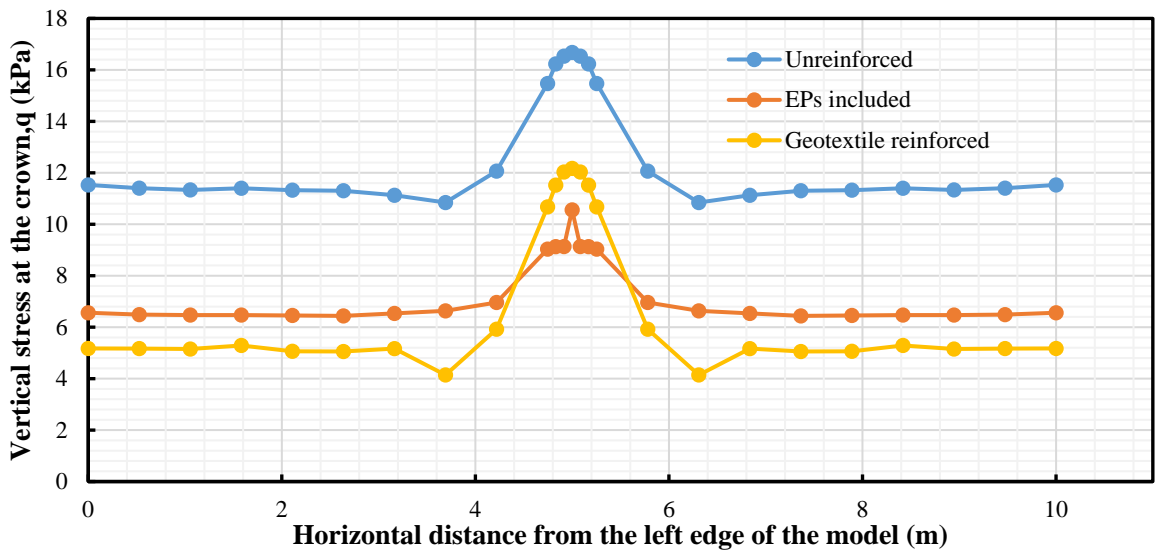


Figure 4.3 Variation of vertical stress at the crown of the pipe along the length of the pipe in fly ash fill

Figure 4.4 presents the variation of vertical pressure on the top of the pipe as the applied pressure (single wheel load) is increased in different fill materials under different trench conditions (unreinforced, EPS included and geotextile reinforced). In all three types of backfill materials, the pipe with the inclusion of EPS geofoam received the lowest amount of vertical stress when it is compared with the unreinforced and geotextile reinforced trenches. For 13.79 kPa applied pressure, the vertical stress at the top of the pipe with EPS geofoam inclusion was recorded as 10.557 kPa, 11.34 kPa, and 9.42 kPa under fly ash, stone dust and soil respectively. For clear understanding, the vertical stress on the crown of the pipe is presented in bar charts for all types of trench systems under three fill materials as shown in Figure 4.5. Based on these results, using EPS geofoam as a compressible inclusion material reduced the vertical stress on the top of pipe up to 36.67%, 40.1% and 34.3% in fly ash, stone dust and soil respectively when it is compared with the unreinforced case. Such reductions of vertical pressure with the inclusion of EPS geofoam were shown in different literatures (e.g. Kim et al., 2010; Kim et al., 2016; Ma et al., 2019; Meidani et al., 2018; Mohammed,2020). But, the magnitude of the effect of EPS geofoam in those papers is varied due to the location of the EPS geofoam, the pipe material and the loading condition.

The addition of single geotextile reinforcement to the trench at a depth of 0.3B, showed a reduction of vertical stress on the pipe crown as shown in Figure 4.4 and Figure 4.5. Quantitatively, 27.01%, 29.3% and 28.6% reduction of vertical pressure on the pipe crown were observed in fly ash, stone dust and soil fills respectively relative to the unreinforced trench cases. This reduction in vertical pressure at the crown was gained in totally different mechanism from the trenches with EPS included. The mechanism is discussed in section 4.2.5 of this paper. However, it is clearly seen that the amount of reduction in vertical pressure by a single geotextile reinforcement is lower than the reductions observed in EPS geofoam included trench models. Furthermore, it is observed that the effectiveness of geotextile reinforcement is directly related to the loading condition. Because, the reinforcement action of geotextile is mobilized more with increasing pressure. That is why the plots of vertical stress under geotextile reinforced models in Figure 4.4 departed more from the plots of unreinforced models as the applied pressure increased.

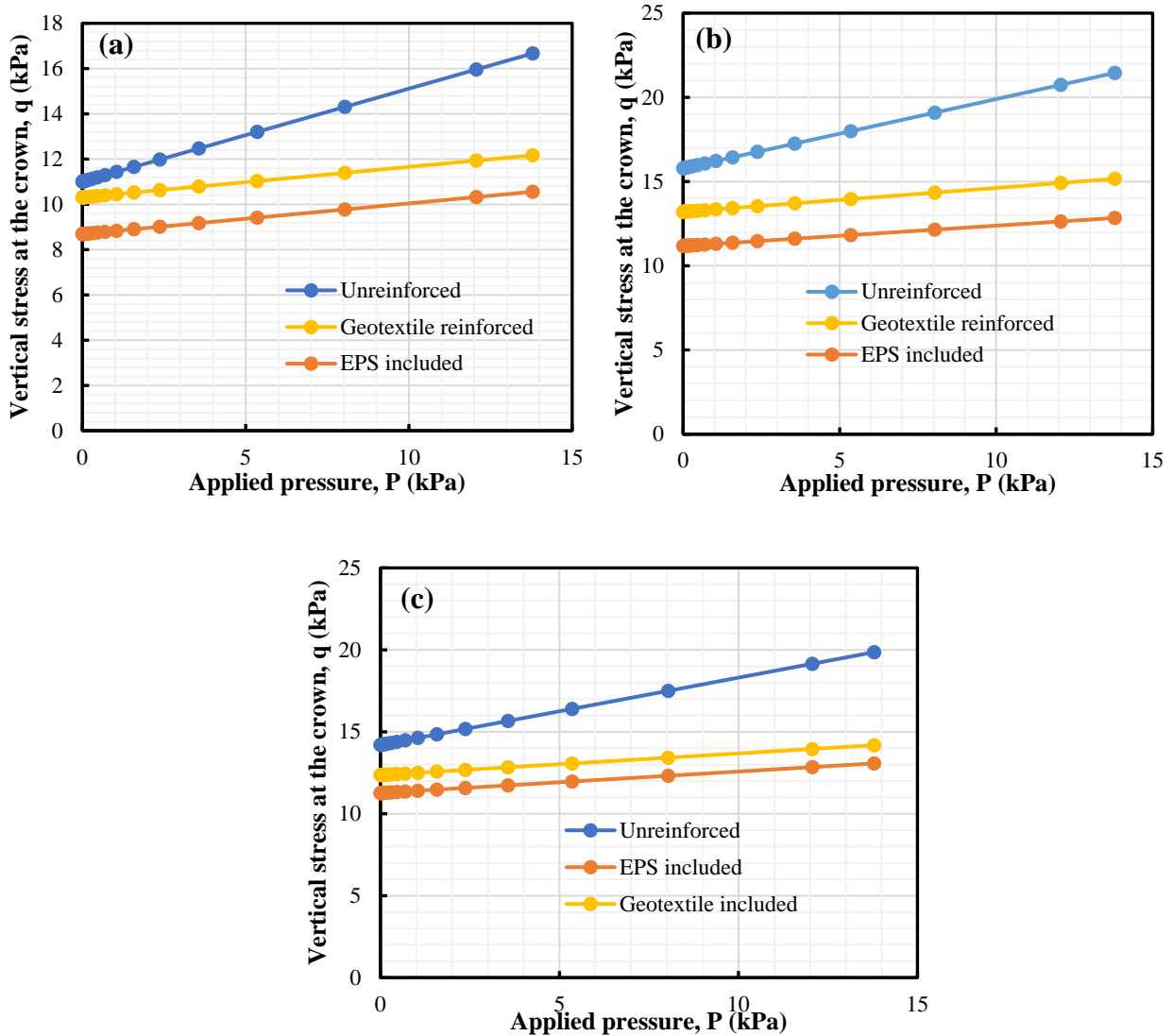


Figure 4.4 Variation of vertical pressure at the crown of the pipe in different backfills (a) fly ash, (b) stone dust and (c) soil

When the vertical stresses are compared based on the fill materials, significant variation was not observed despite the use of EPS geof foam or geotextile. Figure 4.5(a) and 4.5(b) present the vertical stress on the crown of the pipe under different backfills in such a way that the comparison becomes easy. According to Neya et al. (2017), for shallow burial depth, fill materials with a higher value of modulus of elasticity transfer a much lower amount of pressure to the pipe compared with fills with a lower value of modulus of elasticity. This condition will be changed and the effect of mechanical property of fill material becomes insignificant as the burial depth of the pipe gets higher. But in this

research, the pipe under high modulus of elasticity (stone dust fill) received higher amount of vertical stress. As it was explained earlier, the dry density of stone dust is slightly higher than the other fill material which was used in this research. So it will have higher geostatic pressure than the other fill materials. But once the geostatic pressure is applied, the effect of modulus of elasticity explained by Neya et al. (2017) could be observed. Since the amount of applied load used in this research is small, the results are more affected by the weight than the modulus of elasticity of the fill material. That is why the pipe under stone dust fill receives higher amount of vertical stress in all trench conditions (unreinforced, reinforced and EPS included).

In the present research, the difference in vertical stress ratio of the pipe in each fill material under different trench conditions laid below 5%. This condition strengthens the idea of using stone dust and fly ash as an alternative fill material for conventional soils.

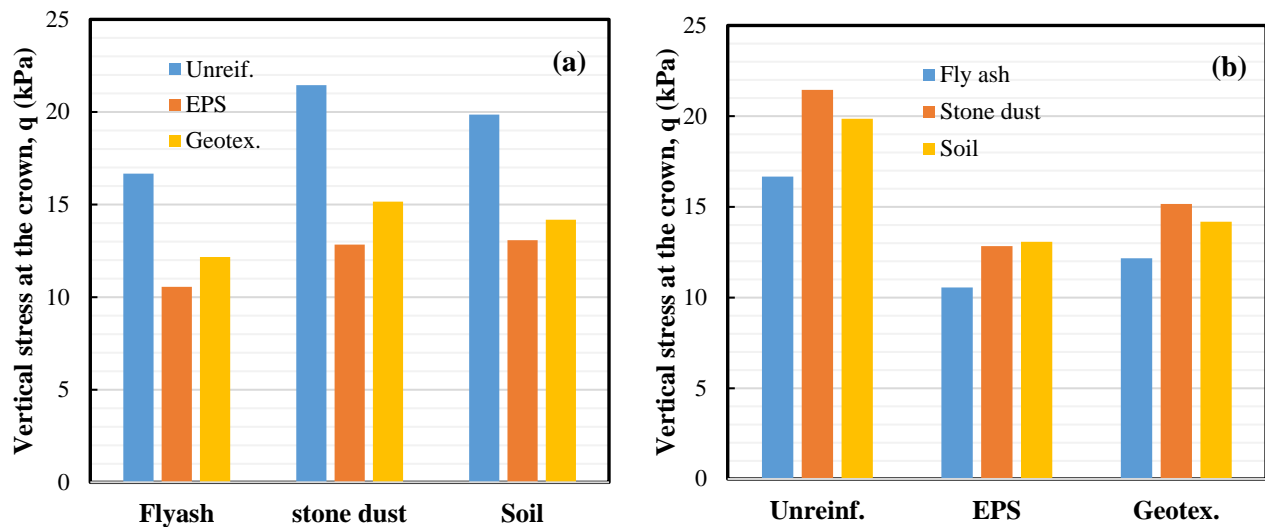


Figure 4.5 Comparisons of stress ratio on the crown for different fill materials

4.2.3 Circumferential Strain

Circumferential strain is a worthy parameter to express the effect of external and internal loads on the wall of the pipes. It is expressed by the horizontal strains at the crown and invert of the pipe, the vertical strains at the spring lines and tangential strains at shoulder and haunch areas. It is developed by the bending stress and wall thrust at the wall of the pipe. Therefore, in this research, the circumferential strain on the external face of the midsection of the pipe was collected from the finite element analysis and it is drawn in a

radar plot as shown in Figure 4.6. In this figure, the strain (ε) was represented in dimensionless units of microstrain ($\mu\varepsilon$), where 1000 $\mu\varepsilon$ equals 0.1% strain and compressive strains (inward strain towards the center of the pipe) were taken as negative. Based on this figure, the pipes, which were modeled with EPS geofoam inclusion, showed lower strain at the crown and the two spring lines than the unreinforced and geotextile reinforced models. However, the effect of EPS geofoam was lowered at the invert of the pipe because unlike the upper side of the pipe, the upward pressure from the foundation bed was directly transferred to the pipe. This condition could be improved by using additional EPS geofoam blocks under the the pipe. Similarly, the walls of the pipes in geotextile reinforced trench models showed lower strain throughout the perimeter of the pipe than unreinforced cases. The type of backfill in which the pipes were installed did not bring a significant difference in the values of the strain because the backfills considered in this thesis have comparable shear strength.

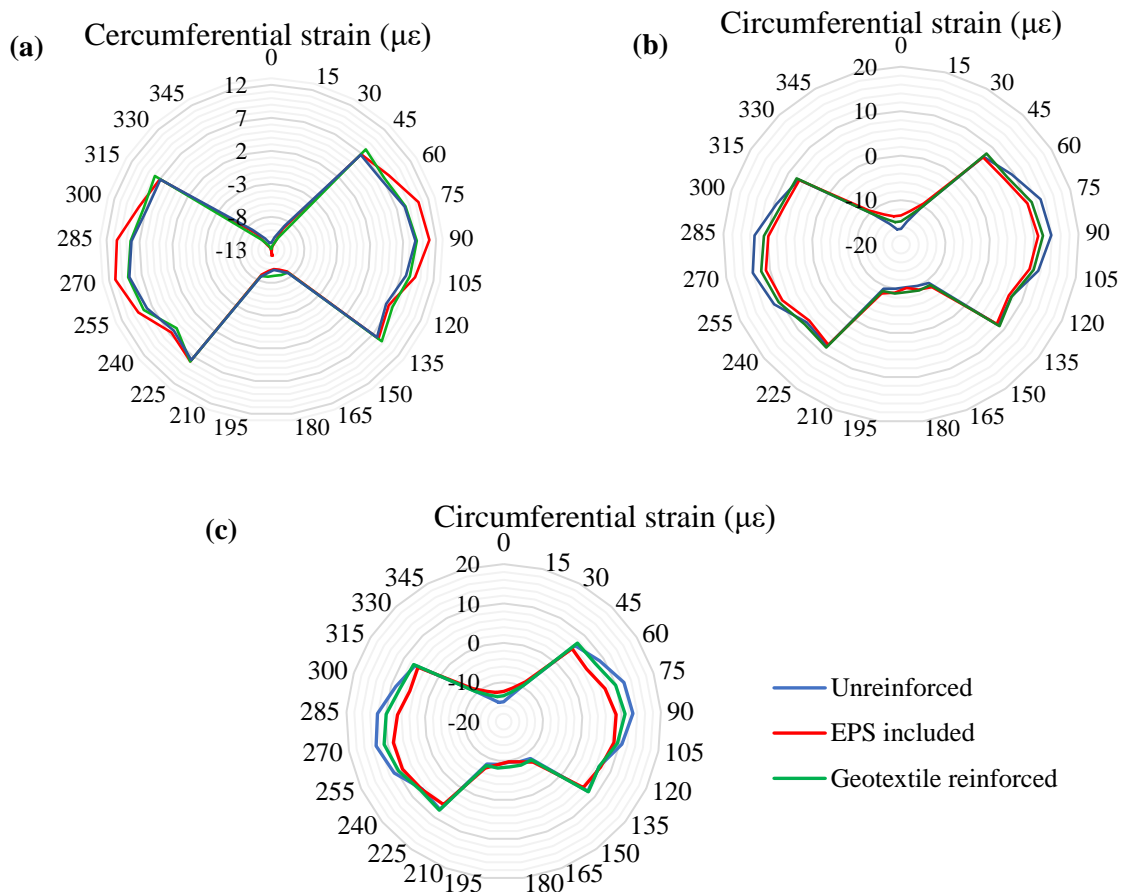


Figure 4.6 Circumferential strain (a) in fly ash fill, (b) in stone dust fill and (c) in soil fill

4.2.4 Performance of EPS Geofilm

As it was explained earlier, EPS geofilm works its magic with its high compressibility. At the end of the analysis, the center of EPS geofilm was found deformed 16.7 mm, 17.9 mm and 19.3 mm in fly ash, stone dust and soil fill respectively. This indicates that the EPS geofilm deformed almost equally in those three backfill materials except there was a slight difference due to the weight of the backfill materials. This result strengthens the idea that EPS geofilm behaved in a similar way in the three backfills.

At the end of the analysis, the thickness of EPS geofilm reduced up to 19.6% of the original thickness and the top surface of the EPS geofilm settled up to 12.4 mm, 12.8 mm and 13.4 mm in flash, soil and stone dust fills respectively. That is about 14% higher than the adjacent soil prism/fill prism which was at the same horizontal plane before loading and which is within the width of the loading plate. The difference in settlement arose from a higher compressible property of EPS geofilm than the compacted side fill. This differential settlement initiates the transmission of shear stress between the two differentially settling soil masses, which is called arching according to Terzaghi (1943). This condition is shown in Figure 4.7. In this figure the concave downward shape at the center of the EPS geofilm was created due to higher stiffness valued of the pipe more than the fill materials. Therefore, it is possible to say, the reduction in vertical stress on the pipe due to the inclusion of EPS geofilm came from this positive arching.

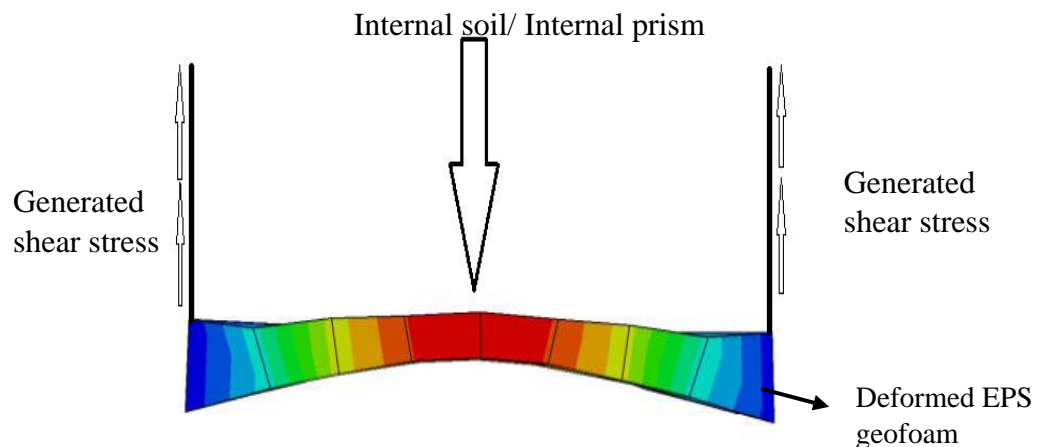


Figure 4.7 Performance of EPS geofilm

4.2.5 Performance of Geotextile

It was explained in section 2.51, the reinforcement function of geotextile is met through a membrane and confining effects. To mobilize that membrane and confining effect of geotextile, some amount of settlement is needed. Figure 4.8(a) presents the deformed (strained) shape of sample geotextile in the fly ash fill model after the analysis was finished. If the reinforcement action needs to be mobilized, the deformation of the geotextile should not be created by sliding between the fill surfaces. Most of the time, this sliding is created when the friction between the fill material and the geotextile is not good enough to resist the movement. If this is the case, the desired tension on the reinforcement material will not be created. Then, the anticipated membrane and confining effects, to create reinforcement, will not be mobilized. In the present study, the settlement of the geotextile was not created by sliding only. If the geotextile was settled simply by sliding, the horizontal strain of the geotextile surface would be zero and the colour contours of displacement shown in Figure 4.8(a) would have been coded in a single color. Again, Figure 4.8(b) showed how the center of the geotextile tensioned at the end of the analysis along the center of the geotextile in different backfills (at section A-A). Section A-A, in Figure 4.8(a), was drawn perpendicular to the length of the pipe. Generally in the analysis that involves geotextile, there was a settlement and this settlement created horizontal stress on the surface of the geotextile membrane. This condition met the criteria to initiate one of the reinforcement mechanisms by geosynthetic as explained by Shukla (2016). Therefore, it can be said that the vertical stress reduction on the pipes and the surface settlement reduction in trench models with the geotextile layer came from the reinforcement action of the geotextile.

The reinforcement effect of the geotextile was observed in all types of backfills almost in similar magnitude. However, to compare the effectiveness of the reinforcement material in each type of fill material, Figure 4.8(b) could be considered. As it can be seen, the geotextile in stone dust fill showed a relatively higher amount of stress than the geotextile in the other fill materials. This was happened because of the fact that stone dust has a relatively higher value of friction angle due to sharp-edged particles. This will create higher interface friction between the geotextile and fill and mobilizes more reinforcement action.

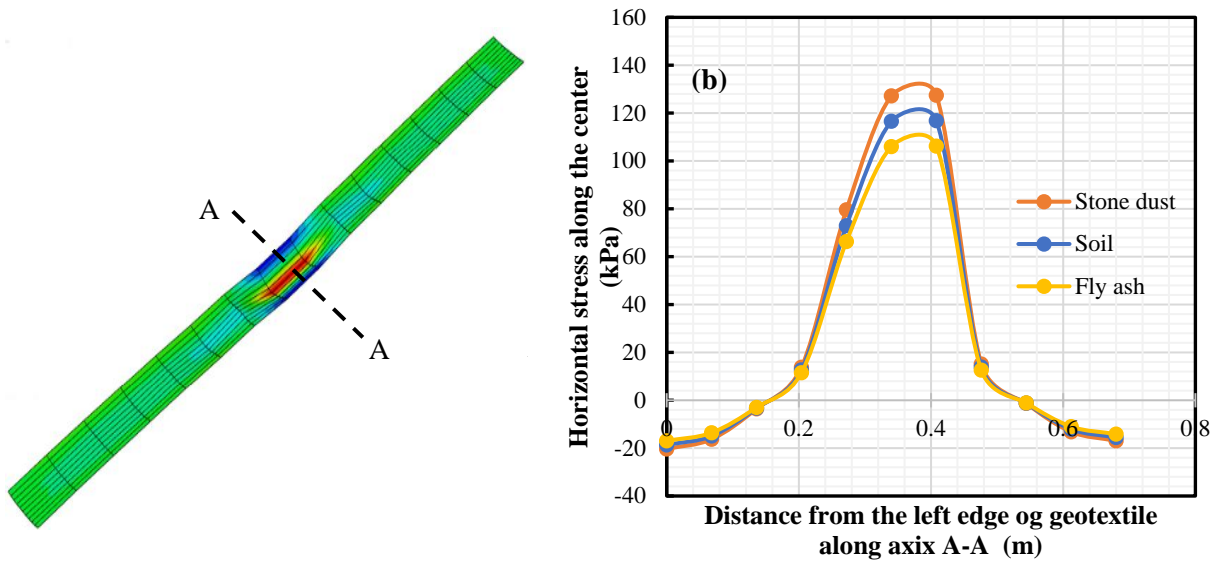


Figure 4.8 Performance of geotextile (a) Sample strained geotextile reinforcement surface, (b) Variation of horizontal stress along section A-A

4.3 Parametric Study

4.3.1 Effect of Pipe Diameter

Pipes are fabricated in different diameters and dimensions depending on the desired function. Diameter directly affects the stiffness of the pipe. When we see the pipes in the market, as the diameters are changed, the thickness of the pipe will also be changed. This will help to treat the difference in stiffness, which arises from diameter change. In this section of the paper, the effect of diameter in different cases is discussed from the results of finite element analysis. For this purpose, four different commercial pipe diameters were considered as it was shown in Table 3.6. These four types of pipes were modeled under three fill materials (fly ash, stone dust, and soil). The analysis was repeatedly made in geotextile reinforced and EPS included trench systems. To see the effect of diameter, other parameters like depth of cover, loading condition and property fill materials were kept constant as the base models. In addition to this, the property of additional materials (EPS geof foam and geotextile) and way of utilization were kept similar. This way, a total of 36 models were analyzed.

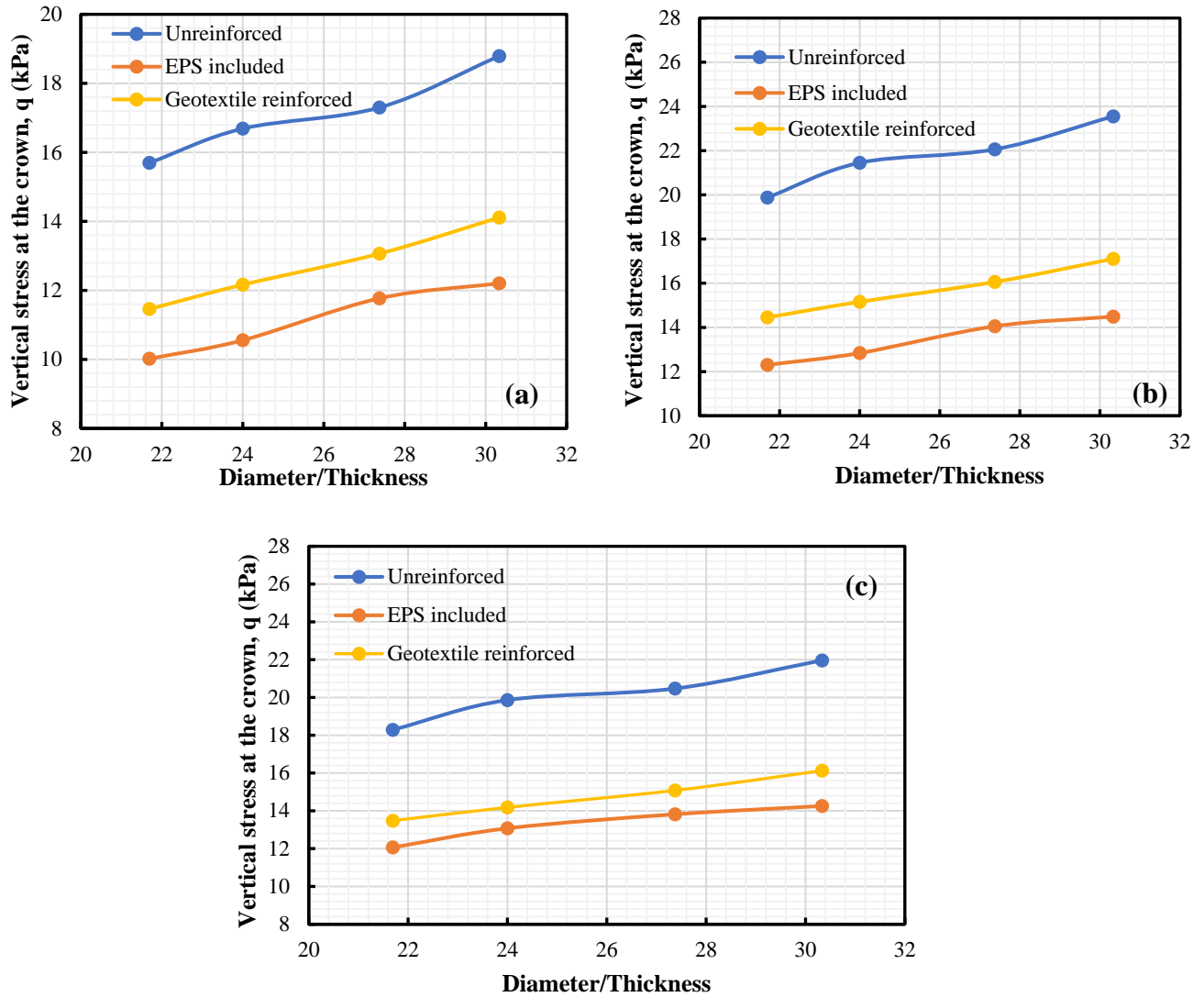


Figure 4.9 Variation of vertical stress ratio with pipe diameter to thickness ratio
(a) fly ash, (b) stone dust, and (c) soil

Table 4.1 Summary of stress ratio results on the crown for minimum and maximum diameter pipe in different trench conditions under (a) in fly ash, (b) in stone dust, (c) in soil

(a) Trench model (fly ash)	Vertical Stress (kPa)		Increment in percentage
	141 mm diam	273 mm diam	
unreinforced	15.696	18.79	19.7
EPS included	10.021	12.206	21.8
Geotextile reinforced	11.461	14.111	21.3

(b) Trench model (stone dust)	Vertical Stress (kPa)		Increment in percentage
	141 mm diam	273 mm diam	
unreinforced	19.876	23.550	18.4
EPS included	12.304	14.489	17.7
Geotextile reinforced	14.454	17.104	18.3

(c) Trench model (soil)	Vertical Stress (kPa)		Increment in percentage
	141 mm diam	273 mm diam	
unreinforced	18.286	21.960	20.1
EPS included	12.065	14.254	18.1
Geotextile reinforced	13.476	16.126	19.6

a. Results in Unreinforced Trench Models

The results of all the analyses were presented in Figure 4.9. In all three backfill materials, the plots of vertical stress (q) vs. pipe diameter to thickness ratio (D/t) of unreinforced cases laid above the reinforced cases. Moreover, as the diameter to thickness ratio of the pipes increased, a higher amount of vertical stresses at the pipe crown was recorded. When the diameter of the pipe increased from 141 mm to 273 mm or as the diameter to thickness ratio increases from 21.69 to 30.33, the vertical stress at the crown of the pipe raised by 19.7 %, 18.4% and 20.1% in fly ash, stone dust and soil fills respectively. This increase in vertical pressure due to higher pipe diameter, shown in Figure 4.9, came from the difference in the width of the soil prism above the pipe. According to Spangler and Handy (1982), the soil arch (soil column) has a width equal to the diameter of the pipe. Therefore, as the diameter increases, the width of this soil arch will also increase and the weight of the fill over the pipe per unit length will be high. This will increase the vertical stress on the crown of the pipe. Another reason for higher vertical stress for larger diameter pipes was the variation of stiffness in the pipes. It was found that those larger diameter commercial pipes, which were used in the analysis, have higher stiffness than lower diameter pipes because of the increase in thickness with the diameter. This condition will make the stiffer pipe to experience a higher amount of load due to negative arching.

b. Results in Geotextile Reinforced and EPS Geofoam Included Models

As the plots in Figure 4.9 show, the increase in diameter of the pipe, which was installed in geotextile reinforced and EPS geofoam included trenches, caused the vertical stress at the crown to go higher. The rise in vertical stress was expected due to the increment of soil column width with pipe diameter as discussed previously. When we compare this increment with the increment, which was recorded in unreinforced cases, it is almost similar for geotextile reinforced models as shown in Table 4.1. As the diameter of the pipe increased from 141 mm to 273 mm or as the diameter to thickness ratio increase from 21.69 to 30.33, the vertical stress at the top of the pipe increased by 21.3%, 18.3% and 19.6% under geotextile reinforced fly ash, stone dust and soil fills respectively. This indicates that the diameter of the pipe did not bring a significant effect on the performance of the geotextile reinforcement. Similarly, the inclusion of EPS geofoam to those different diameter installed trench did not bring significant change on the final result of the vertical stress at the crown of the pipe. As it can be seen clearly in Table 4.1, changing the diameter from 141 mm to 273 mm caused the vertical stress at the crown to rise by 21.8%, 17.7% and 18.1% in fly ash, stone dust and soil fill respectively.

4.3.2 Effect of Pipe Stiffness

In this section, the effect of pipe stiffness on reinforced and unreinforced trench systems under a stone dust fill is discussed. The discussion was made from the results of finite element analysis. For this purpose, five different types of commercial pipes with the same diameter were considered. These are two steel pipes with 200 GPa and 75 GPa modulus of elasticity, a fiberglass reinforced plastic pipe (FRP), a high-density polyethylene plastic pipe (HDPE) and a low-density polyethylene plastic pipe (LDPE). These pipes were selected from the perspective of their difference in modulus of elasticity and their wide range of applications in the pipeline industry. The stiffness of the pipes was determined by an empirical formula (Equation 4.1) as per ASTM standard (ASTM D2412-11) as shown in Table 4.2. Table 4.2 also shows other material properties needed in finite element modeling. All the five pipes were analyzed in unreinforced, geotextile reinforced and EPS included trench cases. The same loading and boundary conditions with the base models were applied.

$$PS = 6.72EI/r^3$$

Equation 4.1

Where PS is pipe stiffness in GPa; E is the modulus of elasticity of the pipe material in kPa; I is the moment of inertia of the pipe wall per unit length in m⁴/m and r is the mean radius of the pipe in m.

In unreinforced cases, one of the steel pipes, which is less flexible, showed a slightly higher amount of vertical stress on the top of the pipe than the other pipes. As clearly indicated in Figure 4.10, a significant difference in vertical pressure was observed when the stiffness of the pipe jumps from 3.7 GPa to 0.118 GPa. Then, the drop in vertical pressure continued slightly for 0.04 GPa pipe stiffness. Quantitatively 16.67 kPa and 6.32 kPa vertical stress at the crown was recorded for 29.6 GPa and 0.037GPa stiffness pipes respectively. That means carbon steel pipe received higher vertical stress than the LDPE pipe. This reduction of vertical pressure in the LDPE pipe came from the positive arching action, which was induced due to the deflection of the flexibility of the LDPE pipe. A similar contribution of positive arching for flexible pipes was also recorded in Kim (2010).

When the trench was modeled with a single geotextile reinforcement at 0.3B, all the pipes experienced lower vertical stress at the crown section than the unreinforced case. Like the unreinforced case, in geotextile reinforced trench, the vertical pressure on the top of the pipe reduced as the stiffness of the pipe decreased. In the case of carbon steel pipe, the installation of geotextile reduced the vertical pressure at the top of the pipe from 16.67 kPa (in unreinforced case) to 12.85 kPa, i.e., a 27.01% drop. Similarly, the vertical pressure ratio at the top of the LDPE pipe reduced from 6.32 kPa to 4.354 kPa due to the installation of single geotextile reinforcement. That is also a 31.11% drop. From these results, it can be noticed that the reinforcing mechanism of the geotextile was not significantly influenced by the stiffness of the pipe. However, this condition might be changed as the pipe and the geotextile are installed closer to each other. This is because of the fact that as the vertical difference between pipe and geotextile is reduced, the upward pressure from the pipe to the geotextile will increase. This will neutralize the tensile stress created on the surface of the geotextile due to the vertical pressure above it.

As the third plot in Figure 4.10 illustrates, the vertical stress on the top of the pipe, which was installed under the inclusion of EPS geofoam, showed a similar pattern with the

unreinforced and geotextile reinforced trench cases. Quantitatively, a 7.178 kPa vertical stress difference was observed between the carbon steel and the LDPE pipe. That is about 6% higher than the unreinforced case. This shows that the stiffness of the pipe has little effect on the performance of the EPS geofom.

Table 4.2 Summary of stiffness of different pipes

Pipe type	Density (kg/m ³)	E (MPa)	Poission's ratio	PS (GPa)
Carbon steel	7850	200	0.3	29.59696
Cast iron	7850	75	0.3	11.09886
FRP	1950	25	0.35	3.69962
HDPE	970	0.9	0.46	0.118388
LDPE	910	0.25	0.46	0.036996

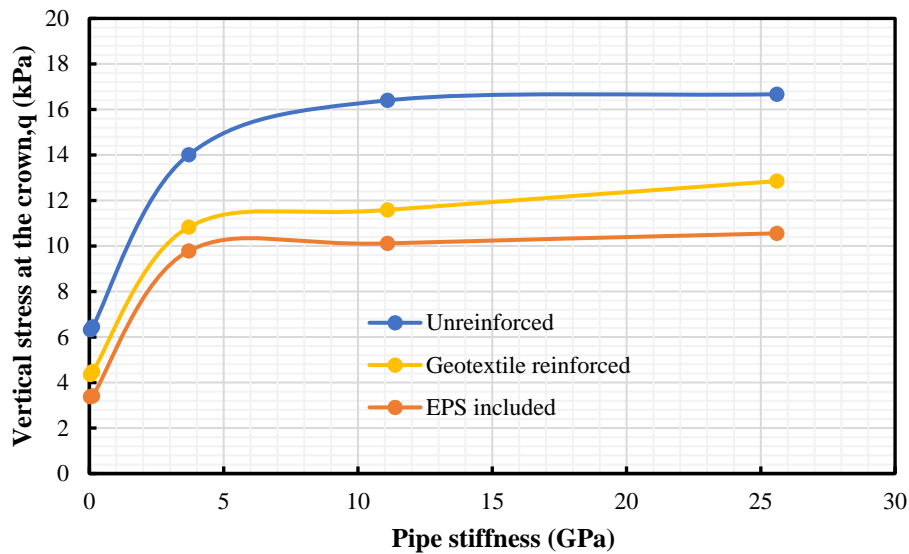


Figure 4.10 Variation of vertical pressure ratio for different pipe stiffness values

4.3.3 Effect of EPS Geofom Thickness

In this section of the paper, the effect of thickness of EPS geofom on the performance of the pipe and the whole trench model is discussed based on the results from the finite element analysis. A single layer of four different thicknesses of EPS geofom blocks was considered, i.e., 20 mm, 40 mm, 60 mm and 80 mm. The rest of the materials and geometrical model of the trench including the boundary and loading conditions were similar to the base model, except the analysis was conducted only in fly ash backfill.

As the results in Figure 4.11(a) indicates, the vertical pressure on the crown of the pipe decreased as the thickness of EPS geofoam increased. At the end of a single ASHTO SH-25 loading, the vertical stress on the top of the pipe reduced from 11.03 kPa to 9.24 kPa when the thickness of EPS geofoam increased from 20 mm to 80 mm. To make the comparison clear, the vertical stress versus the thickness of the EPS geofoam graph is plotted as shown in Figure 4.11(b). Based on this plot, changing the thickness of EPS geofoam from 20 mm to 80 mm brought a 16.24% reduction in vertical stress on the crown. From this result, it can be understood that higher thickness EPS geofoam in trench system contributed to an additional arching effect. However, as the thickness of the EPS geofoam increased it may cause higher amount of settlement at the surface, especially in high loading conditions. So special attention is needed when applying higher thickness EPS geofoam blocks geotechnical sites. A similar reduction of vertical pressure on the pipe and increment of settlement at the surface due to higher EPS thickness blocks were also observed in Beju & Mandal (2017a) when they were working on the protection of a flexible pipe.

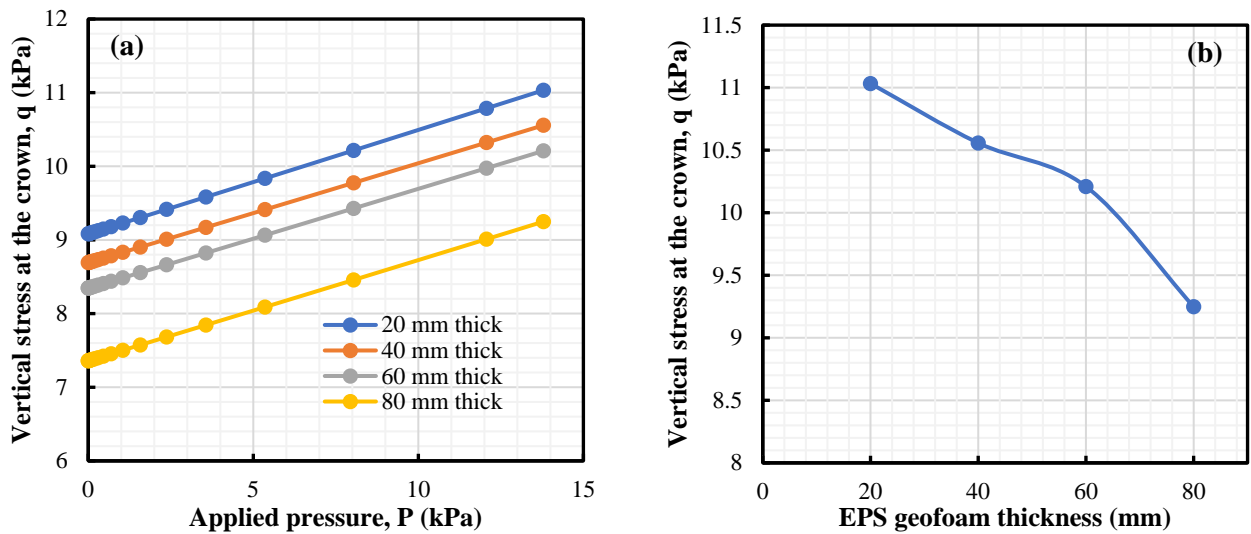


Figure 4.11 Effect of EPS geofoam thickness on the performance of the trench
 (a) Vertical stress – applied pressure curve, (b) Comparison of maximum vertical stress for different thickness EPS geofoams

4.3.4 Effect of EPS Geofoam Location

This section of the paper presents the results and discussions on the effect of the location of a single EPS geofoam block on a pipe, which is installed at 3D from the surface of the

trench. The analysis was conducted using 40 mm thick EPS15 geofoam in a fly ash fill. The location of the EPS geofoam was varied from 0D (directly at the top of the pipe) to 0.75D from the top of the pipe. The rest of the material properties, the geometries and the loading conditions were kept the same with the base model.

Figure 4.12 presents the results of the analysis with different EPS locations. This result shows that as the EPS geofoam block was installed far from the top of the pipe, the vertical stress at the crown increased, i.e., as the EPS geofoam distance from the top of the pipe varied from 0 to 0.75D, the vertical stress increased from 9.49 kPa to 11.96 kPa. This indicates that the pipe with EPS geofoam closer to it will experience lower vertical pressure on its crown because the length on which the shear force is going to be mobilized will be decreased as the EPS geofoam is installed far from the top of the pipe. Based on the above results, EPS geofoam which was installed directly at the top of the pipe performed better regarding both vertical pressure and surface settlement. Therefore, for shallow trenches, it is recommended that EPS geofoam should be installed on the top of the pipe or very closed to the pipe. Similar results were found in literatures regarding the location of EPS geofoam. For example, according to Beju and Mandel (2017a), EPS geofoam performed better when it was placed below 0.2D from the top of the flexible pipe, which was installed 2D from the surface.

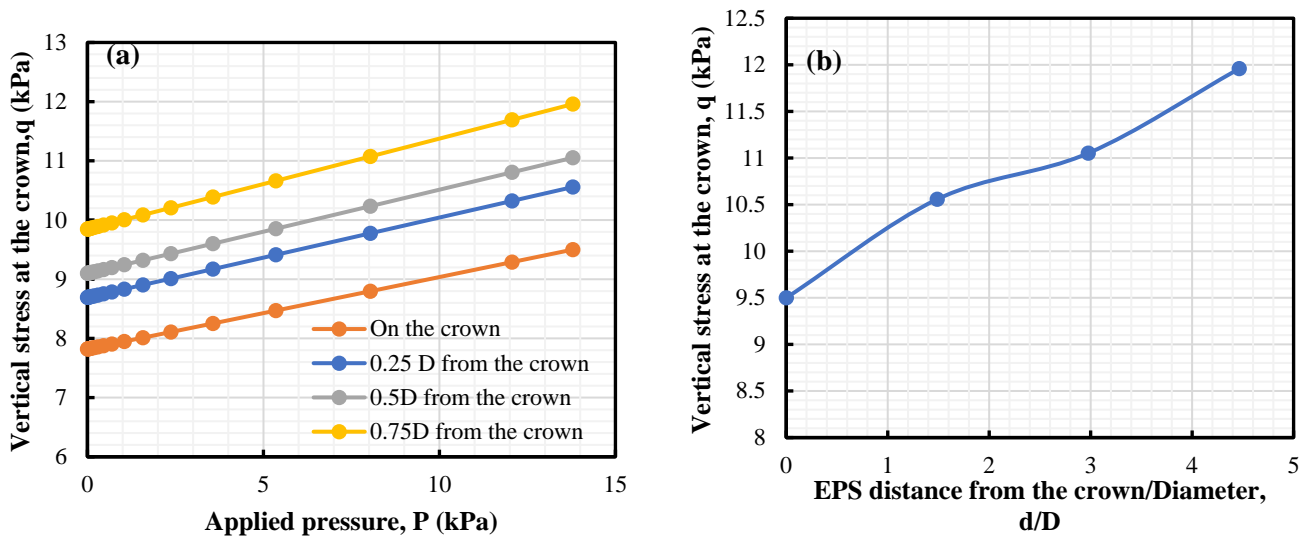


Figure 4.12 Effect of EPS geofoam location on the performance of the trench
 (a) Applied pressure- vertical stress on the crown for different locations of the EPS geofoam, (b) Comparison of vertical stress ratios for different EPS geofoam locations

4.3.5 Effect of Double Layer of EPS Geofoam Blocks

Like the rest of geosynthetic materials, EPS geofoam can be used in trench systems in multiple layers. Therefore, effect of applying different number of layers must be studied. In this section of the paper, the effect of double layer of EPS 15 geofoam block with constant width and thickness, i.e., 1.5D width and 40 mm thick is investigated under fly ash fill numerically. While applying double layer of EPS geofoam for a trench, the spacing between the two blocks must be selected carefully. In the present study, the bottom layer of EPS geofoam block was installed at 0.25D from the top of the pipe and the second block was positioned at four different locations so that the spacing between the two blocks becomes 0.25D, 0.5D, 0.75D, 1D and 1.5D. All the rest of the parameters needed for the finite element analysis were kept constant like the models, which were explained in section 4.2 of this paper.

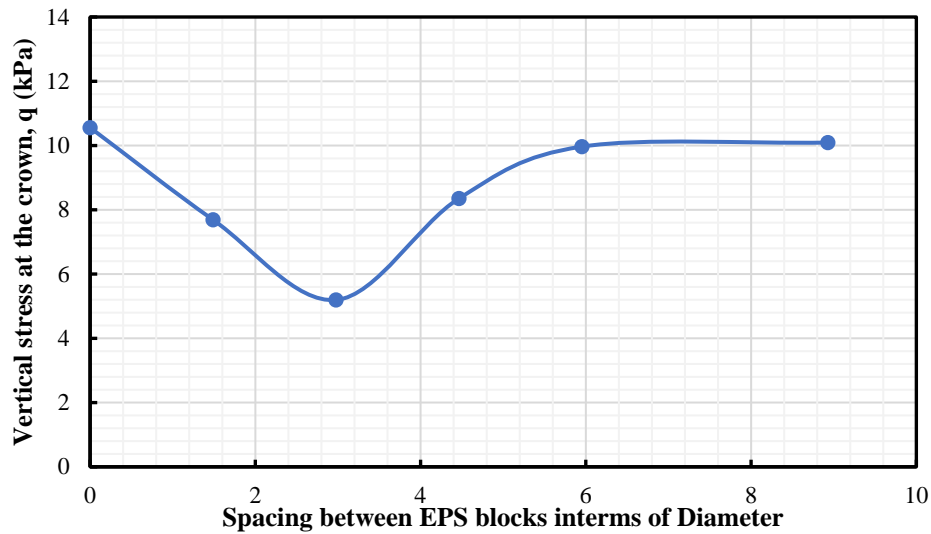


Figure 4.13 Comparison of maximum vertical stress at the crown for different spacings of double EPS geofoam,

The results of the analysis are presented in Figure 4.13. This figure shows the variation of vertical pressure on the crown of the pipe with the spacing of EPS blocks to the diameter ratio. For comparison purpose, a result of a trench model with a single EPS geofoam is inserted in the plot by taking the ratio of spacing and diameter of the pipe as zero. As it can be noticed in this plot, all the pipe with double layer of EPS geofoam block experienced lower amount of vertical pressure on the crown. However, the effect of spacing between

the EPS blocks went in two ways. First, when the spacing increased, the vertical stress on the crown of the pipe decreased. But after 0.5D spacing, additional increase caused the pipe to receive higher vertical stress. The second case might be different if the pipe was buried at deeper positions. Because both EPS geofabric blocks will have enough distance to mobilize the full shear strength along the sides of the soil prisms. From literatures, Kim et al. (2010) investigated that for shallow trench condition, double layer of EPS with the spacing equal to the pipe diameter is more beneficial than a single layer of EPS to reduce the earth pressure.

4.3.6 Effect of Tensile Stiffness of Geotextile Reinforcement

As it was explained earlier, the reinforcement function of geotextile arises from its tensile strength. Therefore, it is obvious to assess the effect of tensile stiffness of the geotextile on the performance of buried pipes. For this purpose, the property of four different HP series commercial geotextiles, which are the product of MIRAFI Company, was used. The tensile stiffness of these geotextiles varies from 17.5 kN/m to 52.5 kN/m as shown in Table 3.9. The analysis was conducted in fly ash backfill with 168 mm outside diameter steel pipe installed in it and the same loading condition with the base models was applied. The models were built in a single layer reinforcement at 0.3 m from the surface.

Figure 4.14 presents the comparison of vertical stress on the top of the pipe under different tensile strength of geotextile reinforcements. To see the effect of tensile stiffness of geotextile on the pipe, the vertical stress is plotted with time. This time express the last two steps of loading, i.e. the geostatic load of the backfill and the static wheel load. As this graph indicates, as the tensile strength of the geotextile increased, the amount of vertical pressure, which reaches, on the crown of the pipe also increased. This is because of the fact that high tensile stiffness geotextiles need higher amount of stress to mobilize their reinforcement action (membrane and confinement effect). But if the amount of loading, in this model, was increased the pipe in higher tensile stiffness geotextile reinforced trench would have received a lower amount of vertical stress. Such dependency of the geotextile performance on applied pressure was observed in Guido et al. (1986) and Ashkan & Sadighi (2020), when they were comparing the performance of geotextile and geogrid reinforced soils.

Generally, for this specific amount of loading, Figure 4.14 illustrates that for increasing the tensile stiffness of reinforcement from 17.5 kN/m to 52.5 kN/m, a 21.3% increment of vertical stress at the crown was recorded. The effect of geotextile would have been higher if the comparison were made under weak backfills or under a backfills compacted in low dry density. This condition was observed in Negi and Singh (2019) when they were investigating the performance of geotextile reinforced sand and weak clay subgrade.

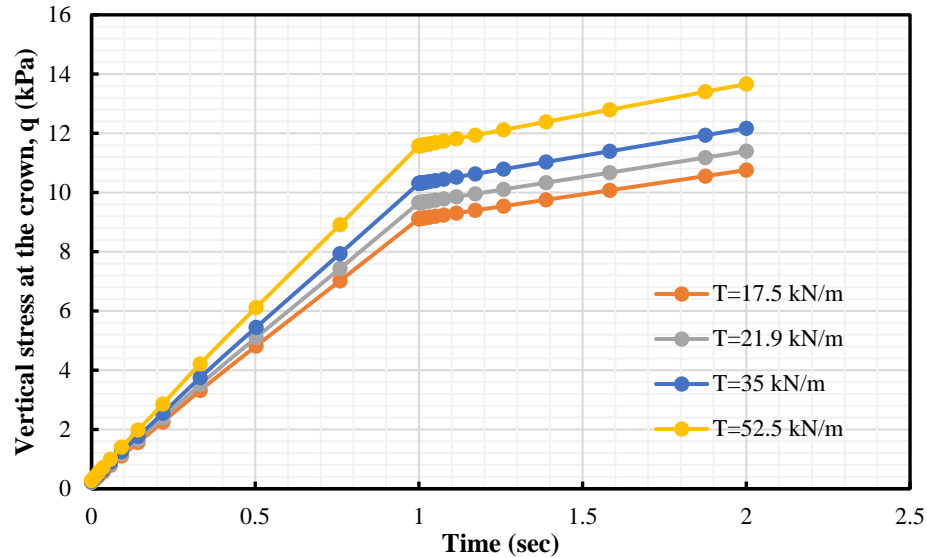


Figure 4.14 Variation of vertical pressure at the crown with time for different tensile strength geotextiles

4.2.7 Effect of Number of Geotextile Reinforcement Layers

To investigate the effect of number of reinforcement on the performance of buried pipes, trench models with single, double and triple geotextile reinforcements were prepared. According to Shukla (2016), applying more than three layers of geosynthetic to a foundation soil is not beneficial and many literatures supports this idea (e.g. Guido et al., 1986). In finite element modeling, the first reinforcement layer was layied at a depth of 0.3B from the surface, where B is the width of the loading plate. Shukla (2016), suggested that the spacing between geosynthetic reinforcement layers to be 0.2B-0.4B. Therefore, the vertical spacing between the reinforcements was modeled as 0.25B. This will put the third reinforcement layer 0.24 m from the surface. According to Guido et al.(1986), the bottom layer of geotextile reinforcement should be within the depth equal to B. With 0.3 m width of loading plate in the models, the criteria of Guido et al. (1986) was also met. The analysis

was conducted under fly ash fill and 168 mm outside diameter steel pipe installed in it, like the base models. The property of HP 570 geotextile was used for this analysis.

Figure 4.15 illustrates the variation of vertical stress at the crown of the pipe with time for different number of reinforcement layers and corresponding result of unreinforced trench system. This figure indicates that increasing the number of geotextile layer reduced the vertical stress on the crown of the pipe. Applying single, double and tripple reinforcement layers caused the pipe crown to experience 27.01%, 36.93% and 42.14% lesser vertical stresses than the unreinforced trench system. Here it can be seen that as number of reinforcement layers increased, the rate of reduction of the vertical stress was reduced. Similar conditions was obserbed in Tahmasebipoor (2012), and Guido (1986).

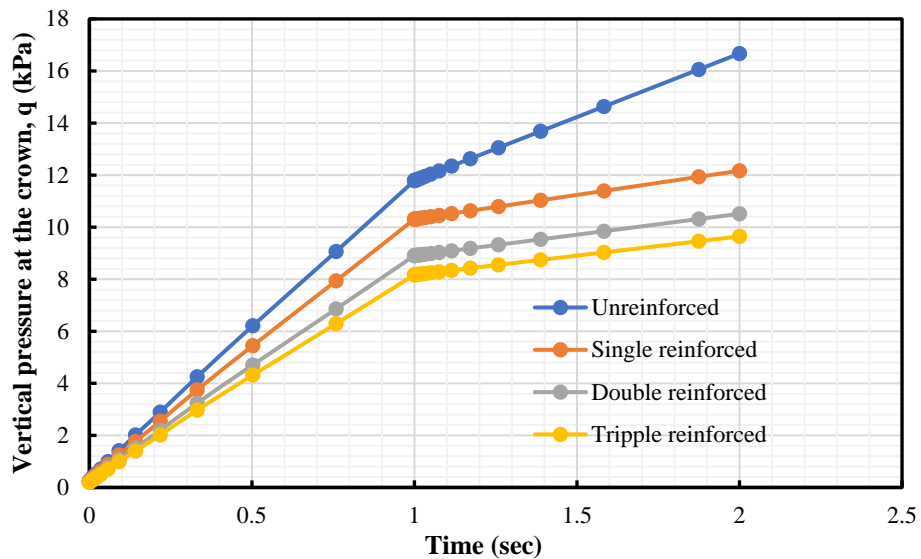


Figure 4.15 Variation of vertical stress at the crown with time for different no of geotextile reinforcement layers

4.4 Combined Use of EPS Geofoam and Geotextile

When EPS geofoam is used in shallow depth trenches under high loading conditions, the plane of equal settlement, which will be created due to settlement of EPS geofoam, might not be found within the trench depth. This will create higher surface settlement compared with unreinforced trenches and the subgrade modulus reaction of the fill-EPS geofoam composite structure will be lower. Such a problem has been observed in different

literatures. In addition to this, it is planned to study how the combined use of EPS geofoam and geotextile affect the vertical stress at the crown of the pipe.

To solve this problem the combined use of EPS geofoam and geotextile was analyzed numerically. For this purpose, all the material properties, loading and boundary conditions, which were used in the base models, were also used here, except the analysis was conducted only in fly ash fill. The configuration of the whole trench system in a two-dimensional plot is shown in Figure 4.16.

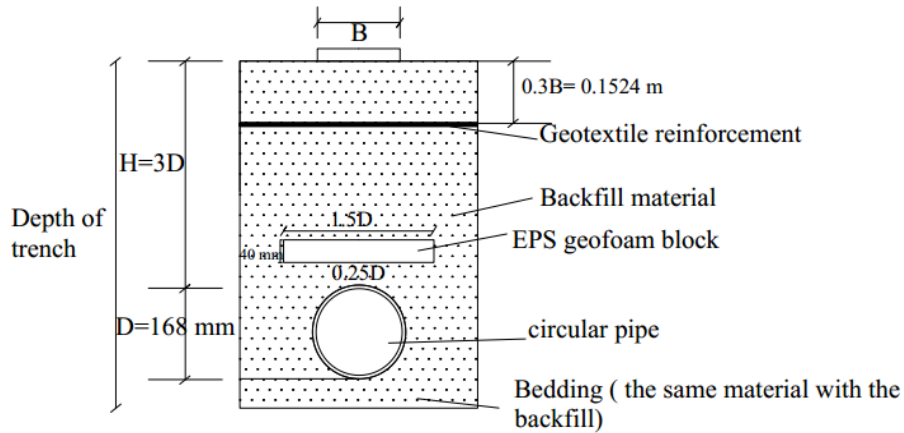


Figure 4.16 Schematic representation of combined use of EPS geofoam and geotextile

The result of the combined use of EPS geofoam and geotextile, and the comparison of it with the previously analyzed models are presented in Figure 4.17. From these graphs, it is understood that the vertical stress, which reaches the crown of the pipe, decreased more in the combined use of EPS geofoam and geotextile than the application of each material separately. The use of EPS geofoam and geotextile reduced the vertical pressure by 37.6% and 23.7% respectively compared with the unreinforced case. However, applying both materials simultaneously reduced the vertical pressure by 49.1%. Reinforcing the EPS included shallow trench system with geotextile might reduce the height above the EPS on which shear stress is going to mobilize. Due to this, the performance of EPS geofoam will decrease. However, this will be compensated by the reinforcement of geotextile. In fact, not only compensation but also additional reduction of vertical pressure on the crown of the pipe will be provided.

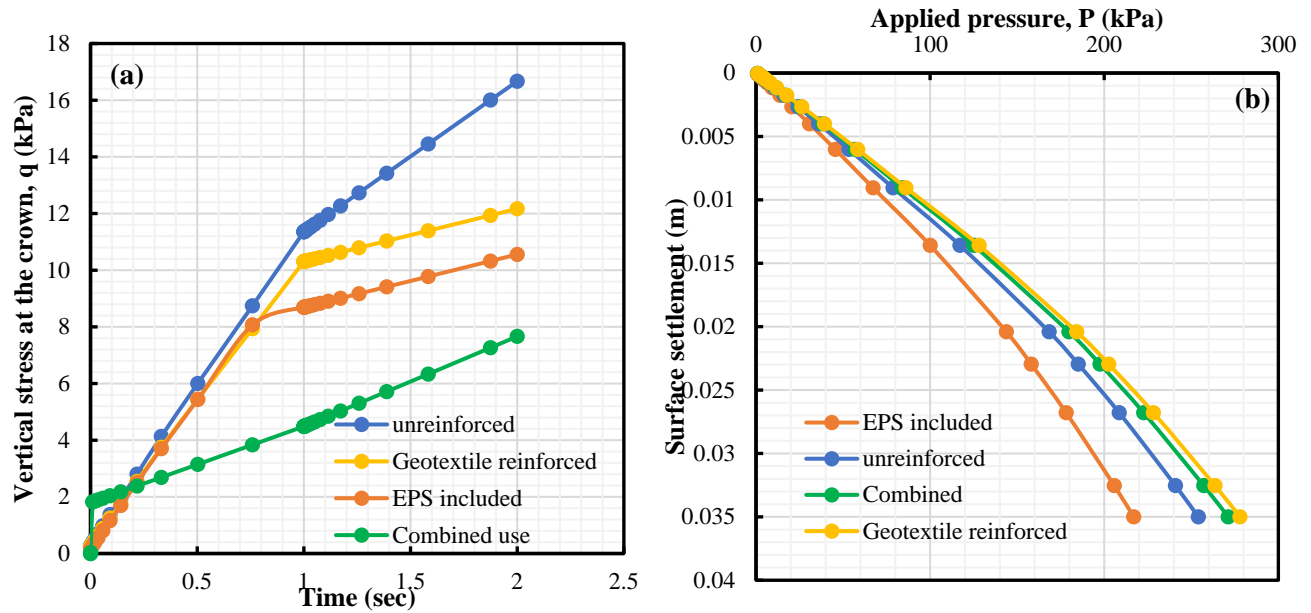


Figure 4. 17 Comparison of combined used of EPS geofoam and geotextile with other case of trench system (a) Variation of vertical stress on the crown with time, (b) Variation of surface settlement with applied pressure

To compare and understand the condition of surface settlement, a 35 mm vertical displacement was applied to the above models at the same area where the load was applied in the previous trench models and the load-settlement graph of these models is presented in Figure 4.17(b). For 35 mm of settlement, 216.93 kPa and 277.94 kPa pressure were needed for EPS geofoam included and geotextile reinforced trenches respectively. However, for the combined use, it took 271.16 kPa. That is about 24.9% more than the EPS included trench. The results clearly showed that EPS included trenches needed a lower amount of applied pressure than the unreinforced trench models to create the 35 mm vertical displacement at the surface. This is because of the high compressibility property of EPS geofoam. On the contrary, geotextile reinforce trenches needed a higher amount of applied pressure to cause the same amount of vertical displacement at the surface. However, when the EPS geofoam and geotextile were used simultaneously, the amount of pressure, which was needed to cause 35 mm settlement in EPS geofoam block, was increased by 24.9 %. That means the surface of a trench with the combined use of EPS geofoam and geotextile was stronger. It was even stronger than the unreinforced trench surface. However, the amount of pressure needed to cause the geotextile reinforced trench surface 35 mm remains higher than the combined trench case. Tafreshi et al. (2020)

successfully reduced the surface settlement in EPS geofilm included trench in higher amount. But, Instead of geotextile, they used geocell as a reinforcement which uses a different reinforcing mechanism from geotextile. That is why they got a higher amount of reduction of surface settlement. Regarding the use of both EPS geofilm and geotextile, only single literature was found, i.e., Beju and Mandel (2017a) and they were fruitful in reducing the vertical pressure on flexible pipe with similar combination of those materials.

Chapter 5

Conclusions and Recommendations

5.1 Conclusions

After a preliminary survey showed that buried pipes in the cities are always prone to damage, a series of numerical analyses were conducted on a full scale trench model with the surrounding soil to investigate the application of EPS geof foam and geotextile for the protection of steel pipe using a finite element software (Abaqus). The trenches were modeled under fly ash, stone dust and conventional soil with a strong intention of utilizing the waste materials. The property of the fill materials was determined by laboratory tests. In this study, the performance of the pipe was examined and compared in different fills and trench conditions, i.e., geotextile reinforced, EPS geof foam included and without those protecting methods. Moreover, some parametric studies were performed on the trench models. Based on the results from those analyses, the following conclusions were made.

1. The performance of the medium-sized steel pipe under fly ash and stone dust fill was comparable with the respective steel pipe, which was modeled under a conventional soil. Therefore, it is possible to use those waste materials as a backfill. Simultaneously, the disposal problem of the waste materials could be minimized and a healthy environment could be created, especially in areas where those wastes are produced.
2. The vertical pressure, which reaches on the top of the steel pipe, was successfully reduced with the reinforcement action of woven geotextile.
3. The use of EPS geof foam as a compressible material in a trench model, with a pipe installed in it at 3D from the surface, reduced the vertical pressure up to 40.1%. However, it caused higher surface settlement than the unreinforced trench models.
4. The performance of EPS geof foam and geotextile was not significantly affected by the type of backfills because the backfill materials, which were used in the trench models, had a comparable shear strength. However, the sharp edged particles of stone dust caused a little higher tensile stress at the geotextile than the other fill materials.

5. The pipe with 3D burial depth was found to be affected by its diameter. As the diameter of the pipe increased, the soil prism above the pipe also increased. Therefore, the vertical pressure on the pipe increased. This condition was true for EPS geof foam included and geotextile reinforced trench models.
6. The effect of pipe stiffness under the three backfill materials (stone dust, fly ash and soil) was significant when the pipe stiffness value lowered below 4 GPa. As the pipe stiffness lowered, the positive arching action also increased. Therefore, the vertical pressure on the top of the pipe decreased.
7. The trench model was affected by the thickness and location of the EPS geof foam block. Thicker EPS blocks reduced the vertical pressure on the pipe. In addition, the best location of EPS geof foam for shallow depth trenches was found to be directly on the pipe or very close to the pipe.
8. With the specific models used in the study, maximum benefit of double EPS geof foam block was mobilized when the spacing between the two blocks is 3D.
9. Applying multiple geotextile layers reduced the vertical pressure on the top of the pipe further.
10. The performance of the geotextile was found to be a function of its tensile strength and applied pressure. Surprisingly, lower tensile strength geotextiles performs better. Because, higher tensile strength geotextiles needed higher applied pressure to mobilize the reinforcement action (membrane and confining mechanisms) within the trench models.
11. The combined use of EPS geof foam and geotextile gave positive impact in reducing the vertical pressure on the pipe. It also successfully tackled the surface settlement problem, which could be encountered in highly loaded EPS geof foam included trenches.

5.2 Recommendations

Based on the conclusions made earlier, the first recommendation from the writer goes to governmental companies and service providers, which use pipes. They should consider utilizing waste materials as a backfill material, and start to play their role in keeping the environment clean. In addition to this, if they apply EPS geof foam and geotextile in

trenching, at least in sensitive areas, they could protect their pipes and save a lot of money, which they are spending by repairing and maintenance.

When using Stone dust and fly ash as a backfill, a thin layer of soil or other fills should be provided at the surface because dry stone dust/fly ash could be removed easily by wind or other things unless we keep them moist all the time, which is not feasible.

When applying multiple layers of EPS geofoam and geotextile in a trench, special supervision should be made by professionals because simple mistakes could lead to the malfunction of those protecting materials.

Other researchers who are interested in this area could repeat the research for large diameter and deeply buried pipes. In addition to this, the protection of buried pipes with a different configuration of EPS geofoam and geotextile should be studied to keep special and sensitive parts of pipelines from damage.

References

- Abdollahi, M., & Tafreshi, S. N. (2017). Numerical investigation on performance of expanded polystyrene geofoam block in protecting buried lifeline structures. *International Journal of Geotechnical and Geological Engineering*, 11, 183-198.
- Abebe, M. S., & Qiu, H. S. (2016). Numerical modeling of geotextile reinforcement of soft subgrade ballasted railway under high speed train. *EJGE*, 21, 4327-4343.
- Agrawal, V., Shah, P., Gupta, A., & Shah, R. (2017). The utilization of quarry dust as fine aggregates in concrete. *International Conference on Research and Innovations in Science, Engineering*, 01, 170-175.
- Al-Naddaf, M., Han, J., & Xu, C. (2019). Geofoam stiffness effect on surface load distribution on buried box culverts installed with the induced trench method. *Geosynthetics conference*. Houston.
- Anil, Ö., Erdem, R. T., & Kantar, E. (2015). Improving the impact behavior of pipes using geofoam layer for protection. *International Journal of Pressure Vessels and Piping*, 132, 52-64.
- Aria, S., Shukla, S. K., & Mohyeddin, A. (2017). Optimum burial depth of geosynthetic reinforcement within sand bed based on numerical investigation. *International Journal of Geotechnical Engineering*, 5, 1-11.
- Ashkan, F., & Sadighi, H. (2020). Numerical and laboratory investigation of effect of soil reinforcement on settlement of strip foundations. *Journal of Geology and Mining Research*, 12(4), 107-117.
- ASTM standard C618-12. (2013). Standard specification for coal fly ash and raw or calcined natural pozzolan for use in concrete. West Conshohocken, ASTM International.
- ASTM standard D6817-13. (2013). Standard Specification for Rigid Cellular Polystyrene Geofoam. West Conshohocken, ASTM International.
- ASTM Standard D2216-98. (1998). Standard test method for laboratory determination of water (moisture) content of soil and rock by mass. West Conshohocken: ASTM international.
- ASTM standard D2321-14. (2014). Standard practice for underground installation of thermoplastic pipe for sewers and other gravity flow applications. West Conshohocken: ASTM International.
- ASTM Standard D2321-11 (2011). Standard practice for underground installation of thermoplastic pipe for sewers and other gravity flow applications. ASTM International, West Conshohocken.
- ASTM Standard D2487-98. (1998). Standard practice for classification of soils for engineering purposes. West Conshohocken: ASTM International.

- ASTM Standard D4318-00. (2000). Standard test methods for liquid limit, plastic limit, and plasticity index of soils. West Conshohocken: ASTM international.
- ASTM Standard D4767-02. (2002). Standard test method for consolidated undrained triaxial compression test for cohesive soils. West Conshohocken: ASTM international.
- ASTM Standard D698-00. (2000). Standard test methods for laboratory compaction characteristics of soil using standard effort. West Conshohocken: ASTM international.
- ASTM Standard D-854-00. (2000). Standard test methods for specific gravity of soil solids by water pycnometer. West Conshohocken: ASTM international.
- Athanasopoulos, G. A. (1996). Results of direct shear tests on geotextile reinforced cohesive soil. *Geotextiles and Geomembranes*, 14, 619-644.
- Atmatzidis, D K; Missirlis, E G; Chryssikos, D A. (2001). An investigation of EPS geofam behavior in compression. *EPS geofam*. salt Lake city.
- Aytekin, M. (1997). Numerical modeling of eps geofam used with swelling soil. *GeotextilesandGeomembrane*, 15, 133-146.
- Banerjee, S., & Chakraborty, J. (2016). Replacement of cement by fly ash in concrete. *International Journal of Civil Engineering*, 03, 40-42.
- Bartlett, S. F., ASCE, M., E., p., & Lingwall, B. N. (2014). Protection of pipelines and buried structures using EPS geofam. *Ground Improvement and Geosynthetics GSP*, 547-556.
- Bartlett, S. F., Lingwall, B. N., & Vaslestad, J. (2015). Methods of protecting buried pipelines and culverts in transportation infrastructure using EPS geofam. *Geotextiles and Geomembranes*, 43, 450-461.
- Beju , Y. Z., & Mandal, J. N. (2018). Expanded polystyrene (EPS) geofam: preliminary characteristic. *procedia engineering*, 189, 239-246.
- Beju, Y. Z., & Mandal, J. N. (2017). Combined Use of Jute Geotextile-EPS Geofam to Protect Flexible Buried Pipes: Experimental and Numerical Studies. *Int. J. of Geosynth. and Ground Eng*, 3.
- Beju, Y. Z., & Mandal, J. N. (2017). Numerical analysis on protection of buried pipelines using geotextile reinforced fly ash bed. *Indian Geotechnical Conference-GeoNEst*, 1-4.
- Boldon, B. A., & Jeyapalan, J. K. (1986). Performance and selection of rigid and flexible pipes. *Journal of Transportation Engineering*, 112(5), 507-524.
- Bourdeau , P. L. (1989). Modeling of membrane action in a two - layer reinforced soil system. *Computers and Geotechnics*, 7, 19-36.

- Bowles, J. E. (1997). *Foundation analysis and design*, McGraw-Hill Companies (5th edition). Singapore.
- Coltin, W., & Mamdouh, E.-B. (2018). Finite element analysis of in-situ decommissioned steel pipelines subjected to surface live load. Fredericton, Canada.
- David, P. M., & Lidija, Z. (1999). *Finite element analysis in geotechnical engineering*. London: Thomas Telford publishing.
- De Beer, E. E. (1970). Experimental determination of the shape factors and the bearing capacity factors of sand. *Geotechnique*, 20(4), 387-411.
- Deb Nath, B., Ali Molla, M., & Sarkar, G. (2017). Study on strength behavior of organic soil stabilized with fly ash. *International Scholarly Research Notices*, 6 pages.
- Edgar, B. (1914). On physically similar systems; illustrations of the use of dimensional equations. *Phys. Rev.*, 4, 345-376.
- EDO. (1992). Expanded polystyrene construction method.
- ElKhadem, S. (2001). Effects of Pipe stiffness and installation methods on performance Of GRP pipes Based on the latest AWWA M- 45 design methods and critical evaluation of past performance of GRP pipes in Egypt. Sixth International Water Technology Conference, IWTC 2001, 143-154.
- Forum on Ethiopian investment (2011). *Water and Energy Resource Potential of Ethiopia Status of Development and Investment Opportunities*.
- Ghosh, A., Ghosh, A., & Bera, A. K. (2005). Bearing capacity of square footing on pond ash reinforced with jute-geotextile. *Geotextiles and Geomembranes* 23 (2005) 144–173, 23, 144-173.
- Guido, V. A., Chan, D. K., & Sweeney, M. A. (1986). Comparison of geogrid and geotextile reinforced earth slabs. *Can. Geotech. J.*, 23, 435-440.
- Handy, R. L. (2004). Anatomy of an error. *Geotechnical and geoenvironment engineering*, ASCE, 130, 768-771.
- Hegde, A. M., & Sitharam, T. G. (2015). Experimental and numerical studies on protection of buried pipelines and underground utilities using geocells. *Geotextiles and Geomembranes*, 43, 372-381.
- Horvath, J. S. (1994). Expanded Polystyrene (EPS) Geofoam: An Introduction to material behavior. *Geotextiles and Geomembranes*, 13, 263-280.
- Horvath, J. S. (1997). The compressible inclusion function of EPS geofoam. *Geotextiles and Geomembranes*, 15, 77-120.

- Horvath, J. S. (2005). Expanding the use of expanded polystyrene (EPS) geof foam. Boston
society of civil engineerins section/American soceity ofcivil engineers geo institute
engineering seminar. Whaltam.
- Ioannis, K. (2018). Fundamentals of finite element analysis. UK: CPI Group (UK) Ltd.
- Jewell, A. R. (1990). Reinforced bond capacity. *Geotechnique*, 40(3), 513-515.
- Kang, J., Parker, F., & Yoo, C. H. (2008). Soil–structure interaction for deeply buried
corrugated steel pipes Part II: Imperfect trench installation. *Engineering Structures*,
30, 588-594.
- Karthik, s., E., Ashok. k., P., Gowtham., G., Elango., D., Gokul., & S, Thangaraj. (2014).
Soil stabilization by using fly ash. *Journal of Mechanical and Civil Engineering* ,
10, 20-26.
- Khoshnoud, H. R., & Marson, A. K. (2011). Prototype and scaled computational model
behavior for rc frame with masonry infill walls.
- Kifle, K. (2019). Optimum Utilization of Coal Ash in Cement.
- Kim, H., & Witthoeft, A. F. (2016). Numerical investigation of earth pressure reduction on
buried pipes using EPS geof foam compressible inclusions. *Geosynthetics
International*, 1072-6349.
- Kim, H., Choi, B., & Kim, J. (2010). Reduction of earth pressure on buried pipes by EPS
geof foam inclusions. *Geotechnical Testing Journal* , 33, 1-10.
- Koarner, R. M. (1993). *Designing with geosynthetics* (5th ed.). United States of America.
- Kou, Y., Mohyeddin, A., & Shukla, S. K. (2018). Experimental investigation for pressure
distribution on flexible conduit covered with sandy soil reinforced with geotextile
reinforcement of varying widths. *Tunnelling and Underground Space Technology*
, 80, 151-163.
- Leo, C. J., Kumruzzaman, M., w. H., & yin, H. j. (2008). Behavior of EPS geof foam in true
triaxial compression tests. *Geotextiles and Geomembranes*, 26, 175-180.
- Lopes, M. D., & Lopes, M. P. (2001). Shear Behaviour of Geosynthetics in the Inclined
Plane Test – Influence of Soil Particle Size and Geosynthetic Structure.
Geosynthetics International, 8(4), 327-342.
- Lopes, M. P. (1999). Soil-geosynthetic interaction – influence of soil particle size and
geosynthetic structure. *Geosynthetics International*, 6(4), 261-282.
- Luca, F., Jean-Frederic, G., Fabio, N., & Alfio, Q. (2002). Numerical treatment of defective
boundary conditions for the Navier-Stokes equations. *Siam J. Numer. Anal*, 40(1),
376-401.

- Lytton, R. L. (1989). Use of geotextiles for reinforcement and strain relief in. *Geotextiles and Geomembranes*, 8, 217-237.
- Mohamed. G., Mmohamed. M., & Hegazy. R. (2017). An investigation on the mechanical behavior of expanded polystyrene (EPS). *international journal of plastics and technology*, 21, 1-7.
- Ma, Q., Ku, Z., & Xiao, H. (2019). Model tests of earth pressure on buried rigid pipes and flexible pipes underneath expanded polystyrene (EPS). *Advances in Civil Engineering*.
- Madhav. R., & POOROOSHASB, H. B. (1988). A new model for geosynthetic reinforced soil. *Computers and Geotechnics*, 6, 277-290.
- Mahmood, A. A., Ahmad, F., & Zakaria, N. (2000). Studies on geotextile/soil interface shear behavior. *Electronic Journal of Geotechnical Engineering*.
- Mandal, J. N. (2012). Behavior of expanded polystyrene (EPS) geofoam under triaxial loading conditions. *EJGE*, 17, 2543-2553.
- Mandal, J. N., & Sah, H. S. (1992). Bearing capacity tests on geogrid-reinforced clay. *Geotextiles and Geomembranes*, 11, 327-333.
- Marston, A., & Anderson, A. O. (1913). The theory of loads on pipes in ditches and tests of cement and clay drain tile and sewer pipe. *Bulletin 31*. Ames: Iowa.
- Meguid, M. A., & Ahmed, M. R. (2020). Earth pressure distribution on buried pipes installed with geofoam. *International journal of geosynthetics and ground engineering*.
- Meguid, M., Hussein, M., Ahmed, M., Z.Omeman, & Whalen, J. (2017). Investigation of soil-geosynthetic-structure interaction associated. *Geotextiles and Geomembranes*, 45(4), 320-330.
- Meidani, M., Meguid, M. A., & Chouinard, L. E. (2018). Estimating earth loads on buried pipes under axial loading condition: insights from 3D discrete element analysis. *International journal of Geo-Engineering*, 9(5).
- Mohammed, A. A. (2020). Stress reduction on buried conduits using EPS geofoam. *Global Journal of Engineering Sciences*, 6(4).
- Mohammed, A., & Hughes, T. G. (2005). Comparison of prototype and 1/6th model scale behaviour under compressive loading. 10th Canadian Masonry Symposium. Banff, Alberta.
- Moser, A. P., & Folkman, S. (2008). *Buried Pipe Design*. (3. edition, Ed.) New York: The McGraw-Hill Companies, Inc.
- Negi, M. S., & Singh, S. K. (2019). Experimental and numerical studies on geotextile reinforced subgrade soil. *International Journal of Geotechnical Engineering*.

- Neya, B. N., Ardeshir, M. A., Delavar, A. A., & Roshan Bakhsh, M. Z. (2017). Three-dimensional analysis of buried steel pipes under moving loads. *Open Journal of Geology*, 7, 1-11.
- Parihar, N. S., Shukla, R. P., & Gupta, A. K. (2015). Effect of reinforcement on soil. *International Journal of Applied Engineering Research*, 10, 4147-4151.
- Parihar, N. S., & shukla, R. P. (2015). Unconfined compressive strength of geotextile sheets reinforced. *International Journal of Earth Sciences and Engineering*, 08, 1379-1385.
- Prakash, K. S., & Rao, C. H. (2016). Study on compressive strength of quarry dust as fine aggregate in concrete. *Advances in Civil Engineering*.
- Prakash, K. S., & Rao, C. H. (2017). Highway embankment design by using quarry dust. *Electronic Journal of Geotechnical Engineering*, 22, 1621-1632.
- Harbert, R. & Leach, G., (1990). Damage control procedures for distribution mains. 56th Autumn meeting of The Institution of Gas Engineers.
- Butterfield, R., (1999). Dimensional analysis for geotechnical engineers. *Geotechnique*, 49, 357-366.
- Rai, A. K., Paul , B., & Singh, G. (2010). A study on backfill properties and use of fly ash for highway embankments. *Journal of Advanced Laboratory Research in Biology*, 01(5), 110-114.
- Rajeev, P., & Kodikara, J. (2011). Numerical analysis of an experimental pipe buried in swelling soil. *Computers and Geotechnics*, 38, 897-904.
- Robbert, C. D. (1995). Finite element modeling for stress analysis. United State of America: Jhon Wiley & Sons, Inc.
- Robert, K. M. (2005). Designig with geosynthetic (5th ed.). New Jersey: Pearson Prentice Hall.
- Saboya, F. A., Santiago, P. d., Martins, R. R., Tibana, S., Ramires, R. S., & Araruna , J. T. (2012). Centrifuge test to evaluate the geotechnical performance of anchored buried pipelines in sand. *Ournal of Pipeline Systems Engineering and Practice*, 3(3), 84-97.
- Satyanarayana, K. G., Sukumaran, K., Mukherjee, R. S., Pavithan, C., & Pillai, S. K. (1990). Natural fibre-polymer composites. *Cement & Concrete Composites*, 12, 117-136.
- Schofield, A. N. (1980). Cambridge geotechnical centrifuge operations. *Geotechnique*, 30(3), 227-268.

- Shirazi, G. M., A. Rashid, S. A., Nazir, B. R., Moavedi, H., Horpibulsuk, S., Samingthong, W., & Moayedi, H. (2020). Sustainable soil bearing capacity improvement using natural limited life geotextile. *Minerals*, 10, 479.
- Shukla, K. S. (2016). *An introduction to geosynthetic engineering*. EH Leiden,: CRC Press/Balkema.
- shukla, S. K., & Chandra, S. (1994). A study of settlement response of a geosynthetic reinforced compressible granular fill-soft soil system. *Geotextiles and Geomembranes*, 13, 627-639.
- Sinha, S., Khan, N., & Soni, P. (2017). An experimental study on effects of quarry dust as partial replacement of sand in concrete. *International Research Journal of Engineering and Technology (IRJET)*, 04, 2021-2023.
- Soni, D. K., & Saini, J. (2014). Mechanical properties of high volume fly ash (HVFA) and concrete subjected to evaluated 1200c temperature. *International Journal of Civil Engineering Research*, 05, 241-248.
- Soylemez, B., & Huvaj, N. (2018). Effect of geofoam location and density on the improvement of buried flexible pipe. *engineering structures*, 224-232.
- Spangler, M. G. (1941). *The structural design of flexible pipe culverts*. Bulletin 153. Ames: Iowa Engineering Experiment Station.
- Spangler, M. G., & Handy, R. L. (1982). *Soil Engineering*. (4. edition, Ed.) New York.
- Spangler, M. G., & Handy, R. L. (2007). *Geotechnical engineering, soil and foundation principles and practices*. (5. edition, Ed.) New York.
- Stone, K. L., & Newson, T. A. (2006). Uplift resistance of buried pipelines: an investigation of scale effects in model tests.
- Subramanian, K., & Kannan, A. (2013). An Experimental study on usage of quarry dust as partial replacement for sand in concrete and mortar. *Australian Journal of Basic and Applied Sciences*,, *Australian Journal of Basic and Applied Sciences*, 955-967.
- Tadesse, M. (2016). *Optimum Utilization of Coal Ash as Additive For Blended Cement Production*.
- Tafreshi, S. M., Darabi, N. J., & Dawson, A. R. (2020). Combining EPS geofoam with geocell to reduce buried pipe loads and trench surface rutting. *Geotextiles and Geomembranes*, 48(3), 400-418.
- Tahmasebipoor , A., Noorzad, R., Shooshpasha, E., & Barari, A. (2012). A parametric study of stability of geotextile-reinforced soil above an underground cavity. *Arab J Geosci*, 5, 449-456.
- Terzaghi, K. (1943). *Theoretical soil mechanics*. united states of america: John Wiley & Sons, Inc.

- Trott, J. J., Taylor, R. N., & Symons, I. F. (1984). Tests to validate centrifuge modelling of flexible pipes. *Ground Engineering*, 14-28.
- Tuna, S. C., & Altun, S. (2012). Mechanical behaviour of sand-geotextile interface. *Scientia Iranica*, 19, 1044-1051.
- Watkins, R. K., & Anderson, L. R. (2000). *Structural mechanics of buried pipes*. New York: CRC Press LLC.
- Watkins, R., Keil, B., Mielke, R., & Rahman, S. (2010). Pipe zone bedding and backfill: A Flexible Pipe Perspective. *pipelines*, 426-433.
- Yang, G., Yu, T., & Liu, H. (2011). Numerical simulation of undrained triaxial test using 3d discrete element modeling. *Geotechnical Special Publication*, 222, 99-106.
- You-chang, H., Hai, S., & Zheng-jun, Z. (2009). Experimental study on behavior of geotextile-reinforced soil. *Geotextiles and Geomembranes*, 16(3), 2393-2402.

Appendix

1. Moisture content and liquid limit

Table A.1 .1 Water content of conventional soil

Measurement/Calculation	Variable	Units	Sample		
			1	2	3
Can Number	---	---	CN-1	CN-2	CN-2
Mass of Empty Can	M_C	(g)	17.71	18.52	18.34
Mass of Can & Moist Soil	M_{CMS}	(g)	52.50	71.02	40.51
Mass of Can & Dry Soil	M_{CDS}	(g)	47.83	63.92	37.56
Mass of Soil	M_S	(g)	30.12	45.40	19.22
Mass of Water	M_w	(g)	4.67	7.10	2.95
Water Content	w	(%)	15.50	15.64	15.35
Average moisture content	w_{avg}	(%)		15.50	

2. Atterberg limit of soil

a. Liquid Limit of the Soil

Table A.2.1 Liquid Limit Determination (cassagrandia method)

Sample no	1	2	3	4
Moisture can and lid number	CN-1	CN-2	CN-3	CN-4
M_c , Mass of empty, clean can, lid (g)	18.4	17.9	18.7	18.3
M_{cms} , Mass of can, lid, and moist soil (g)	22.1	23.6	26.2	24.4
M_{cds} , Mass of can, lid and dry soil (g)	21.1	21.91	23.8	22.3
M_s , Mass of soil solids (g)	2.7	4.01	5.1	4
M_w , Mass of pore water (g)	1	1.69	2.4	2.1
W , Water content (%)	37%	42%	47%	52%
No drops(N)	33	29	27	21

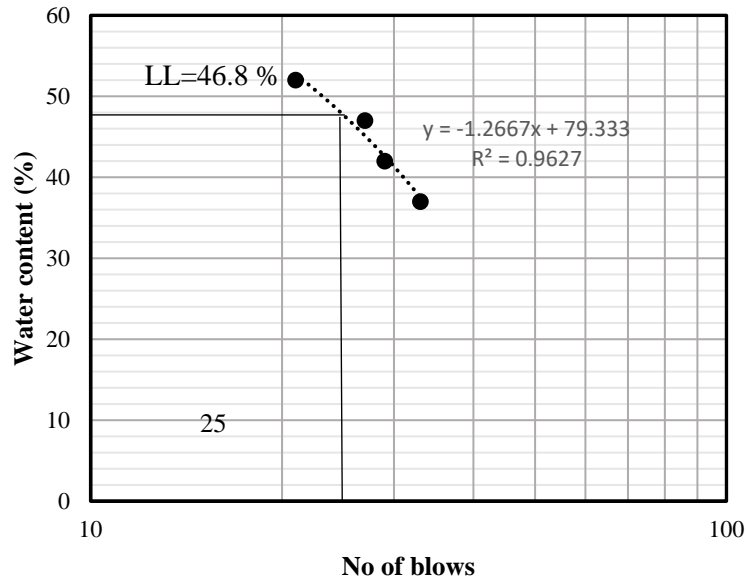


Figure A.2.1 Variation of water content with logarithm of number of blows

b. Plastic Limit of Soil

Table A.2.2 Plastic Limit determination for soil

Sample no	1	2	3
Moisture can and lid number	T1	T2	T3
Mc, Mass of empty, clean can,lid(g)	18.1	18.3	18.3
Mcms, Mass of can,lid ,and moist soil (g)	19.3	19.8	19.9
Mcds, Mass of can,lid and dry soil (g)	19.1	19.5	19.6
Ms, Mass of soil solids (g)	1	1.2	1.3
Mw, Mass of pore water (g)	0.2	0.3	0.3
w=Water content w%	20.2	21.3	23.5
Average plastic limit	21.7		

3. Specific gravity

Table A.3.1 Specific gravity determination for stone dust

Trial	1	2	3
Pycnometer No.	1	2	3
Mass of Pycnometer(empty, clean) (g)	193.88	203.5	186.13
Mass of empty Pycnometer + Dry soil (g)	218.88	228.5	211.13
Mass of Dry soil (No. 10 sieve) (g)	25	25	25
Mass of Pycnometer full of water (g)	693.82	719.16	715.34
Mass of Pycno + Soil + full of water (g)	710.01	735.33	731.52
Specific gravity (uncorrected)	2.8377	2.8313	2.8345
Correction factor, k	0.9991	0.9991	0.9991
Specific Gravity corrected	2.835	2.829	2.832
Average Specific Gravity		2.832	

Table A.3.2 Specific gravity determination for fly ash

Trial	1	2	3
Pycnometer No.	1	2	3
Mass of Pycnometer(empty, clean) (g)	193.88	203.5	186.13
Mass of empty Pycnometer + Dry soil (g)	218.88	228.5	211.13
Mass of Dry soil (No. 10 sieve) (g)	25	25	25
Mass of Pycnometer full of water (g)	693.82	719.16	715.34
Mass of Pycno + Soil + full of water (g)	707.85	733.16	729.35
Specific gravity (uncorrected)	2.2789	2.2727	2.2748
Correction factor K	0.9991	0.9991	0.9991
Specific Gravity corrected	2.277	2.271	2.273
Average Specific Gravity		2.273	

Table A.3.3 Specific gravity determination for soil

Trial	1	2	3
Pycnometer No.	1	2	3
Mass of Pycnometer(empty, clean) (g)	193.88	203.5	186.13
Mass of empty Pycnometer + Dry soil (g)	218.88	228.5	211.13
Mass of Dry soil (No. 10 sieve) (g)	25	25	25
Mass of Pycnometer full of water (g)	693.82	719.16	715.34
Mass of Pycno + Soil + full of water (g)	709.38	734.71	730.91
Specific gravity (uncorrected)	2.6483	2.6455	2.6511
Correction factor K	0.9991	0.9991	0.9991
Specific Gravity corrected	2.646	2.643	2.649
Average Specific Gravity	2.646		

4. Particle size of backfill materials

Table A.4.1 Sieve analysis for soil

Sieve opening (mm)	Wt.of Sieve (g)	Wt.of Sieve + Soil Retained (g)	Wt.of Soil retained (g)	Percent retained (%)	Cumulative percent retained (%)	Percent finer (%)
20	413.55	454.44	40.89	2.5663	2.5663	97.4337
14	402.6	538.42	135.82	8.52	11.09	88.91
6.3	402.35	961.06	558.71	35.07	46.16	53.84
5	406.01	537.75	131.74	8.27	54.42	45.58
2	391.11	763.97	372.86	23.40	77.83	22.17
1.18	351.7	466.68	114.98	7.22	85.04	14.96
0.6	314.64	413.22	98.58	6.19	91.23	8.77
0.3	288.23	352.02	63.79	4.00	95.23	4.77
0.15	283.02	330.16	47.14	2.96	98.19	1.81
0.075	267.24	294.05	26.81	1.68	99.87	0.13
pan	247.22	247.22	2	0.13	100.00	0.00
Total			1593.32	100		

Table A.4.2 Sieve analysis for stone dust

Sieve opening (mm)	Wt.of Sieve (g)	Wt.of Sieve+ Soil Retained(g)	Wt.of Soil retained (g)	Percent retained (%)	Cummulative percent retained (%)	Percent finner (%)
9.5	402.35	402.35	0	0.00	0.00	100.00
6.3	406.01	490.908	84.8983	5.66	5.66	94.34
4.75	391.11	506.682	115.572	7.70	13.36	86.64
2	351.7	494.096	142.396	9.49	22.86	77.14
1.18	314.64	436.517	121.877	8.13	30.98	69.02
0.6	288.23	439.78	151.55	10.10	41.09	58.91
0.425	283.02	526.409	243.389	16.23	57.31	42.69
0.075	267.24	301.096	33.8563	2.26	59.57	40.43/23.3
pan	247.22	853.693	606.473	40.43	100.00	0.00
Total			1500.01	100.00	-----	-----

Table A.4.4 Sieve analysis for fly ash

Sieve No	Sieve opening (mm)	Mass of Sieve(g)	Mass of sieve with retained soil(g)	Mass of retained soil(g)	Percentage Retained (%)	Cumulative Percentage Retained (%)	Percent Finer (%)
10	2	391.11	405.62	14.51	0.97	0.97	99.03
16	1.18	351.7	426.25	74.55	4.97	5.94	94.06
30	0.6	314.64	370.52	55.88	3.73	9.66	90.34
40	0.425	288.23	352.02	63.79	4.25	13.92	86.08
50	0.3	283.02	330.16	47.14	3.14	17.06	82.94
100	0.15	267.24	360.89	93.65	6.24	23.30	76.70
200	0.075	267.24	390.25	123.01	8.20	31.50	68.50
pan	-----	247.22	2635.71	1027.47	95.69	-----	-----
total				1500			

Table A.4.3 Hydrometer analysis for stone dust

Time (min)	AHR	COMP	CHR	L	TEMP	K	D	p	comb p
0.75	1.0158	0.0025	1.0133	12.12058	21.2	0.0129	0.0519	41.11965	16.63
1	1.0135	0.0024	1.0111	12.72898	21.6	0.0115	0.0410	34.3179	13.88
2	1.0129	0.0024	1.0105	12.88769	21.8	0.01283	0.0326	32.46288	13.13
4	1.0115	0.0024	1.0091	13.25802	21.8	0.01283	0.0234	28.1345	11.38
8	1.0103	0.002	1.0083	13.57544	23.7	0.01262	0.0164	25.66114	10.38
15	1.0091	0.002	1.0071	13.89287	23.5	0.01265	0.0122	21.95109	8.88
30	1.0076	0.0017	1.0059	14.28965	24.5	0.01243	0.0086	18.24105	7.38
60	1.0041	0.0017	1.0024	15.21547	24.8	0.01236	0.0062	7.420087	3.00
120	1.0038	0.0014	1.0024	15.29482	27.4	0.01217	0.0043	7.420087	3.00
240	1.0035	0.0014	1.0021	15.37418	27.5	0.01215	0.0031	6.492576	2.63
480	1.0032	0.0014	1.0018	15.45354	27.6	0.01211	0.0022	5.565066	2.25
1440	1.0032	0.0022	1.001	15.45354	22.3	0.01281	0.0013	3.091703	1.25

Table A.4.5 Hydrometer analysis for fly ash

Time(min)	AHR	COMP	CHR	L	TEMP	K	D	P	COMB P
0.5	1.0205	0.0025	1.018	10.87734	21.4	0.01317	0.0614	64.28	52.60
1	1.0201	0.0025	1.0176	10.98315	21.4	0.01317	0.0436	62.85	43.05
2	1.0182	0.0025	1.0157	11.48574	21.4	0.01317	0.0316	56.07	38.41
4	1.0156	0.0025	1.0131	12.17349	20.9	0.01317	0.0230	46.78	32.05
8	1.0146	0.0025	1.0121	12.43801	20.9	0.01317	0.0164	43.21	29.60
15	1.0129	0.0025	1.0104	12.88769	21.4	0.01317	0.0122	37.14	25.44
30	1.0115	0.0022	1.0093	13.25802	22.3	0.01301	0.0086	33.21	22.75
60	1.0103	0.0022	1.0081	13.57544	22.4	0.01301	0.0062	28.93	19.81
120	1.0091	0.0021	1.007	13.89287	22.8	0.01299	0.0044	25.00	17.12
240	1.0076	0.0017	1.0059	14.28965	24.2	0.01271	0.0031	21.07	14.43
480	1.0041	0.0016	1.0025	15.21547	25.1	0.01256	0.0022	8.93	6.12
1440	1.0032	0.0016	1.0016	15.45354	25.8	0.01242	0.0013	5.71	3.91

5. Compaction

Table A.5.1 Determination of maximum dry density for Stone dust

Moisture Content Determination					
Moisture can-Number	1	2	3	4	5
Mass of can , M_c (g)	17.81	18.43	18.0	18.49	18.93
Mass of can and moist soil, M_{cms} (g)	62.30	52.0	57.8	59.14	65.41
Mass of can and oven dry soil, M_{cds} (g)	59.51	49.52	54.30	55.12	59.81
Water content, w (%)	6.69	8.11	9.66	10.97	13.70
Density Determination					
				Mass of Mold,(g)	3348.3
				Volume of Mold,(cm^3)	944.0
Water content, w (%)	6.69	8.11	9.66	10.97	13.70
Mass of moist soil + mold, M_t (g)	5362.50	5524.00	5610.23	5590.12	5491.12
Mass of moist of soil in the mold, M_m (g)	2014.20	2175.70	2261.93	2241.82	2142.82
Moist density of compacted specimen, ρ_m (g/cm^3)	2.13	2.30	2.40	2.37	2.27
Dry density of compacted specimen, ρ_d (g/cm^3)	2.00	2.13	2.1850	2.14	2.00
Dry density for zero void curve	2.38	2.30	2.22	2.16	2.04

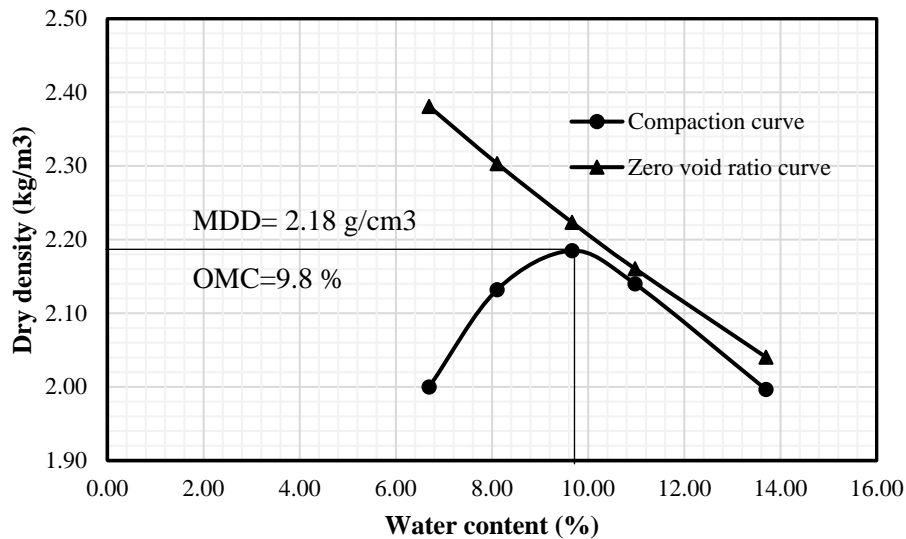


Figure A.5.1 Compaction curve for stone dust sample

Table A.5.2 Determination of maximum dry density for soil

Moisture Content Determination				
Moisture can-Number	1	2	3	4
Mass of can , M_c (g)	17.10	17.57	18.1	18.15
Mass of can and moist soil, M_{cms} (g)	64.10	65.9	65.1	57.48
Mass of can and oven dry soil, M_{cds} (g)	60.50	61.45	59.90	51.80
Water content, ω (%)	8.3	10.2	12.5	16.9

Density Determination				
			Mass of Mold, (g)	3348.3
			Volume of Mold, (cm ³)	944.0
Water content, ω (%)	8.3	10.2	12.5	16.9
Mass of moist soil + mold, M_t (g)	5277.0	5350.0	5430.5	5310.0
Mass of moist of soil in the mold, M_m (g)	1928.7	2001.7	2082.2	1961.7
Moist density of compacted specimen, ρ_m (g/cm ³)	2.04	2.12	2.21	2.08
Dry density of compacted specimen, ρ_d (g/cm ³)	1.89	1.92	1.96	1.78
Dry density for zero void curve	2.169719	2.085155	1.988427	1.829035

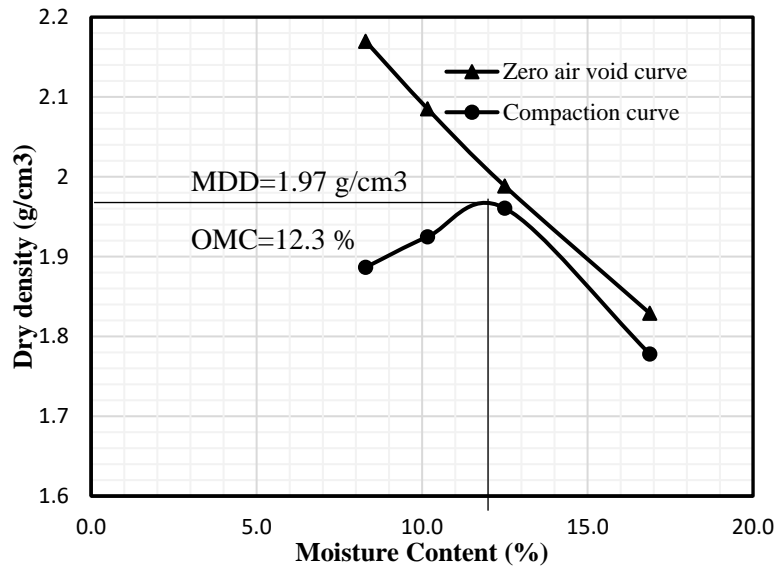


Figure A.5.2 Compaction curve for soil sample

Table A.5.3 Determination of maximum dry density for fly ash

Moisture Content Determination					
Moisture can-Number	1	2	3	4	5
Mass of can , M_c (g)	17.81	18.43	18.0	18.49	18.93
Mass of can and moist soil, M_{cms} (g)	62.30	52.0	57.8	59.14	65.41
Mass of can and oven dry soil, M_{cds} (g)	55.50	46.50	50.08	48.90	53.00
Water content, w (%)	18.0	19.7	24.1	33.7	36.4

Density Determination					
	Mass of Mold, (g)			3348.3	
	Volume of Mold, (cm ³)			944.0	
Water content, w (%)	18.04	19.74	24.08	33.67	36.43
Mass of moist soil + mold, M_t (g)	4740.00	4810.07	4950.18	4930.00	4900.00
Mass of moist of soil in mold, M_m (g)	1391.70	1461.77	1601.88	1581.70	1551.70
Moist density of compacted specimen, ρ_m (g/cm ³)	1.47	1.55	1.70	1.68	1.64
Dry density of compacted specimen, ρ_d (g/cm ³)	1.25	1.29	1.37	1.25	1.20
Dry density for zero void curve	1.61	1.57	1.47	1.29	1.24

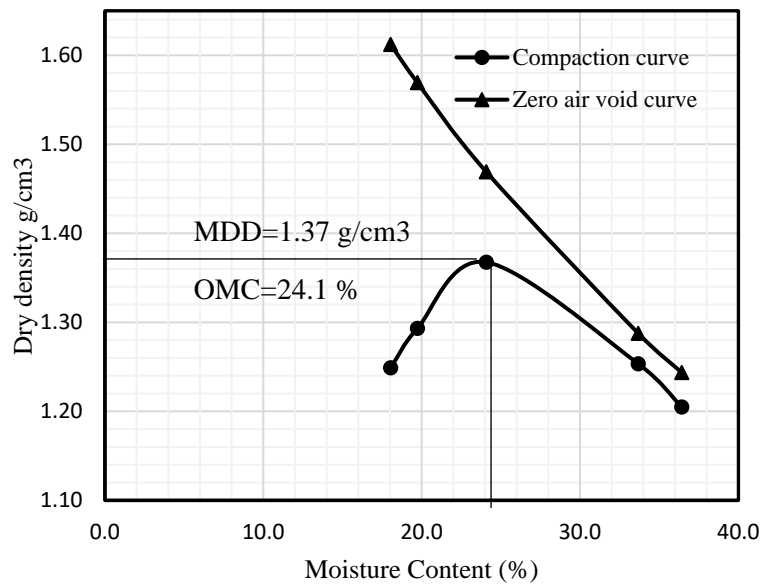


Figure A.5.3 Compaction curve for fly ash sample

6. Photos

6.1 Problems observed in pipelines



6.2 Sample fill materials



6.3 Some pictures of EPS geofabric



6.3 Some pictures of geotextile layers

